GLOBAL SEARCH OF TRIGGERED NON-VOLCANIC TREMOR

A Dissertation
Presented to
The Academic Faculty

by

Tzu-Kai Kevin Chao

In Partial Fulfillment
of the Requirements for the Degree
DOCTOR OF PHILOSOPHY (GEOLOGICAL SCIENCES) in the
School of EARTH AND ATMOSPHERIC SCIENCES

Georgia Institute of Technology
August, 2012

GLOBAL SEARCH OF TRIGGERED NON-VOLCANIC TREMOR

Approved by:

Dr. Zhigang Peng, Advisor
School of Earth and Atmospheric Sciences
Georgia Institute of Technology

Dr. Christian Huber
School of Earth and Atmospheric Sciences
Georgia Institute of Technology

Dr. Josef Dufek
School of Earth and Atmospheric Sciences
Georgia Institute of Technology

Dr. Andrew Newman
School of Earth and Atmospheric Sciences
Georgia Institute of Technology

Dr. Leonid Germanovich
School of Civil and Environmental Engineering
Georgia Institute of Technology

Date Approved: May 17, 2012

To My Family

ACKNOWLEDGEMENTS

The person I would like to thank most is my advisor Zhigang Peng. Without his patience and inspiration throughout my study, I wouldn't have learned so much, not only on the professional knowledge, but also the spirit of dedication toward research. I would also like to thank Josef Dufek, Leonid Germanovich, Christian Huber, and Andrew Newman for spending time as my committee members. Thanks to all co-authors of my papers, Chunquan Wu, Chi-Chia Tang, Cheng-Horng Lin, Amanda Fabian, Lujendra Ojha, Hector Gonzalez-Huizar, Chastity Aiken, Bogdan Enescu, Honn Kao, Aaron Velasco, Kazushige Obara, Takanori Matsuzawa. I'm grateful to my colleagues in the Geophysical group at the School of Earth and Atmospheric Sciences at Georgia Tech for their support and encouragement. These include Jaime Convers, Peng Zhao, Chunquan Wu, Lujia Feng, Cindy Young, Michelle Oakes, Xiaolu Zhang, Xiaofeng Meng, Brendan Sullivan, Chastity Aiken, Gregory Armstrong, Jing Wu, Tao Jiang, Ozge Karakas, Mary Benage, Jenn Telling, Grant farmer, Alice Koerner, Carol Paty, Amanda Thomas, Abhijit Ghosh, Joe Estep, Tina Colbert, Zach Lifton, and Ming-Chu Chen. Also, to Kurt Frankel, I will always remember you.

Last but not least, I want to thank my parents and my dear wife Erica for their support and faith in me. To my daughter Eleanor and my son Adam, you are the best reward.

TABLE OF CONTENTS

LIST OF TABLES

LIST OF FIGURES

SUMMARY

Deep non-volcanic tremor is a newly discovered seismic phenomenon with low amplitude, long duration, and no clear *P*- and *S*-waves as compared with regular earthquake. Tremor has been observed at many major plate-boundary faults, providing new information about fault slip behaviors below the seismogenic zone. While tremor mostly occurs spontaneously (ambient tremor) or during episodic slow-slip events (SSEs), sometimes tremor can also be triggered during teleseismic waves of distance earthquakes, which is known as "triggered tremor". The primary focus of my Ph.D. work is to understand the physical mechanisms and necessary conditions of triggered tremor by systematic investigations in different tectonic regions. These include Taiwan, California, southwest Japan, Alaska and the Aleutian Arc, Cascadia, and New Zealand.

In the first chapter of my dissertation, I conduct a systematic survey of triggered tremor beneath the Central Range (CR) in Taiwan for 45 teleseismic earthquakes from 1998 to 2009 with Mw ≥ 7.5. Triggered tremors are visually identified as bursts of high-frequency (2–8 Hz), non-impulsive, and long-duration seismic energy that are coherent among many seismic stations and modulated by the teleseismic surface waves. A total of 9 teleseismic earthquakes has triggered clear tremor in Taiwan. The peak ground velocity (PGV) of teleseismic surface waves is the most important factor in determining tremor triggering potential, with an apparent threshold of ~0.1 cm/s, or 7–8 kPa. However, such threshold is partially controlled by the background noise level, preventing triggered tremor with weaker amplitude from being observed. In addition, I find a positive

correlation between the PGV and the triggered tremor amplitude, which is consistent with the prediction of the 'clock-advance' model. This suggests that triggered tremor can be considered as a sped-up occurrence of ambient tremor under fast loading from the passing surface waves. Finally, the incident angles of surface waves also play an important rule in controlling the tremor triggering potential.

The next chapter focuses on a systematic comparison of triggered tremor around the Calaveras Fault (CF) in northern California (NC), the Parkfield-Cholame section of the San Andreas Fault (SAF) in central California (CC), and the San Jacinto Fault (SJF) in southern California (SC). Out of 42 large (Mw $\geq$7.5) earthquakes between 2001 and 2010, only the 2002 Mw 7.9 Denali fault earthquake triggered clear tremor in NC and SC. In comparison, abundant triggered and ambient tremor has been observed in CC. Further analysis reveal that the lack of triggered tremor observations in SC and NC is not simply a consequence of their different background noise levels as compared to CC, but rather reflects different background tremor rates in these regions.

In the final chapter, I systematically search for triggered tremor following the 2011 Mw9.0 Tohoku-Oki earthquake in the regions where ambient or triggered tremor has been found before. The main purpose is to check whether triggered tremor is observed in regions when certain conditions (e.g., surface wave amplitudes) are met. Triggered tremor is observed in southwest Japan, Taiwan, the Aleutian Arc, south-central Alaska, northern Vancouver Island, the Parkfield-Cholame section of the SAF in CC and the SJF in SC, and the North Island of New Zealand. Such a widespread triggering of tremor is

not too surprising because of the large amplitude surface waves (minimum peak value of ~0.1 cm/s) and the associated dynamic stresses (at least ~7-8 kPa), which is one of the most important factors in controlling the triggering threshold. The triggered tremor in different region is located close to or nearby the ambient tremor active area. In addition, the amplitudes of triggered tremor have positive correlations with the amplitudes of teleseismic surface waves among many regions. Moreover, both Love and Rayleigh waves participate in triggering tremor in different regions, and their triggering potential is somewhat controlled by the incident angles.

In summary, systematically surveys of triggered tremor in different tectonic regions reveal that triggered tremor shares similar physical mechanism (shear failure on the fault interface) as ambient tremor but with different loading conditions. The amplitude of the teleseismic surface wave is one of the most important factors in controlling the tremor triggering threshold. In addition, the frequency contents and incident angles of the triggering waves, and local fault geometry and ambient conditions also play certain roles in determining the triggering potential. On the other hand, the background noise level and seismic network coverage and station quality also could affect the apparent triggering threshold.

Because triggered tremor occurs almost instantaneously during the teleseismic surface waves, and the tremor amplitude is somewhat controlled by the amplitude of the triggering waves, the occurrence time and the size of the triggered tremor could be somewhat predictable, so long as we know the amplitude and period of surface waves

and associated time-varying dynamic stresses. Hence, further analysis of triggered tremor may provide important new clues on the nucleation and predictability of seismic events.

CHAPTER 1

INTRODUCTION

1.1 Overview of Non-Volcanic Tremor

Deep "non-volcanic" tremor is a newly observed seismic signal occurring away from volcanic regions with non-impulsive arrival, low amplitude, and long duration (Beroza and Ide, 2011; and references therein; Peng and Gomberg, 2010; Rubinstein *et al.*, 2010; Schwartz and Rokosky, 2007). After the initial discovery in southwest Japan (Obara, 2002), tremor has been identified in many regions along major plate boundaries around the Pacific plate (Peng and Gomberg, 2010; Schwartz and Rokosky, 2007). These include the Cascadia subduction zone (Rogers and Dragert, 2003), the San Andreas Fault in central California (Nadeau and Dolenc, 2005), and the subduction zones in Mexico (Payero *et al.*, 2008), Alaska (Peterson and Christensen, 2009), the Aleutian Arc (Peterson *et al*., 2011), the North Island of New Zealand (Kim *et al*., 2011; Ide, 2012), southern Chile (Ide, 2012), and Costa Rica (Brown *et al.*, 2009; Outerbridge *et al.*, 2010). Tremors often accompany SSEs observed from geodetic measurements (Obara and Hirose, 2006; Rogers and Dragert, 2003). Because tremors generally occur in the lower crust below the locked seismogenic zone, a systematic study of tremor and SSEs could help us to better understand deep fault slips in the lower crust (Rubinstein *et al.*, 2010), and their relationship to the occurrence of large earthquakes (Shelly, 2009, 2010).

Recent studies have shown that tremor can be instantaneously triggered by passing surface waves of regional (epicentral distance between 100 and 1200 km) (Guilhem *et al.*, 2010) and teleseismic earthquakes (Fry *et al.*, 2011; Ghosh *et al.*, 2009; Gomberg *et al.*, 2008; Gomberg, 2010; Miyazawa and Mori, 2005; Miyazawa and Mori, 2006;

Miyazawa and Brodsky, 2008; Miyazawa *et al.*, 2008; Peng and Chao, 2008; Peng *et al.*, 2008; Peng *et al.*, 2009; Peng *et al.*, 2010a; Rubinstein *et al.*, 2007; Rubinstein *et al.*, 2009; Shelly *et al.*, 2011). Triggered tremor is mostly found at places where "ambient tremor" (i.e. not associated with teleseismic earthquakes) are identified, and their spectra shapes are similar (Peng *et al.*, 2008; Rubinstein *et al.*, 2007). In addition, at least portions of triggered tremor consists of many low-frequency earthquakes (LFEs) (Peng *et al.*, 2010a; Shelly *et al.*, 2011; Tang *et al.*, 2010), suggesting that triggered and ambient tremors are generated by similar failure processes but with different loading conditions. That is, triggered tremor could be considered as a special case of ambient tremor driven by the dynamic stresses from the surface waves (Gomberg, 2010).

1.2 Motivations

Because tremor episodes often accompany slow-slip events, they can be used as an indicator to study SSEs (Wech and Creager, 2011), especially at regions where the sizes of SSEs are too small to be observed by geodetic instruments (Shelly, 2010; Smith and Gomberg, 2009). The recent finding on migration of SSEs before the 2011 Mw9.0 Tohoku-Oki earthquake (Kato *et al.*, 2012) and the 1999 Mw7.6 Izmit earthquake (Bouchon *et al.*, 2011) provides a new insight on studying evolutions of fault zone behaviors prior to major earthquakes. In addition, recent studies have shown that the occurrence of ETS on the deep portion of subduction zone interface may increase the conditional properties of a megathrust earthquake by several orders of magnitude (Mazzotti and Adams, 2004). These observations suggest that monitoring tremor

behaviors at depth may hold important new clues in the predictability of large earthquakes.

Triggered tremor generally has a higher signal-to-noise ratio (SNR) than ambient tremor, and mostly occurs during the large-amplitude of surface waves. So it is relatively easy to search for triggered tremor in wide regions (e.g. Gomberg *et al.*, 2008), providing a useful tool to identify regions with ambient tremors and SSEs (Gomberg, 2010). Since triggered tremor shares many similar failure mechanism as ambient tremor, a better understanding the characteristics of the dynamics triggering of tremor can help seismologists to understand the interaction between tremor, slow slip, and earthquakes.

1.3 Organization of the Dissertation Chapters

In this Ph.D. dissertation, I include results from two published papers in Chapter 2 (Chao *et al.*, 2012d) and Chapter 3 (Chao *et al.*, 2012a), and one submitted manuscript in Chapter 4 (Chao *et al.*, 2012b). In Chapter 2, I show the results of a systematic survey of triggered tremor in Taiwan during nine teleseismic earthquakes. Chapter 3 focuses on a comparison of triggered tremor in three regions in California. In Chapter 4, I present the results of global survey of triggered tremor following the 2011 Mw9.0 Tohoku-Oki earthquake in eight regions where ambient tremor episodes are active or triggered tremor has been observed before. In the appendix, I include the detailed analysis procedure on how to identify and locate triggered tremor.

CHAPTER 2 (Chao *et al.*, 2012d)

REMOTE TRIGGERING OF NON-VOLCANIC TREMOR AROUND TAIWAN

Summary

We perform a systematic survey of triggered deep "non-volcanic" tremor beneath the Central Range (CR) in Taiwan for 45 teleseismic earthquakes from 1998 to 2009 with Mw ≥ 7.5 and epicentral distance ≥ 1000 km to the broadband station TPUB. Triggered tremors are visually identified as bursts of high-frequency (2–8 Hz), non-impulsive, and long-duration seismic energy that are coherent among many seismic stations and modulated by the teleseismic surface waves. Out of the 45 earthquakes, we identified 9 teleseismic events associated with 9 tremor sources in the southern and 5 in the northern CR. Most of the tremor sources are located within the depth range of 15–25 km in the lower crust above the Moho. We find that the amplitudes of the surface waves play an important role in determining the triggering potential, and the apparent triggering threshold is ~0.1 cm s^{-1}, or 7–8 KPa. However, such threshold is partially controlled by the background noise level, which could prevent weaker tremor triggered by surface waves with smaller amplitudes from being identified. The amplitudes of the triggered tremor show a positive correlation with the amplitudes of the triggering surface waves, consistent with the predictions by the "clock-advance" model. In addition to amplitudes, other factors, such as frequency contents and incidence angles, also affect the triggering potential. We find that intermediate-period (30–10 s) surface waves could

trigger/modulate tremors, suggesting that long-period (> 30 s) surface waves are not always required in long-range triggering. Tremors appear to be triggered by both Love and Rayleigh waves. When the incidence angles are parallel to the strike of the CR, all 6 events triggered tremor primarily during the Rayleigh waves. For strike normal incidence, only the 2001 Mw7.8 Kunlun earthquake showed predominant Love wave triggering. This observation can be qualitatively explained by a simple Coulomb failure for a left-lateral shear on the low-angle detachment fault beneath the southern CR.

2.1 Introduction

Triggered tremor has been observed in many tectonic regions, however, several fundamental questions remain unclear. First, the underlying physical mechanisms of triggered tremor generation are still in debate. Earlier studies have suggested that triggered tremor reflects fluid flow due to changes in dilatational stresses during large-amplitude Rayleigh waves (Miyazawa and Mori, 2005; Miyazawa and Mori, 2006; Miyazawa and Brodsky, 2008; Miyazawa *et al.*, 2008). Recent studies have invoked simple Coulomb failure criteria (Hill, 2008; Hill, 2010) to explain the correlation of triggered tremor with both Love and Rayleigh waves (e.g. Fry *et al.*, 2011; Peng and Chao, 2008; Peng *et al.*, 2008; Peng *et al.*, 2009; Rubinstein *et al.*, 2007; Rubinstein *et al.*, 2009). In addition, the necessary conditions (both ambient environments and incoming surface waves) to favor triggered tremor generation are still unclear. The amplitude of passing surface waves appears to be an important factor in controlling triggered tremors based on the systematic surveys in Parkfield (Peng *et al.*, 2009) and

Cascadia (Rubinstein *et al.*, 2009). Other factors, such as frequency (Guilhem *et al.*, 2010) and incidence angle (Hill, 2010) of surface waves are also possible controlling parameters for triggering tremor. Rubinstein *et al.* (2009) and Gomberg (2010) also suggested that when a fault is close to or undergoing failure, it is more likely to generate triggered tremor. Finally, triggered and ambient tremors occur in certain isolated regions along major plate boundaries (Beroza and Ide, 2009; Beroza and Ide, 2011; Peng and Gomberg, 2010; Rubinstein *et al.*, 2010). While many studies have shown that elevated fluid pressures may favor tremor generation, it is still not clear what is the most important condition that control tremor occurrence.

To further investigate the necessary conditions and underlying mechanisms for triggered tremor, we conduct a systematic search of tremor in Taiwan triggered by large teleseismic earthquakes (Figure 2.1). This study is an extension of our previous work on tremor triggered by the 2001 Mw7.8 Kunlun earthquake (Peng and Chao, 2008), and LFEs triggered by the 2005 Mw8.6 Nias earthquake (Tang *et al.*, 2010). In this study, we examine the passing surface waves from 45 teleseismic earthquakes between 1998 and 2009 with Mw $\geq$ 7.5, and find a total of 9 events that have triggered tremor in Taiwan. We present the results for these cases, and then discuss possible triggering mechanisms and necessary conditions for tremor generation.

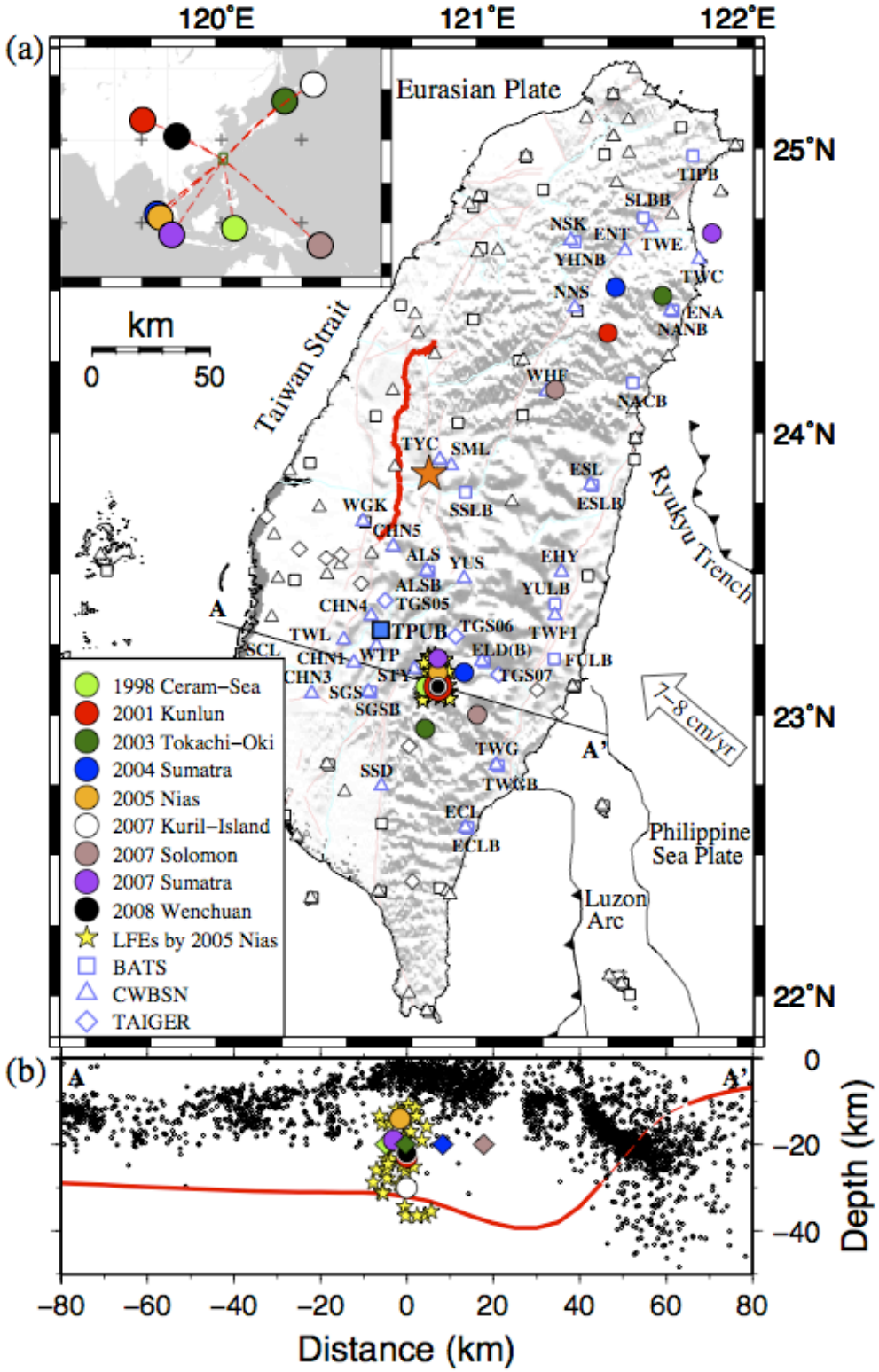

Figure 2.1. (a) The study area around the Central Range (CR) in Taiwan. The circles with different colors correspond to the locations of 14 tremors triggered by 9 teleseismic earthquakes. The yellow stars mark the 41 low-frequency earthquakes (LFEs) (Tang *et*

al., 2010) triggered by the 2005 Nias earthquake. Seismic stations of BATS, CWBSN, and TAIGER are marked by square, triangle, and diamond symbols, respectively. The stations plotted in light blue colors are used in this study. The broadband station TPUB is shown by the blue square. The hypocenter and fault trace of the 1999 Mw7.6 Chi-Chi earthquake are marked by the orange star and red bold line. The inset shows the epicentral locations of the 9 triggering mainshocks. **(b)** A cross-section view along A–A' normal to the strike of the southern CR. Triggered tremors and LFEs are marked by circles and stars, respectively. The diamond symbols mark the tremor locations that are not well constrained and set to be at 20 km. The black dots represent earthquakes with magnitudes greater than 3.0 within 20 km along A–A' between 1991 and 2006 from the CWBSN catalog. The red line marks the Moho depth calculated by the receiver functions (Tang *et al.*, 2011).

2.2 Tectonic Setting and Previous Studies of Tremor and Slow-Slip Events in Taiwan

Taiwan is a seismically active island located at the western portion of the circum-Pacific seismic belt. The high level of seismicity around Taiwan is mostly associated with two tectonic activities: the subduction of the Eurasian plate eastward beneath the Philippine Sea Plate on the southern side of the island, and the subduction of the Philippine Sea plate northward beneath the Eurasian plate on the eastern side along the Ryukyu Trench (Shin and Teng, 2001; Wu *et al.*, 2007). In between, the Luzon Arc collides with the Chinese continental margin with a convergence rate of 7–8 cm yr^{-1} (Yu *et al.*, 1997). The island itself can be divided into two major tectonic provinces, separated by the 160-km-long NNE-striking Longitudinal Valley Fault (LVF). The eastern side contains the Coastal Ranges and several volcanic islands. The western side can be further divided into several NNE-SSW trending structural belts: the Coastal Plain, Western Foothills, the Hsueshan Ranges, and the CR.

Several recent studies have focused on triggered tremors (Peng and Chao, 2008; Tang *et al.*, 2010; Velasco *et al.*, 2009; Yeh, 2011) and slow-slip events (Liu *et al.*, 2009) in Taiwan. Peng and Chao (2008) first identified tremor beneath the southern CR triggered by the surface waves of the 2001 Mw7.8 Kunlun earthquake. The tremor occurs when the Love wave displacement propagated to the southwest direction (parallel to the CR). They suggested that the tremor was generated by the shear slip on the weak detachment fault beneath the CR. Following the work of Guilhem *et al.* (2010) that searched for tremor triggered by regional earthquakes, Yeh (2011) conducted a systematic search of tremor along the CR triggered by 70 regional earthquakes around Taiwan with magnitude from 6.0 to 7.5 and epicentral distance between 100 and 2000 km, and did not find any positive case. One possible reason is that only recordings from surface stations were used in that study, and hence the SNR might be low in the examined frequency range of 2–8 Hz. Recently, Tang *et al*. (2010) used a matched filter technique to identify *P*- and *S*-waves of 41 LFEs within the tremor bursts triggered by the 2005 Mw8.6 Nias earthquake. They detected 1–2 LFEs in each tremor burst, and suggested that the triggered tremors consist of many LFEs, similar to ambient tremor (Shelly *et al.*, 2007). Based on the LFE locations (yellow stars on Figure 1), they proposed that those triggered LFEs (tremors) occurred on the deep extension of the high-angle thrust Chaochou-Lishan fault (CLF) and near a region with modestly high Vp/Vs ratios (1.75–1.85). Velasco *et al*. (2009) studied the tremor triggering mechanism by modeling the triggering preference of surface waves based on the Coulomb failure criteria. They found that the Love wave produces the largest dynamic stress and triggers tremor when it propagates in the direction perpendicular to the strike of CR, while Rayleigh wave generates larger dynamic stress

and triggers tremor when it propagates parallel to the strike of the CR. Moreover, Liu *et al*. (2009) reported slow earthquakes recorded by borehole strainmeter in eastern Taiwan near the LVF. These events generally last for a few hours to a day and half of them are triggered by typhoons.

2.3 Data and Analysis Procedure

The seismic data used in this study come from three major seismic networks in Taiwan: (1) the Broadband Array in Taiwan for Seismology (BATS) operated by the Institute of Earth Sciences (IES), Academia Sinica, (2) the short-period Central Weather Bureau Seismic Network (CWBSN) operated by the Taiwan Central Weather Bureau (CWB), and (3) the CWB Broadband Seismic Network (CWBBB) (Shin and Teng, 2001). An additional temporary deployment, the TAiwan Integrated GEodynamics Research (TAIGER) (http://taiger.binghamton.edu/) was used for the 13 January 2007 Mw8.1 Kuril-Island earthquake. We selected large teleseismic earthquakes from 01 January 1998 to 31 December 2009 listed in the Advanced National Seismic System (ANSS, http://www.ncedc.org/anss/) earthquake catalog. A total of 45 earthquakes (Figure 2.2a) with magnitudes Mw $\geq$ 7.5, depths $\leq$ 100 km, and epicentral distances $\geq$ 1000 km to the BATS station TPUB (Figure 2.1a) were selected for further examination (Table S2.1). These criteria are based on the empirical values used by recent studies of tremor triggered by teleseismic earthquakes in other regions (Peng *et al.*, 2009; Rubinstein *et al.*, 2009).

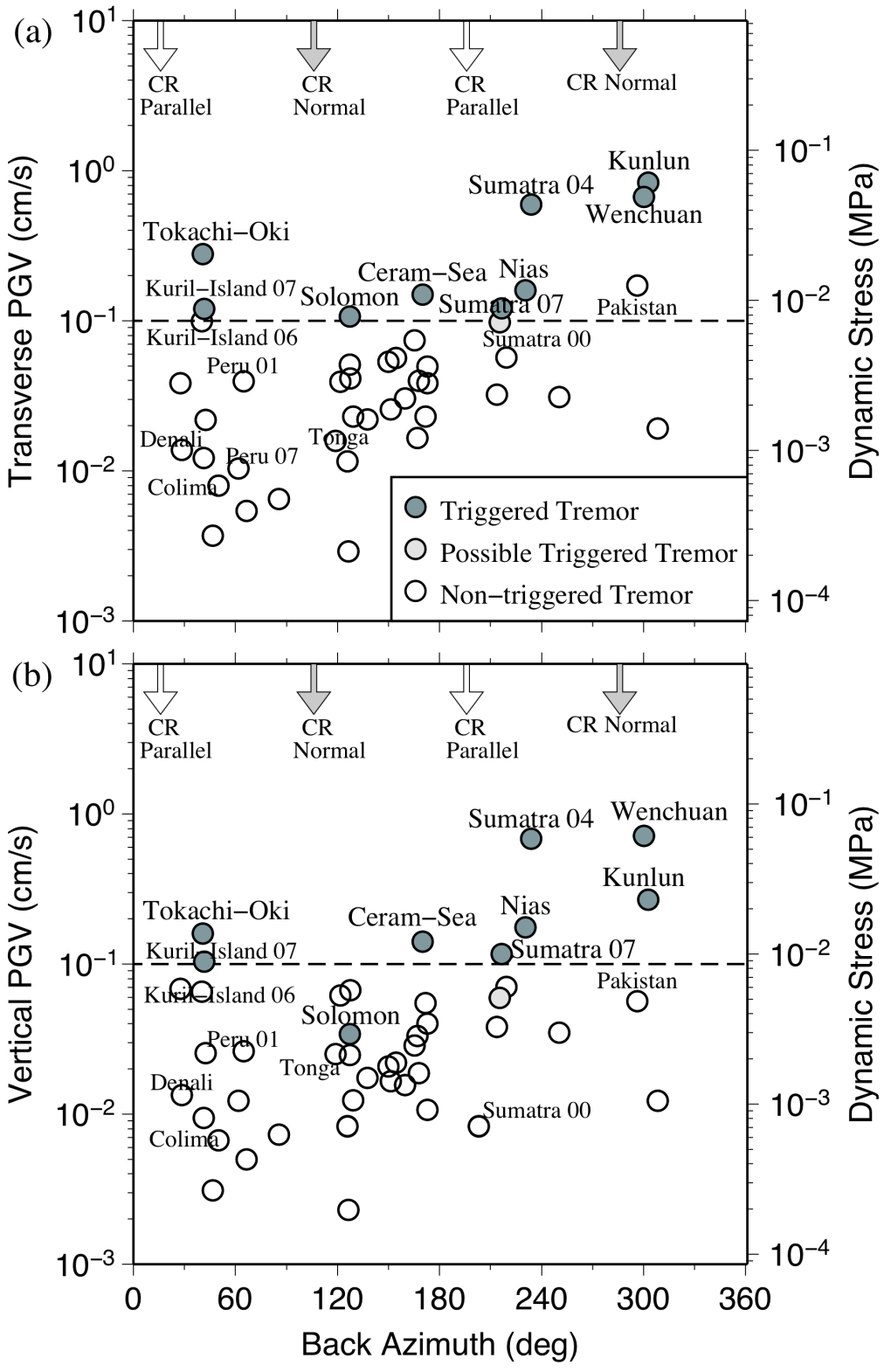

Figure 2.2 The peak ground velocity (left vertical axis) and the corresponding dynamic stress (right vertical axis) versus the back azimuth in transverse **(a)** and vertical **(b)**

components at station TPUB for all 45 teleseismic earthquake with Mw ≥ 7.5 between 1998 and 2009. The dashed line marks the apparent tremor-triggering threshold of 7–8 KPa. The solid white and gray arrows mark the directions parallel and normal to the strike of the Central Range (CR) (N16°E). The detailed earthquake information is listed in Table S2.1.

The analysis procedure generally follows that of Peng and Chao (2008) and Peng *et al*. (2009) and is briefly described here. We first shifted the reference time of three-component (north, east, and vertical) seismograms to the origin time of the teleseismic event, removed mean and instrument response, cut seismograms into the lengths of 1000 s before and 9000 s after the origin time, and applied a 2–8 Hz band-pass-filter. Next, we compared the band-pass-filtered seismograms with the broadband recordings to visually identify triggered tremor during the passage of surface waves. Only the seismic data recorded by the BATS were used in this step because this is the only network with continuous recording throughout the entire time period. We identified triggered tremor as bursts of high-frequency, non-impulsive, and long-duration seismic signals that are coherent among many nearby stations, and in phase with the passing surface waves (Peng *et al.*, 2009). If the comparison with BATS stations showed potential triggered tremor signals, we examined the CWB broadband and short-period data for further evidence of triggered tremor. Only the signals recorded by at least five surrounding stations within 100 km of the potential tremor source with clear move-out (i.e. later arrivals with increasing distances) are classified as positive triggering cases and used in the following analysis.

Next, we used the standard envelope cross-correlation techniques (Peng and Chao, 2008; Peng *et al.*, 2009) to obtain the tremor location by minimizing the root mean square

(RMS) residual between the theoretical travel time difference among station pairs and those observed from cross correlations of band-pass-filtered envelope functions. Based on the tremor move-out and our previous studies, we divided the seismic data into two groups, one around the southern CR, and the other one near the northern CR (Figure 2.1a). We assumed that multiple tremor episodes triggered by the same teleseismic earthquake come from the same location, either in the southern or northern CR. Although tremor (or LFEs) triggered by the same triggering event could come from slightly different sources (Figure 2.1b) (Tang *et al.*, 2010), in general those LFEs triggered by the 2005 Nias earthquake are close to the location (Figure 2.1a) identified by the envelope cross-correlation techniques. Hence in this study we only calculated an average location in southern or northern CR for each triggering event. We used an updated 1-D velocity model (Tang *et al.*, 2010) to compute the *S*-wave arrival times for the tremor from south. This 1-D velocity model (Table S2.2a) is averaged from the 3-D velocity model (Wu *et al.*, 2007) around the southern tremor source region. For the tremor locations in north, we used a slightly different 1-D velocity model (Table S2.2b) computed from the 3-D velocity model (Wu *et al.*, 2007) in that region. Finally, we computed the RMS values using a 1 km grid from 0 to 50 km in depth and within 1 degree of the epicentral distance from the stations ELDB and ENT for the tremor in southern and northern CR, respectively. The best tremor location is obtained from the smallest RMS and the location errors were calculated from the c-square distribution within the 68% confidence limit (Shearer, 1999). An example of the best-fitting tremor locations triggered by the 2005 Nias earthquake is shown in Figure 2.3.

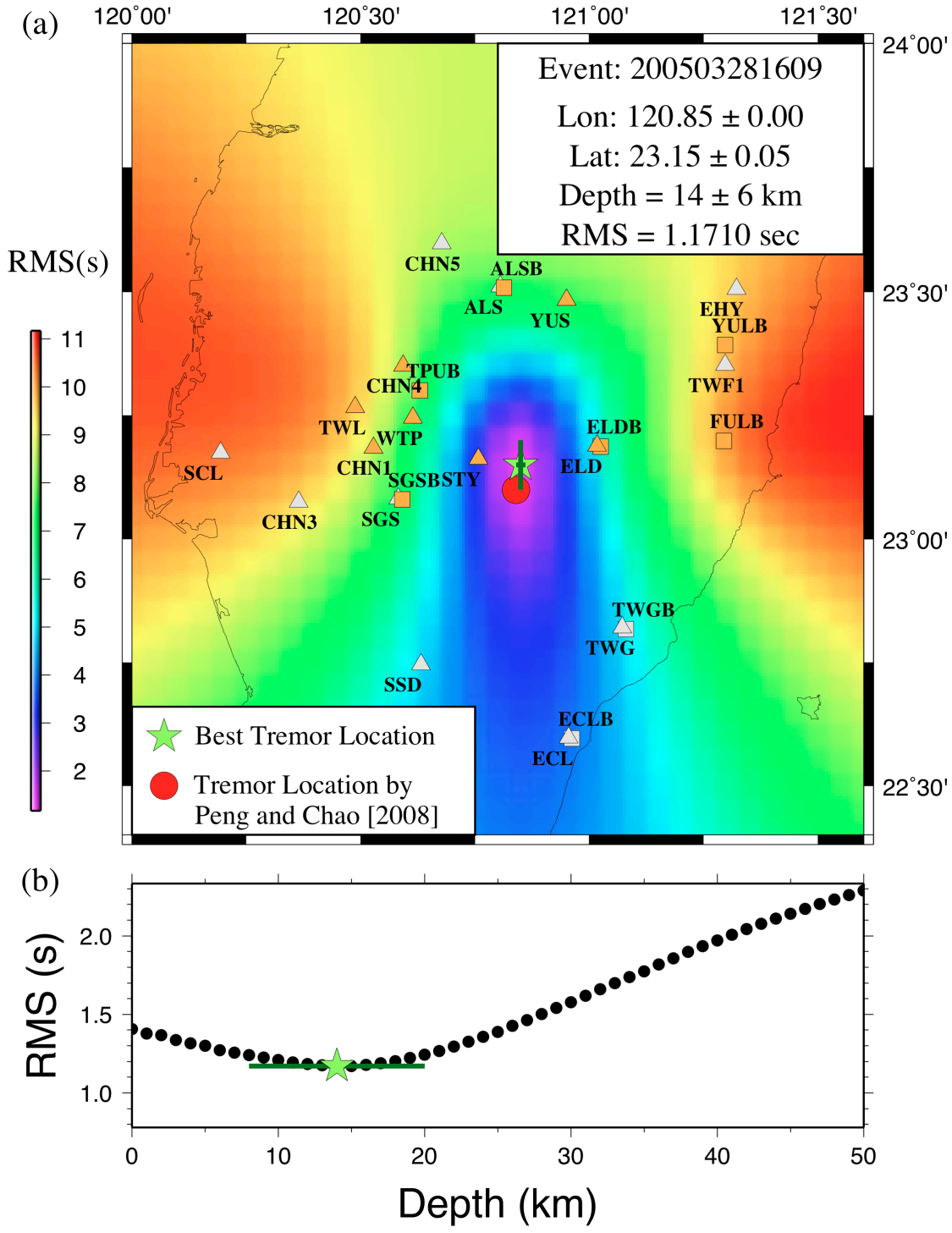

Figure 2.3 (a) An example of tremor location triggered by the 2005 Nias earthquake. The background color marks the root mean square (RMS) residual between the observed and predicted travel time differences, and the best tremor location that corresponds to the minimum RMS is marked by the green star. The red circle marks the hypocenter of tremor triggered by the 2001 Kunlun earthquake (Peng and Chao, 2008). The orange

symbols mark the stations that are used to locate tremor. Other notations are the same as in Figure 2.1. **(b)** The RMS versus depth profile at the hypocenter of the best tremor location. The green star marks the best fitting depth and the horizontal line shows the 68% confidence level.

Figure 2.1a shows the tremor locations in southern and northern CR. The tremors in the southern CR are clustered in a restricted region, while the tremor locations in the northern CR are more scattered. The horizontal and vertical uncertainties in tremor locations are on the order of 10 km (see Table S2.3 for detailed error estimation), which is typical for those locations obtained from the tremor envelope cross-correlation techniques (Obara, 2002; Rubinstein *et al.*, 2010). The depths of tremors were general located between 15 and 25 km (Figure 2.1b). For some events the depths were not well constrained because the RMS value decreasing or increasing monotonically with depth, we used an average value of 20 km in depth for those events (diamond symbols in Figure 2.1b).

2.4 Tremors Triggered by Teleseismic Earthquakes

Among all 45 teleseismic earthquakes (Figure 2.2), we identified 9 earthquakes (Table S2.3) that triggered 9 and 5 tremor sources in the southern and northern CR (Figure 2.1a), respectively. These earthquakes include the (1) 1998 November 29 Mw 7.7 Ceram-Sea, (2) 2001 November 14 Mw7.8 Kunlun, (3) 2003 September 25 Mw8.3 Tokachi-Oki, (4) 2004 December 26 Mw9.2 Sumatra, (5) 2005 March 28 Mw8.6 Nias, (6) 2007 January 13 Mw 8.1 Kuril-Island, (7) 2007 April 1 Mw8.1 Solomon, (8) 2007 September 12 Mw8.4 Sumatra, and (9) 2008 May 12 Mw7.9 Wenchuan earthquakes

(Figures 2.4–2.12). In addition, the 2000 June 4 Mw7.9 Sumatra earthquake (Figure 2.13) is considered as a possible triggering event due to lack of enough recording stations.

To better quantify whether Love or Rayleigh waves trigger tremor in the southern CR, we used the following three criteria to measure the effects of surface waves on tremor activity. Firstly, we checked whether the tremor activity is initiated by the Love or the Rayleigh waves. If tremor starts in the first few cycles of the Love waves, then it is considered as a possible case of Love wave triggering (e.g., Figure 2.4). On the other hand, if tremor did not start until the arrivals of the long-period Rayleigh waves, then it is likely that Rayleigh wave plays a more important role in triggering tremor (e.g., Figure 2.7). Because Rayleigh wave introduces volumetric changes (Miyazawa and Brodsky, 2008), we evaluated Rayleigh wave triggering in upward vertical surface displacement (BHZ in Figures 2.4–2.12b) to represent the positive dilatational (volumetric) stress changes at depth (Peng *et al.*, 2009). The Love wave amplitude decreases with depth and such displacement gradient would cause horizontal shear that either parallel or perpendicular to the wave propagation direction (Hill 2008). Because most of the tremor-triggering events have incidence angles that are either parallel or perpendicular to the strike of the CR, we used the peak of the Love wave displacement in the transverse component (BHT seismogram in Figures 2.4-2.12b) as a proxy to represent shear stresses at depth where tremor occurred (Peng and Chao, 2008). We computed the *S*-wave travel time at the station with best tremor signals and shifted the trace back to the tremor source region. Similarly, we time shifted the surface waves traces based on phase velocities of 4.1 km/s and 3.5 km/s for the Love and Rayleigh waves, respectively. Finally, we

compared the peaks of the tremor bursts on the time-shifted 2-8 Hz band-pass-filtered envelope functions, with the time-shifted surface wave peaks. Secondly, we compared the peak displacement amplitudes ratio of Rayleigh and Love waves (R/L) and used it as a proxy for the strength of the associated dynamic stresses. When the R/L value is greater than 1, it means that the Rayleigh-wave amplitude is larger than the Love-wave amplitude, and vice versa. We noted that the peak amplitudes are measured on the surface, and they decay differently with depth. Nevertheless, their amplitude ratios provide a first-order approximation of the induced stress perturbations. Thirdly, we computed the correlation coefficient (CC) between time-shifted tremor envelope functions and Love (CC-Lo) and Rayleigh (CC-Ra) waves. Ideally, if tremor is mostly triggered by certain types of surface waves, then we would expect to see a relatively high positive CC values between surface waves and tremor envelopes. Hence, we used the CC value as a measure of their correlations.

In the following subsections, we describe the observed triggered tremors and quantify their relationships to the surface waves for all nine triggering earthquakes. Figures 2.4–2.12 are presented in the order from the maximum to minimum transverse peak ground velocity (PGV) recorded at the BATS station TPUB (Figure 2.2a). In each event, we considered it as a Love or Rayleigh wave triggering case if at least 2 of 3 three aforementioned criteria is met.

2.4.1 The 2001 November 14 Mw7.8 Kunlun Earthquake

The 2001 November 14 Mw7.8 Kunlun earthquake generated the largest transverse PGV (Figure 2.2a) at the station TPUB, and has triggered microearthquakes near Beijing (Wu *et al.*, 2011) , and tremor in central California (Peng *et al.*, 2009). This event also triggered clear tremor beneath the southern CR in Taiwan (Peng and Chao, 2008), and the results are briefly summarized here. The 2–8 Hz band-pass-filtered seismograms show clear triggered tremor (Figure 2.4a) from at least two tremor sources, one near the southern CR where the majority of the triggered tremor (Figure 2.1a) and LFEs (Tang *et al.*, 2010) are located, and another is located in the northern portion of the CR (Figure 2.1a). Additional tremor bursts appeared later with the long duration surface waves until 1350 s. Tremor sources appear to be initiated by the Love wave (Figure 2.4b) and the amplitude ratio is less than 1 (R/L=0.21). Hence this event is considered as Love wave triggering (Peng and Chao, 2008) even though the tremor bursts are correlated better with the small amplitude Rayleigh wave (CC-Ra=0.36 and CC-Lo=0.03).

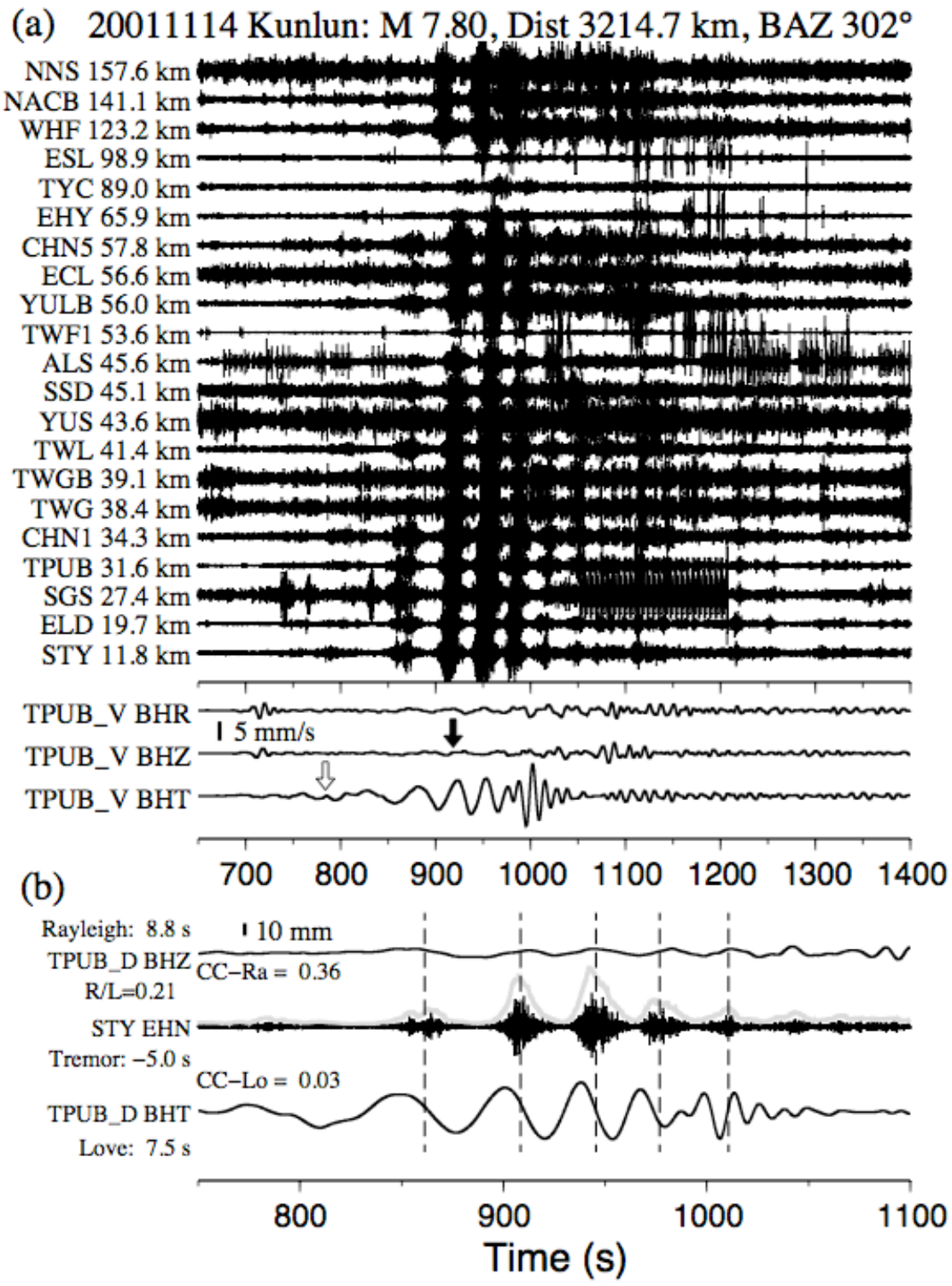

Figure 2.4 Tremor triggered by the 2001 Mw7.8 Kunlun earthquake. **(a)** The 2–8 Hz band-pass-filtered seismograms in the north (N) component showing the move-out of tremor from two source regions. The seismograms are plotted according to the best tremor location in the southern CR. The hypocentral distance between each station and

tremor source is shown next to the station name on the left side of each trace. The occurrence date (year/month/day) of the mainshock, its magnitude (M), and the epicenter distance (Dist) and back azimuth (BAZ) relative to the broadband station TPUB are shown on the top. The lower panel of (a) shows the radial (R), vertical (Z), and transverse (T) component velocity (V) seismograms recorded at station TPUB. The thick vertical bars mark the amplitude scale of surface waves. The zero time corresponds to the origin time of the mainshock. The open and black vertical arrows indicate the predicted arrivals of the Love and Rayleigh waves with the apparent velocity of 4.1 and 3.5 km/s, respectively. **(b)** A detailed comparison between the displacement (D) seismograms in Z component for Rayleigh wave and T component for Love wave at TPUB and 2–8 Hz band-pass-filtered N-component seismogram at a CWB station STY. Each seismogram has been time-shifted back to the tremor occurrence time to reflect the relationship between the surface waves and tremor at the source region. The adjusted times for Rayleigh waves, Love waves, and tremor are marked next to the station names. The maximum amplitude ratio of Rayleigh/Love (R/L) waves is measured during the tremor occurrence time. The vertical dotted lines mark the peaks of tremor envelope functions. The correlation coefficient (CC) between time-shifted tremor envelope functions and Love (CC-Lo) and Rayleigh (CC-Ra) waves are shown by each seismogram. The time windows used to compute the CC values (Table S2.3) generally started around the predicted arrivals and centered around the peaks of the Love and Rayleigh waves.

2.4.2 The 2008 May 12 Mw7.9 Wenchuan Earthquake

The 2008 May 12 Mw7.9 Wenchuan earthquake generated the second largest PGV (Figure 2.2a) in transverse components at the station TPUB, and has the closest epicentral distance of about 1900 km to TPUB among all 45 teleseismic earthquakes. This event also triggered widespread microearthquakes in continental China (Jiang *et al.*, 2010; Peng *et al.*, 2010b), tremor in southwest Japan (Miyazawa *et al.*, 2008), Cascadia (Gomberg, 2010), and central California (Peng *et al.*, 2009). Interestingly, this event only triggered tremor signals (Figure 2.5a) that are barely above the background noise levels during the mainshock coda between 600 s and 850 s near the southern CR in Taiwan. After shifting both the tremor and the surface waves back to the tremor source region, we find that tremor did not occur during the first few cycles of Love wave starting at ~600 s (Figure

2.5b), but are modulated by the following Rayleigh waves (~680 s). Also the tremor and Rayleigh wave is correlated better (CC-Ra=0.50 and CC-Lo=0.20), thus we classified this event is triggered by Rayleigh waves.

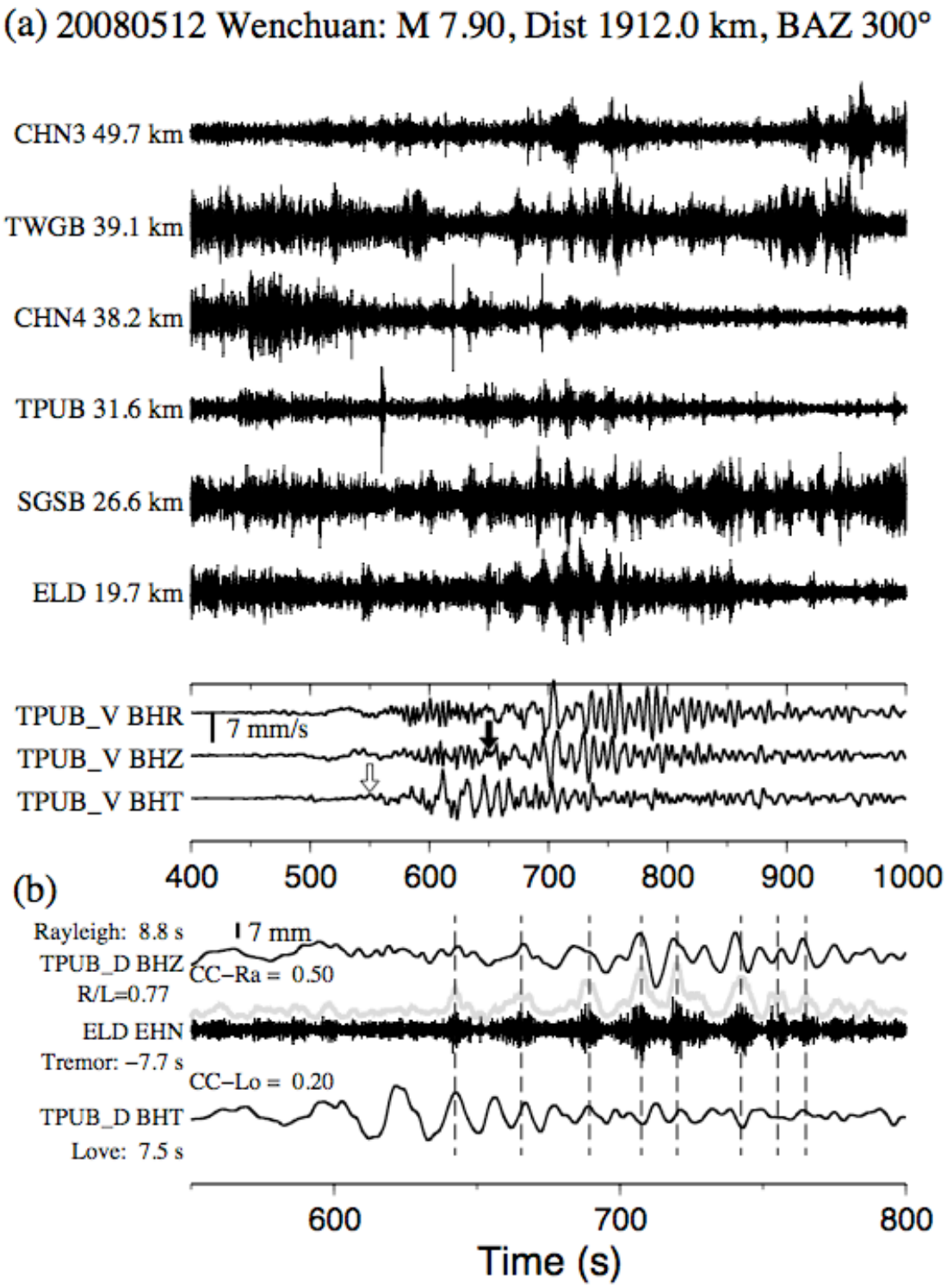

Figure 2.5 Tremor triggered by the 2008 Mw7.9 Wenchuan earthquake. **(a)** The 2–8 Hz band-pass-filtered N-component seismograms showing move-out of triggered tremor during the passing surface waves between 600 and 850 s. **(b)** A detailed comparison

between the displacement seismograms at TPUB and band-pass-filtered seismogram at CWB station ELD. Other notations are the same as in Figure 2.4.

2.4.3 The 2004 December 26 Mw9.0 2004 Sumatra Earthquake

The 2004 December 26 Mw9.0 Sumatra earthquake has the largest magnitude among all the analyzed events and generated the third largest transverse PGV (Figure 2.2a) among all nine triggering events in Taiwan. This event also triggered tremor in central California (Ghosh *et al.*, 2009; Peng *et al.*, 2009), Cascadia (Rubinstein *et al.*, 2009), and southern Japan (Miyazawa and Mori, 2006; Miyazawa and Brodsky, 2008), and microearthquakes near Beijing, China (Wu *et al.*, 2011) and Alaska (West *et al.*, 2005). The 2004 Sumatra earthquake generated clear multiple tremor sources in both southern and northern CR in Taiwan (Figure 2.6a). Some tremor bursts started to appear at 950 s and the large-amplitude tremor bursts occurred between 1150 s and 1450 s. Small tremor bursts appeared until 1600 s. The tremor bursts show better correlation with larger amplitude of Rayleigh waves (R/L=1.28, CC-Ra=0.23, and CC-Lo=–0.44) (Figure 2.6b). Hence, we consider this as a case of Rayleigh wave triggering.

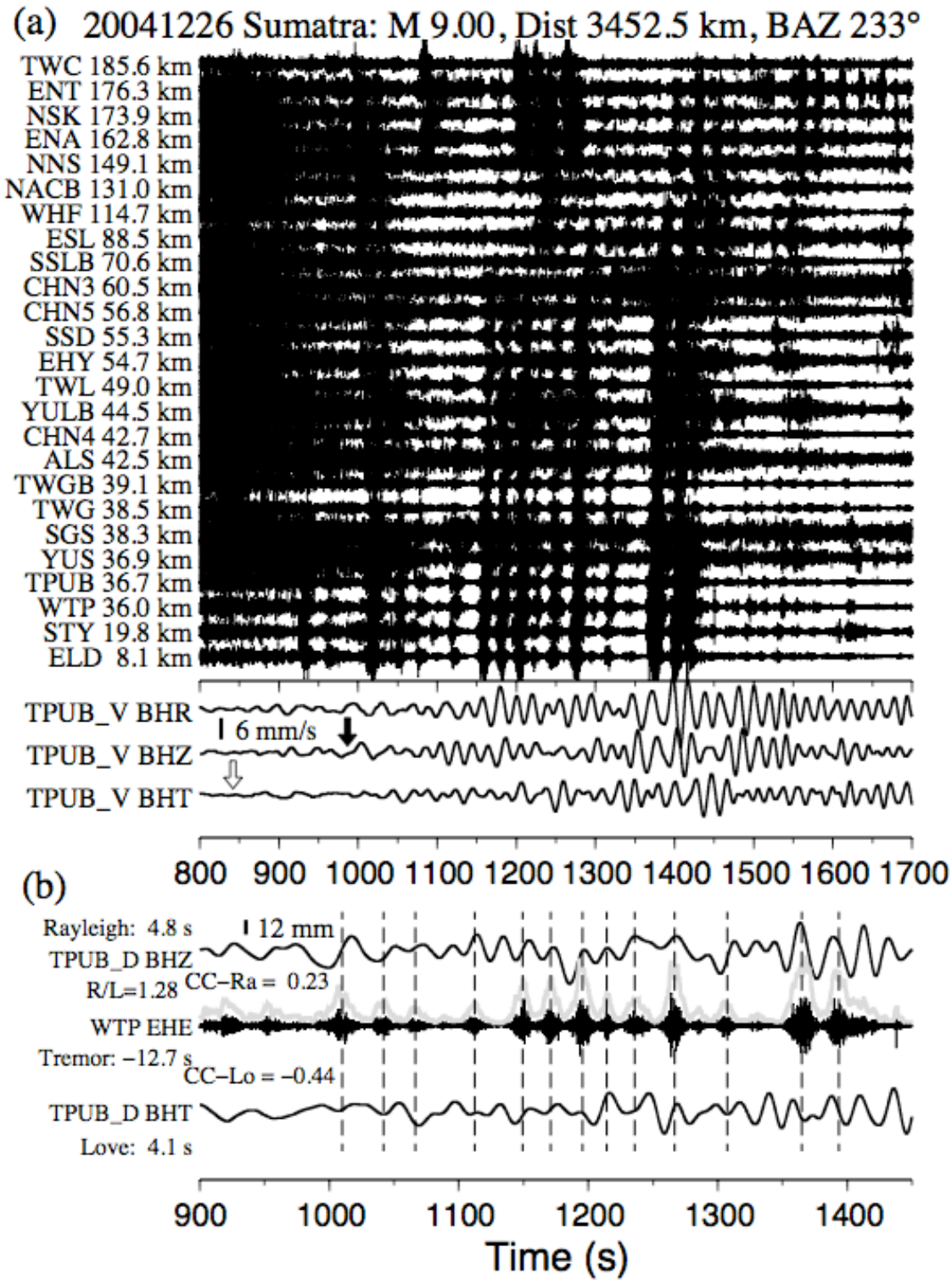

Figure 2.6 Tremor triggered by the 2004 Mw9.0 Sumatra earthquake. **(a)** The 2–8 Hz band-pass-filtered E-component seismograms showing move-out of tremor from multiple source regions. **(b)** A detailed comparison between the displacement seismograms at

TPUB and band-pass-filtered seismogram at WTP. Other notations are the same as in Figure 2.4.

2.4.4 The 2003 September 25 Mw8.3 Tokachi-Oki Earthquake

The 2003 September 25 Mw8.3 Tokachi-Oki earthquake in Japan has the fourth largest transverse PGV (Figure 2.2a). This event triggered shallow microearthquakes near Beijing (Wu *et al.*, 2011), tremor in southwest Japan (Miyazawa and Mori, 2005; Miyazawa *et al.*, 2008), central California (Peng *et al.*, 2009), and multiple tremor sources in Taiwan (Figure 2.7a). Tremors triggered by this event are shown between 750 and 1200 s (Figure 2.7a). Due to lack of continuous CWBSN data during this time, we only used data from BATS and CWBBB networks to analyze this event. After shifting time back to the tremor source region, we found that the first tremor burst in the southern portion occurred at ~780 s after the first arrival of Love waves (Figure 2.7b). On the other hand, the tremor peaks corresponded well with the peaks of Rayleigh waves (Figure 2.7b, CC-Ra=0.39 and CC-Lo=–0.24), hence this event is considered as triggered by Rayleigh waves.

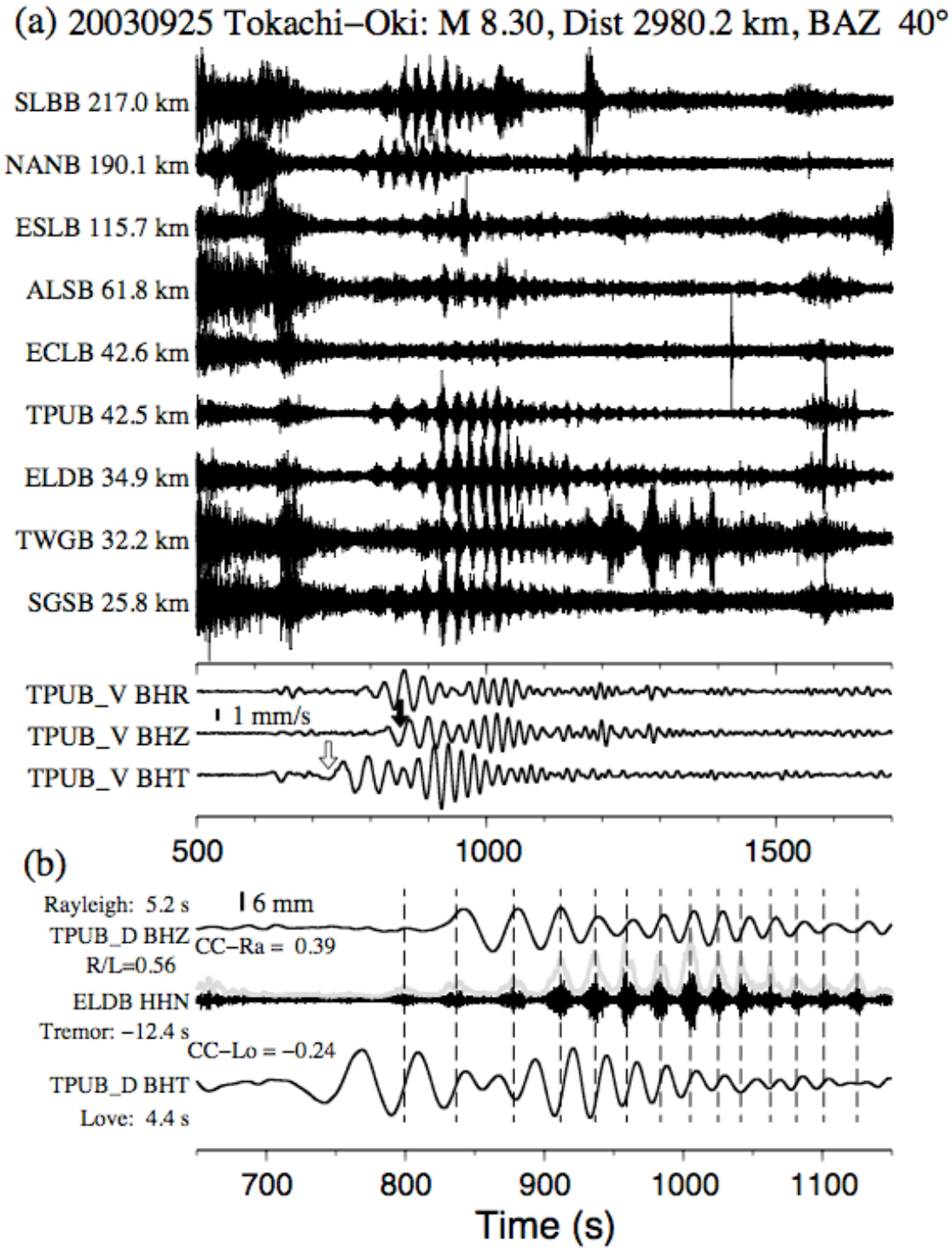

Figure 2.7 Tremor triggered by the 2003 Mw8.3 Tokachi-Oki earthquake. **(a)** The 2–8 Hz band-pass-filtered N-component seismograms showing move-out of tremor from multiple source regions. **(b)** A detailed comparison between the displacement seismograms at TPUB and band-pass-filtered seismogram at ELDB. Other notations are the same as in Figure 2.4.

2.4.5 The 2005 March 28 Mw8.6 Nias Earthquake

The 2005 March 28 Mw8.6 Nias earthquake in Sumatra, Indonesia has the second largest magnitude and has the 5th largest transverse PGV among all nine triggering earthquakes. This event generated a single tremor source in the southern CR. The clear tremor bursts were shown between 950 s and 1300 s (Figure 2.8a), and the long duration tremor bursts were continuously shown up until 2200 s. The large-amplitude signals recorded at around 1400 s, 1750 s, and 2150 s possibly came from three local earthquakes (marked by vertical gray arrows in Figure 2.8a) with M2.3 near Chiayi City (120.37^{o}E, 23.53^{o}N, and 9 km in depth), M2.7 at about 40 km north of Hualien City (121.73^{o}E, 24.25^{o}N, and 13 km in depth), and M2.2 at about 37 km north of Hualien City (121.72^{o}E, 24.25^{o}N, and 12 km in depth), respectively. After adjusting the times of tremor and surface waves, the comparison indicates that the tremors were more likely associated with Rayleigh waves (Figure 2.8b, R/L=2.53, CC-Ra=0.48, and CC-Lo=0.39). Again, we consider this as a Rayleigh wave triggering case.

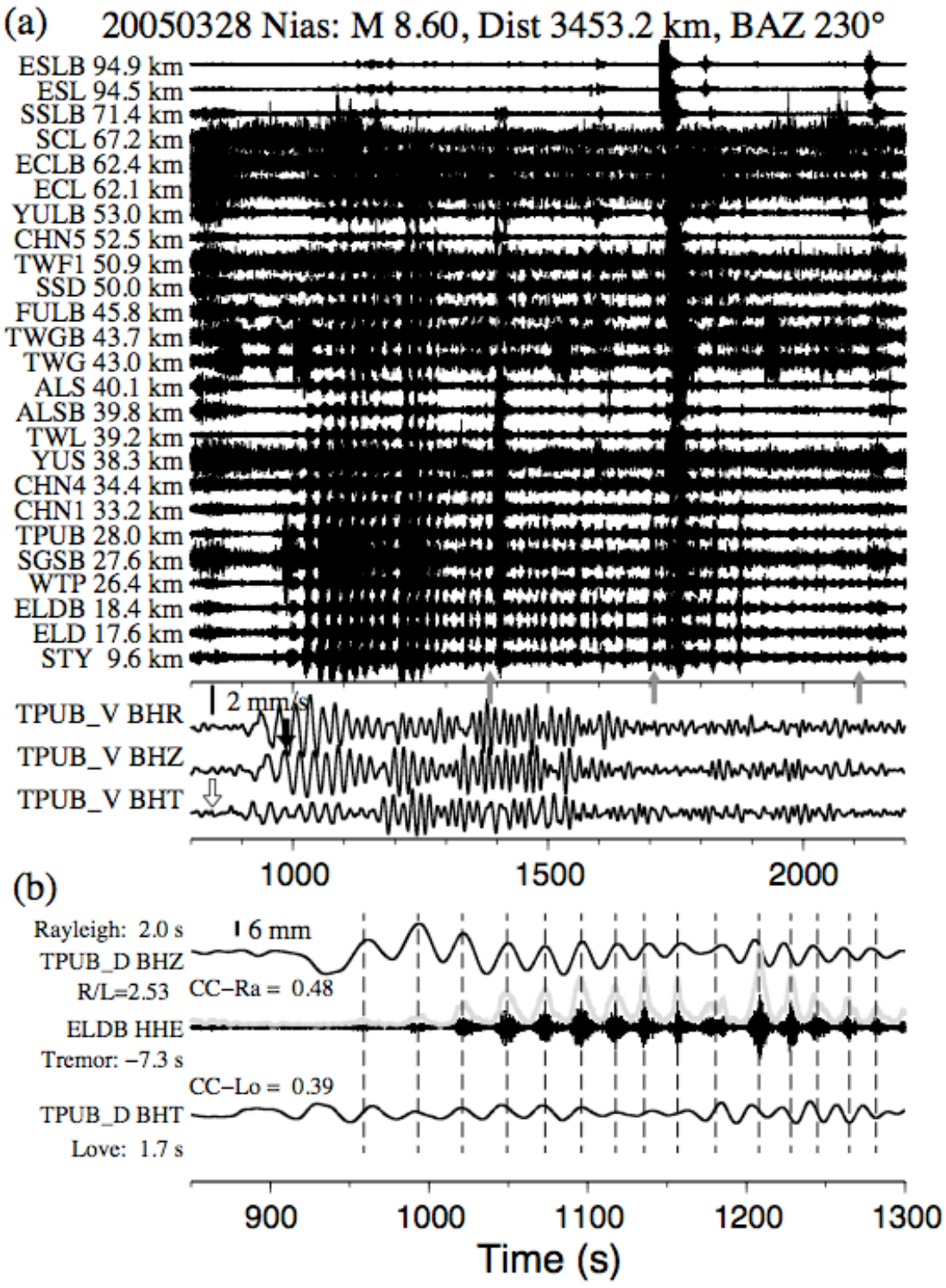

Figure 2.8. Tremor triggered by the 2005 Mw8.6 Nias earthquake. **(a)** The 2–8 Hz band-pass-filtered E-component seismograms showing move-out of tremor from the southern CR. The vertical gray arrows mark the origin times of local earthquakes from the CWB

catalog. **(b)** A detailed comparison between the displacement seismograms at TPUB and band-pass-filtered seismogram at ELDB. Other notations are the same as in Figure 2.4.

2.4.6 The 1998 November 29 Mw7.7 Ceram-Sea Earthquake

The 1998 November 29 Mw7.7 Ceram-Sea earthquake has the smallest magnitude among all the 9 tremor triggering events and has the second closest epicentral distance of about 2800 km to TPUB. This event generated triggered tremors in the south of the CR shown between 850 and 1000 s (Figure 2.9a). The tremor bursts were barely above the background noise level, and mostly occurred during the Rayleigh waves (Figure 2.9b, R/L=1.54, CC-Ra=0.28, and CC-Lo=–0.07).

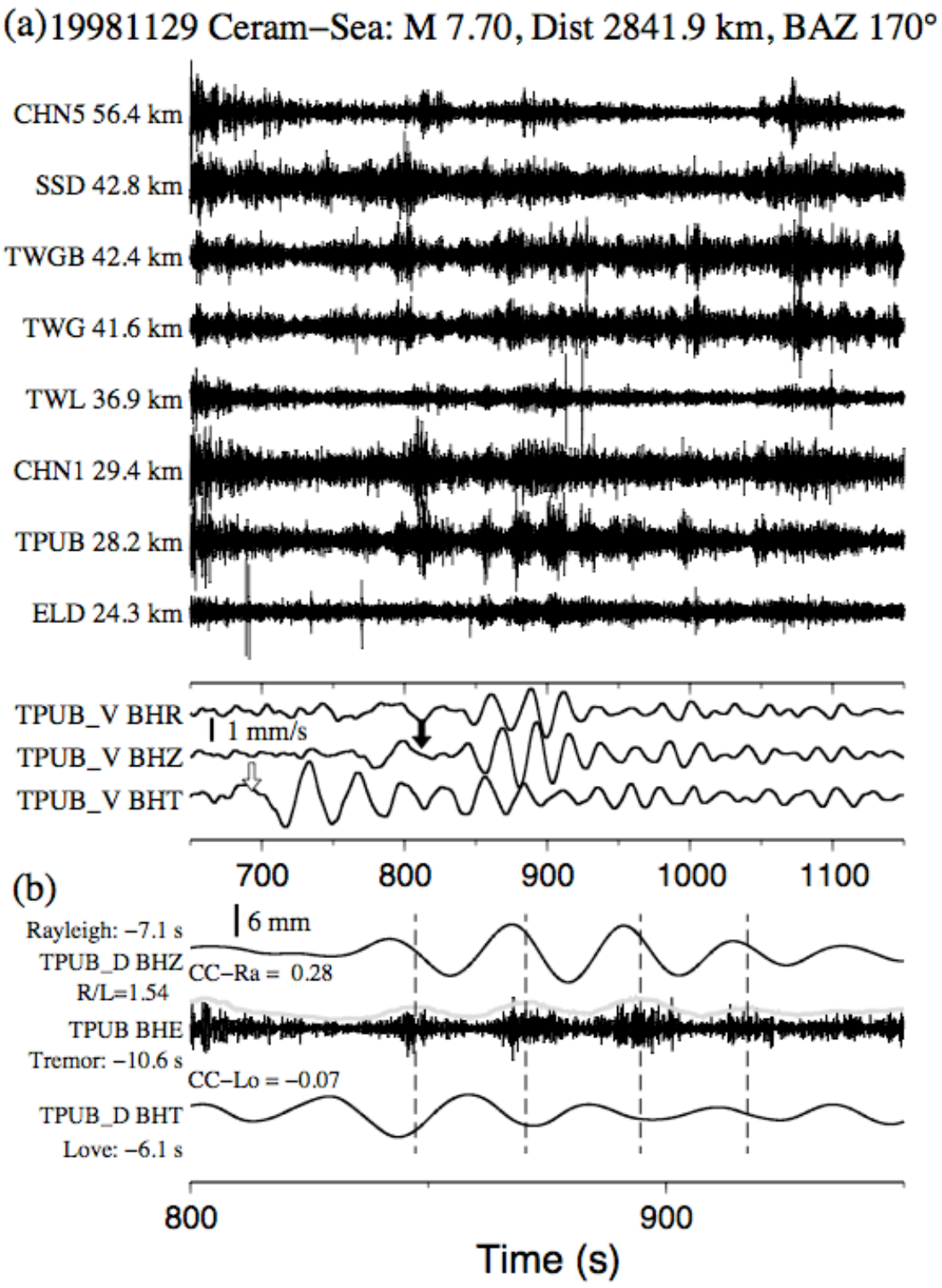

Figure 2.9 Tremor triggered by the 1998 Mw7.7 Ceram-Sea earthquake. **(a)** The 2–8 Hz band-pass-filtered seismograms in the E-component showing the move-out of tremor from the southern CR. **(b)** A detailed comparison between the displacement seismograms

and band-pass-filtered seismogram recorded at TPUB. Other notations are the same as in Figure 2.4.

2.4.7 The 2007 September 12 Mw8.4 Sumatra Earthquake

The 2007 September 12 Mw8.4 Sumatra earthquake has one of the smallest transverse PGV (Figure 2.2a) and generated two clear tremor sources in both southern and northern CR (Figure 2.1a). The clear tremor bursts from the southern CR occurred between 1000 s and 1900 s during the passing surface waves (Figure 2.10a). Tremors around the northern CR occurred during 1100 s to 1500 s and were recorded by three stations TIPB, ENT, and NANB. Based on the comparison between surface waves and tremor bursts in Figure 2.10b, the tremor sources from the south of the CR were mainly associated with the Rayleigh waves (R/L=2.37, CC-Ra=0.35, and CC-Lo=0.04).

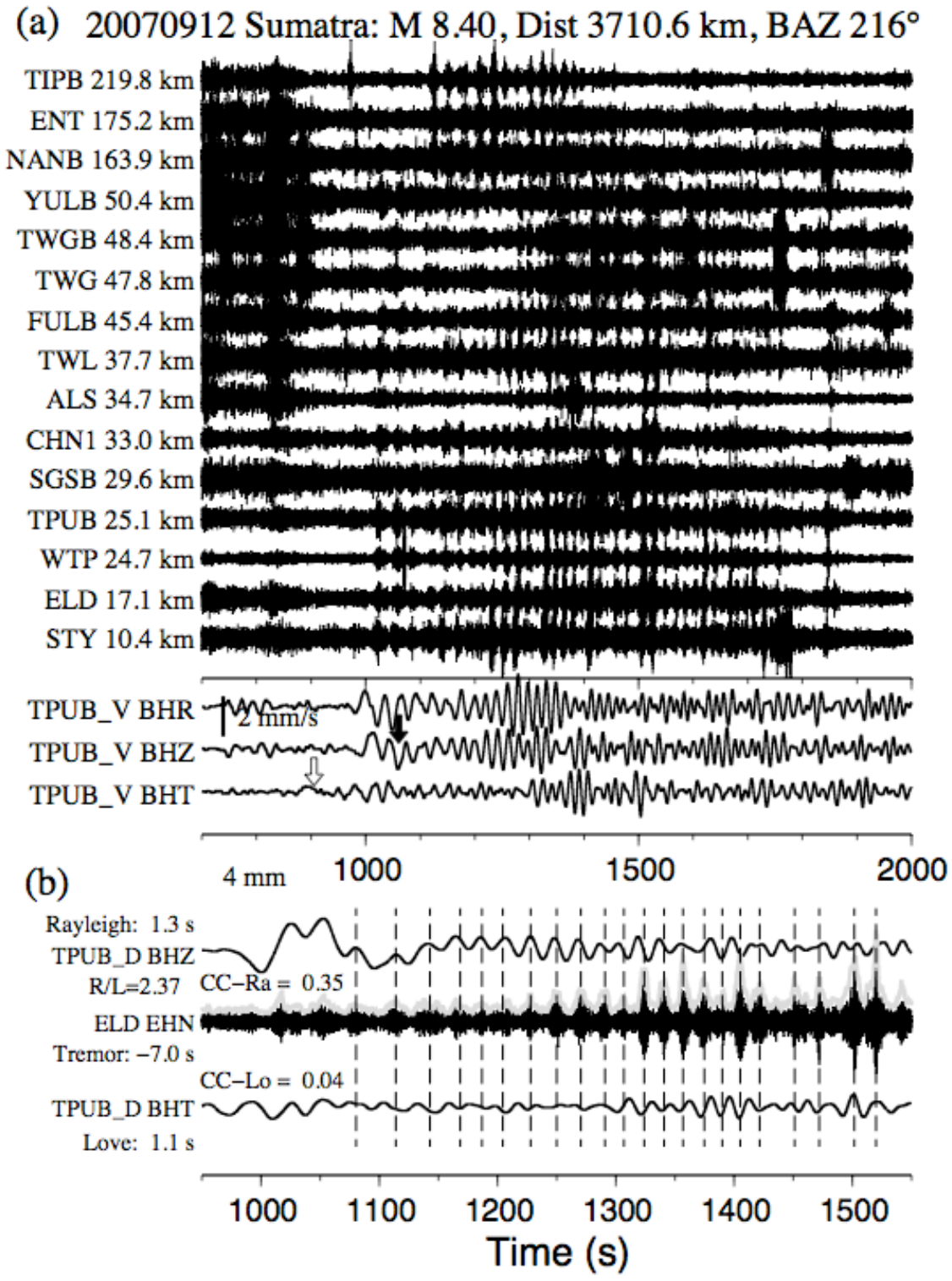

Figure 2.10 Tremor triggered by the 2007 Mw8.4 Sumatra earthquake. **(a)** The 2–8 Hz band-pass-filtered seismograms in the N-component showing the move-out of tremor from the multiple sources. **(b)** A detailed comparison between the displacement

seismograms at TPUB and band-pass-filtered seismogram at ELD. Other notations are the same as in Figure 2.4.

2.4.8 The 2007 January 13 Mw8.1 Kuril-Island Earthquake

The 2007 January 13 Mw8.1 Kuril-Island earthquake in Japan has one of the smallest transverse PGV (Figure 2.2a) among all nine triggering earthquakes. This earthquake and the previous Mw8.3 Kuril-Island earthquake occurred on 2006 November 15 both triggered tremors in central California (Peng *et al.*, 2009). In Taiwan, although the measured transverse PGVs for both events are very close (Figure 2.2a), only the 2007 Kuril-Island event show clear triggered tremor signals in the southern CR. The tremor bursts started at 1100 s and continuously appeared until 2100 s (Figure 2.11a). The impulsive signals recorded at around 2100 s came from a local earthquake (marked by vertical gray arrow in Figure 2.11a) with M3.0 located at the Pacific Ocean around 90 km outside the Hualien City (122.47^{o}E, 24.15^{o}N, and 45 km in depth). After adjusting the occurrence time of surface waves and tremors back to the tremor sources, we found that tremor started during the Rayleigh waves. In addition, the tremor bursts correlated better with Rayleigh wave (CC-Ra=0.23 and CC-Lo=0.11). Hence we also consider this is triggered by Rayleigh waves.

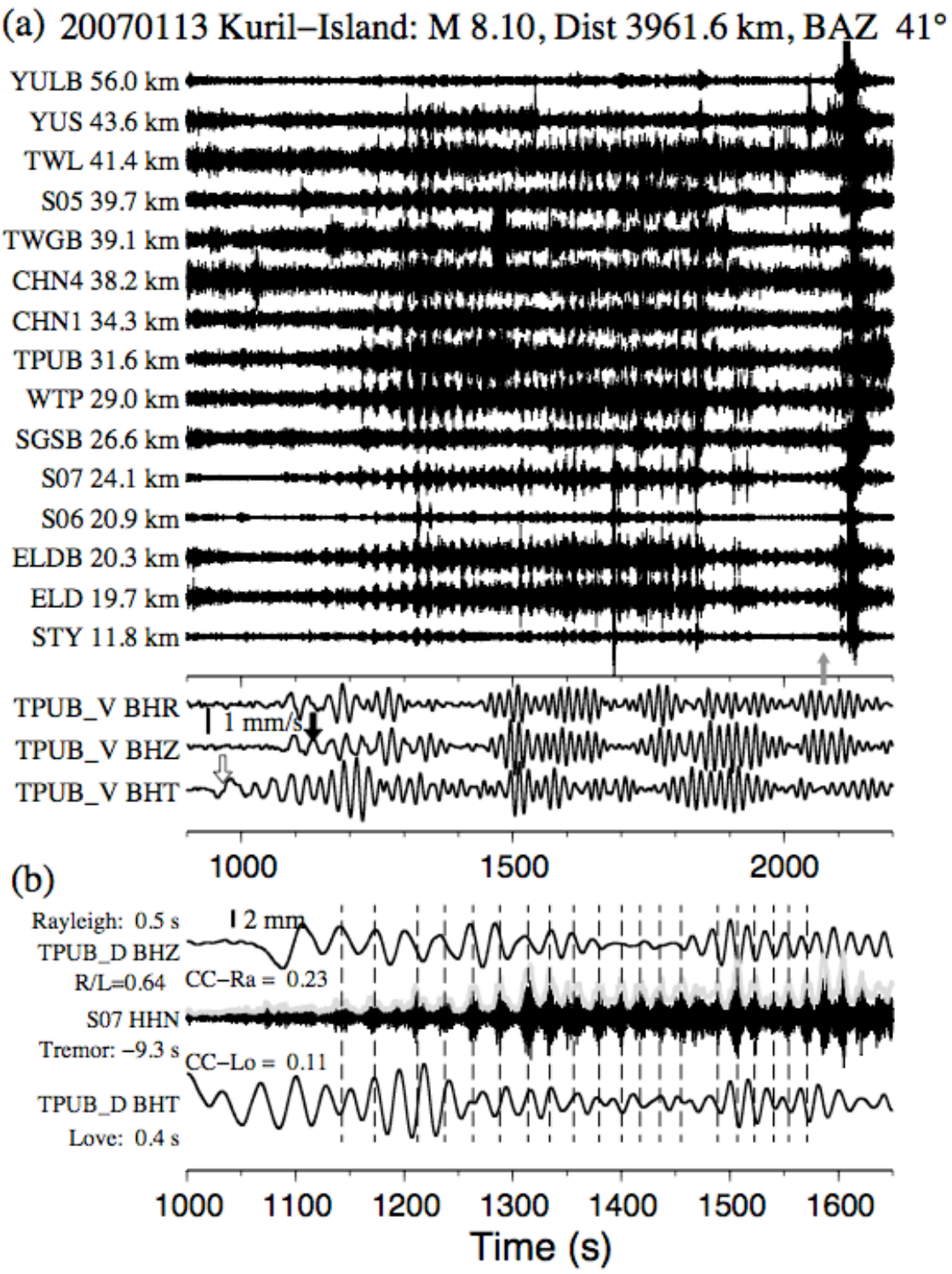

Figure 2.11 Tremor triggered by the 2007 Mw8.1 Kuril-Island earthquake. **(a)** The 2–8 Hz band-pass-filtered seismograms in the N-component showing the move-out of tremor from the southern CR. The vertical gray arrow marks the origin time of a local earthquake from the CWB catalog. **(b)** A detailed comparison between the displacement

seismograms at TPUB and band-pass-filtered seismogram at TAIGER station TGS07. Other notations are the same as in Figure 2.4.

2.4.9 The 2007 April 1 Mw8.1 Solomon Islands Earthquake

The 2007 April 1 Mw8.1 Solomon Islands earthquake has the least transverse and vertical PGV (~0.1 cm s^{-1}) at TPUB (Figure 2.2). This event also generated triggered tremors in the southwest Japan (Miyazawa *et al.*, 2008). In Taiwan, this event triggered multiple tremor sources with low SNR between 1350 s and 1450 s (Figure 2.12). The tremor source around the southern CR was located further to the southeast as compared with other tremor sources (Figure 2.1). Another tremor source located in the north (Figure 2.1a) was recorded at stations with epicentral distance greater than 100 km. After adjusting time back to the tremor source region in the southern CR, we found that the tremor bursts occurred far after the arrival of Love waves (at ~1250 s). Also the tremor bursts correlate better with larger amplitude of Rayleigh waves (R/L=1.89, CC-Ra=0.23, and CC-Lo=0.13), hence we considered this is triggered by Rayleigh waves.

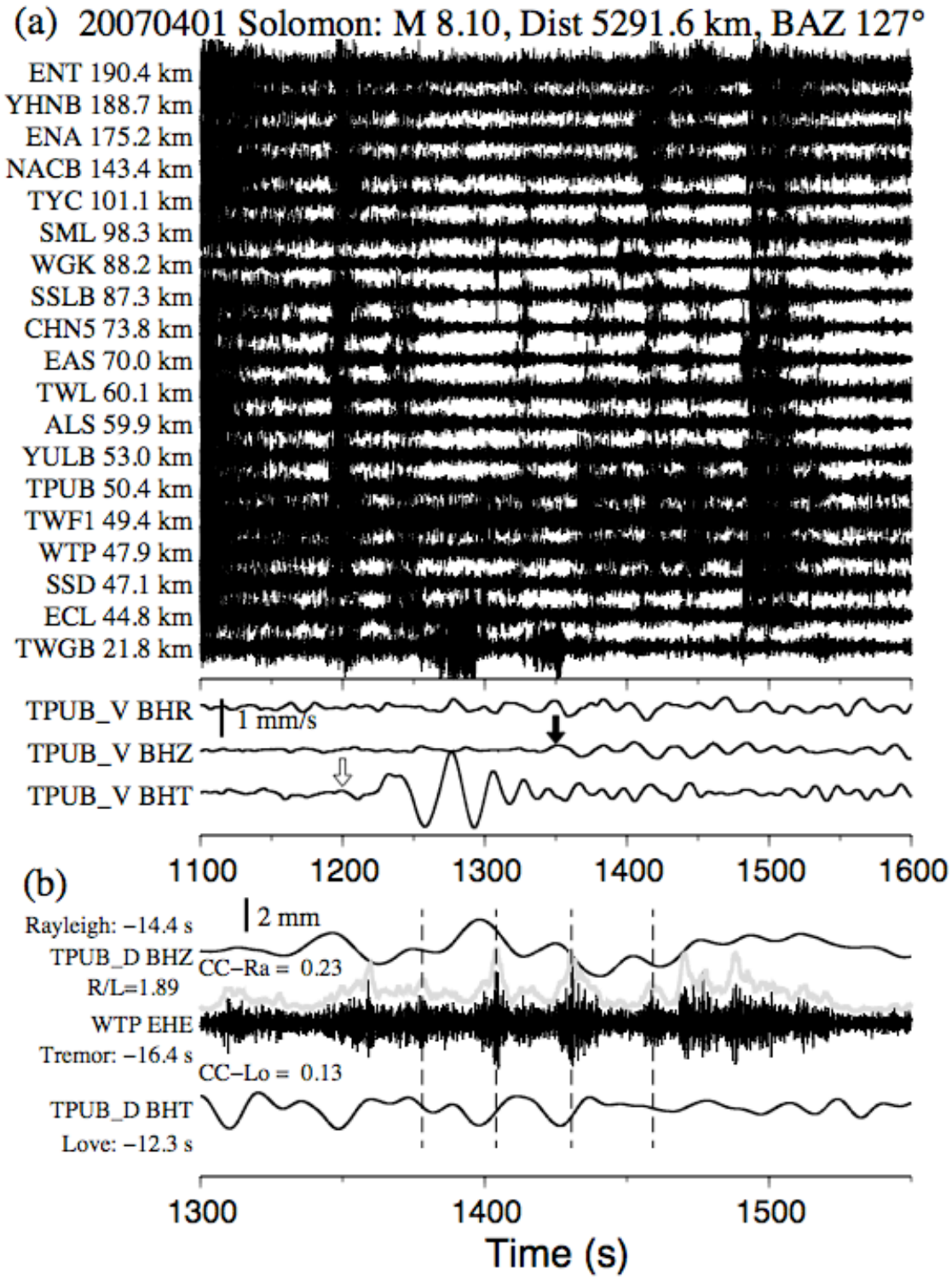

Figure 2.12 Tremor triggered by the 2007 Mw8.1 Solomon earthquake. **(a)** The 2–8 Hz band-pass-filtered seismograms in E-component showing the move-out of tremor from the southern CR. **(b)** A detailed comparison between the displacement seismograms at

TPUB and band-pass-filtered seismogram at WTP. Other notations are the same as in Figure 2.4.

2.4.10 The 2000 June 4 Mw7.9 Sumatra Earthquake

The 2000 June 4 Mw7.9 Sumatra earthquake has one of the smallest transverse and vertical PGV by comparing with the other 9 triggering events (Figure 2.2). We found clear tremor bursts consistent with the cycles of Rayleigh waves between 1000 and 1400 s (Figure 2.13) at TPUB station of BATS. However, due to the lack of continuous CWBSN data during this time to further confirm and locate the tremor, we considered this as a case of possible triggered tremor. The impulsive signal recorded at around 640 s came from a local earthquake with magnitude 2.8 located at the Pacific Ocean around 30 km southeast of the Yilan City (121.97^{o}E, 24.38^{o}N, and 28 km in depth). The double peaks at around 900 s during the large-amplitude Love waves likely correspond to a regional earthquake (with *S*-*P* time of ~15 s) because no local earthquakes are listed in the CWB catalog during this time period.

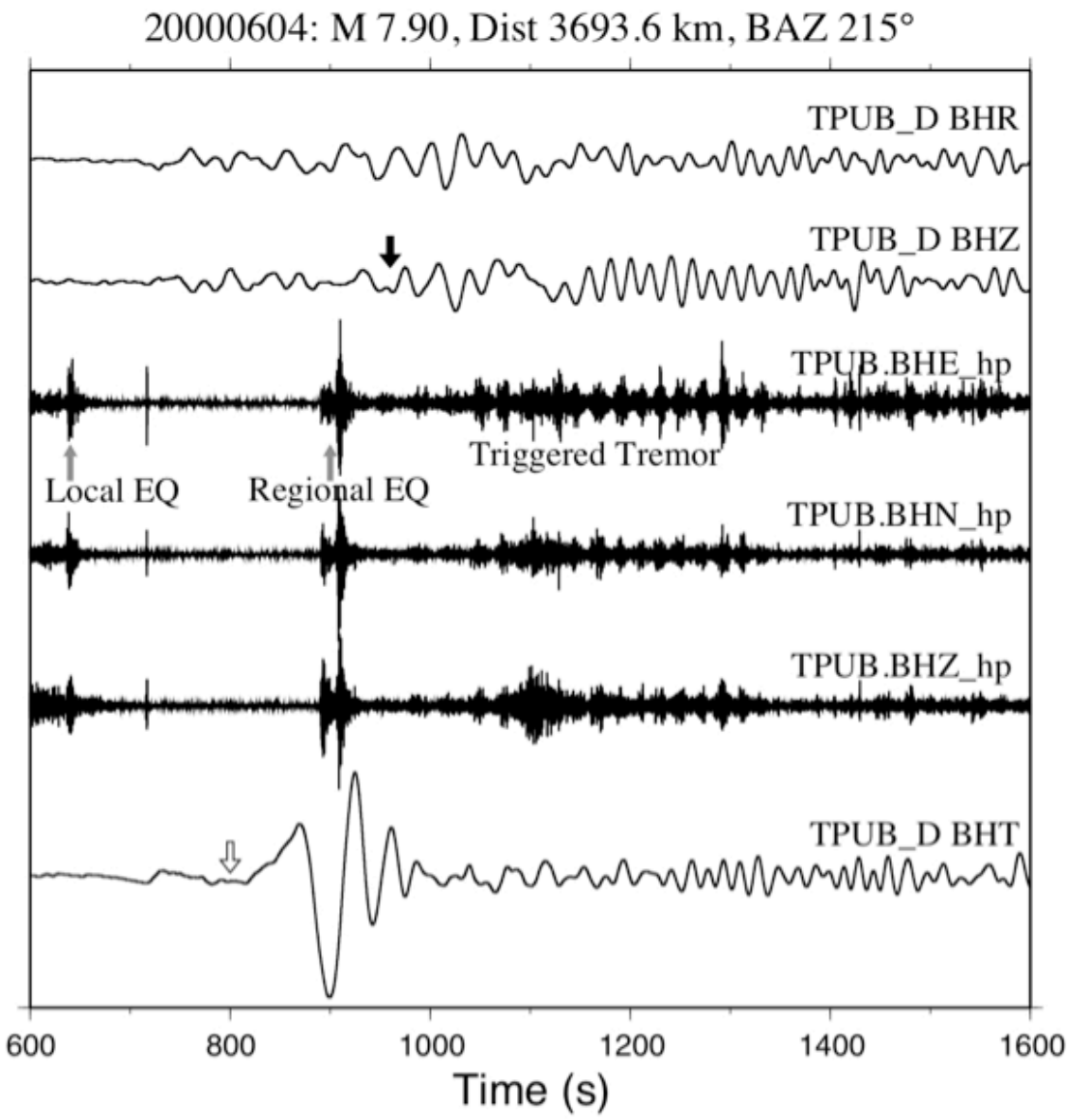

Figure 2.13 A comparison between the broadband displacement seismograms and 5 Hz high-pass-filtered seismograms at station TPUB showing possible tremor triggered by the 2000 Mw7.9 Sumatra earthquake. The open and black vertical arrows mark the approximate arrivals of the Love and Rayleigh waves. The gray arrows mark the origin times of local and regional earthquakes.

2.5 Triggering Potential

As briefly mentioned before, previous studies have suggested that the PGV of the teleseismic surface wave is one of the most important factors in controlling the potential of triggering tremor (Peng *et al.*, 2009; Rubinstein *et al.*, 2009). However, it is still not clear whether triggering potential also depends on frequency (Brodsky and Prejean, 2005; Guilhem *et al.*, 2010; Peng *et al.*, 2009; Rubinstein *et al.*, 2009), incidence angle (Hill, 2008; Hill, 2010; Rubinstein *et al.*, 2009), background tremor rate (Rubinstein *et al.*, 2009), background noise (Gomberg, 2010), or other factors. In this section, we quantified the triggering threshold in terms of the amplitude (PGV), incidence angle, and frequency of the distant surface waves. In addition, we also evaluated the relationship between the amplitudes of the triggering waves and triggered tremors and use them to test the "clock-advance" model for earthquake triggering (Gomberg, 2010) and the role of background noise level on the triggering threshold.

2.5.1 Amplitude (PGV)

Figure 2 shows the PGV and the corresponding peak dynamics stress σ_d measured from the transverse (Figure 2.2a) and vertical (Figure 2.2b) components for all 45 teleseismic earthquakes. To calculate the corresponding dynamic stress s_d, we used the equation $\sigma_d = G\dot{u}/v_s$ (Jaeger and Cook, 1979), where G is the shear modulus, $\dot{u}$ is the PGV, and v_s is the phase velocity. For all nine triggering earthquakes, the measured transverse PGV ranges from 0.10 cm s^{-1} to the 0.835 cm s^{-1}, which corresponds to the peak dynamic stress of 7.8 to 61.1 KPa, if we use a nominal shear modulus of 30 GPa and a constant Rayleigh waves velocity of 3.5 km s^{-1} (Miyazawa and Brodsky, 2008).

The PGV of 0.1 cm s^{-1} appears to separate most of triggering and non-triggering earthquakes in both transverse and vertical components, which corresponds to an apparent tremor-triggering threshold 7–8 KPa. It is worth noting that some events with the transverse PGVs (Figure 2.2a) just above (the 2005 October 8 Mw7.6 Pakistan) or below (the 2006 November 15 Mw8.3 Kuril-Island earthquake) the aforementioned threshold did not trigger tremor, while one event (the 2000 June 4 Mw7.9 Sumatra earthquake) just below the threshold is considered as possible triggered tremor. For the vertical component (Figure 2.2b), the 2007 Mw8.1 Solomon event with relative low PGV (0.03 cm s^{-1} or 2.4 KPa) below the inferred 0.1 cm s^{-1}, still trigger tremor. Nonetheless, we suggest that while the PGV is one of the most important parameters in controlling the trigger thresholds.

2.5.2 Incidence Angle

To examine the triggering potential of surface waves coming from different angles, we modeled the dynamic stress caused by the passage of Love and Rayleigh waves with an arbitrary incidence angle on critically-stressed faults (Figure 2.14) under the Coulomb failure criteria (Gonzalez-Huizar and Velasco, 2011; Hill, 2010; Wu *et al.*, 2011), and then compared the modeling results with our observations. The triggering potential is controlled by the Coulomb failure function that depends on fault types, orientations, incident angles, and types of surface waves.

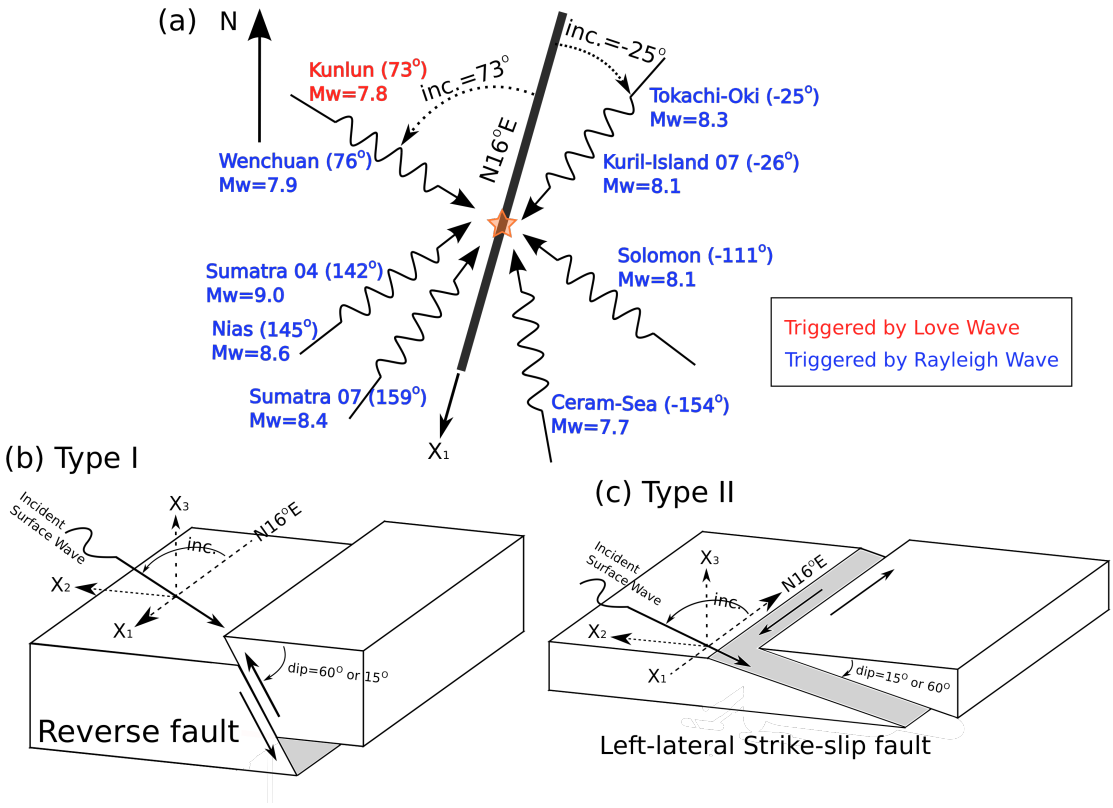

Figure 2.14 Schematic diagram showing multiple tremor source models. **(a)** A map view of the strike of the CR (N16°E), and the incident angles of the nine tremor triggering earthquakes. The events that show triggering with the Love and Rayleigh types of waves are marked in red and blue colors, respectively. **(b)** Type I: A reverse fault model with high or low (60° or 15°) dipping angles. **(c)** Type II: A low-angle oblique-slip fault plane model with high or low dipping angles.

The modeling procedure generally follows Wu *et al.* (2011) and is briefly described here. We assume tremor was triggered at an average depth of 20 km (Figure 2.1b) by the surface waves with 20-s periods. Based on the fault models and slip directions from our previous studies (Peng and Chao, 2008; Tang *et al.*, 2010), we tested four fault-plane models in different fault types and dipping angles: (1) the high-angle (dip=60°) reverse (Figure 2.14b and 2.15a) and low-angle (dip=15°) reverse (Figure 2.14b and 2.15b) fault models that are parallel to the CR (i.e. strike=N16°E) (Suppe, 1981), and (2) the high-angle left-lateral (LL) strike-slip (Figure 2.14c and 2.15c) and low-angle LL strike-slip

(Figure 2.14c and 2.15d) models. The triggering potentials for the Love and Rayleigh waves have been normalized assuming comparable displacement amplitudes at the surface for both types of surface waves. Note that the incidence angle in Figure 2.15 is defined as counterclockwise (Hill, 2010; Wu *et al.*, 2011) from the strike of the CR (Figure 2.14a), and is different from the definition of back azimuth in Figure 2.2.

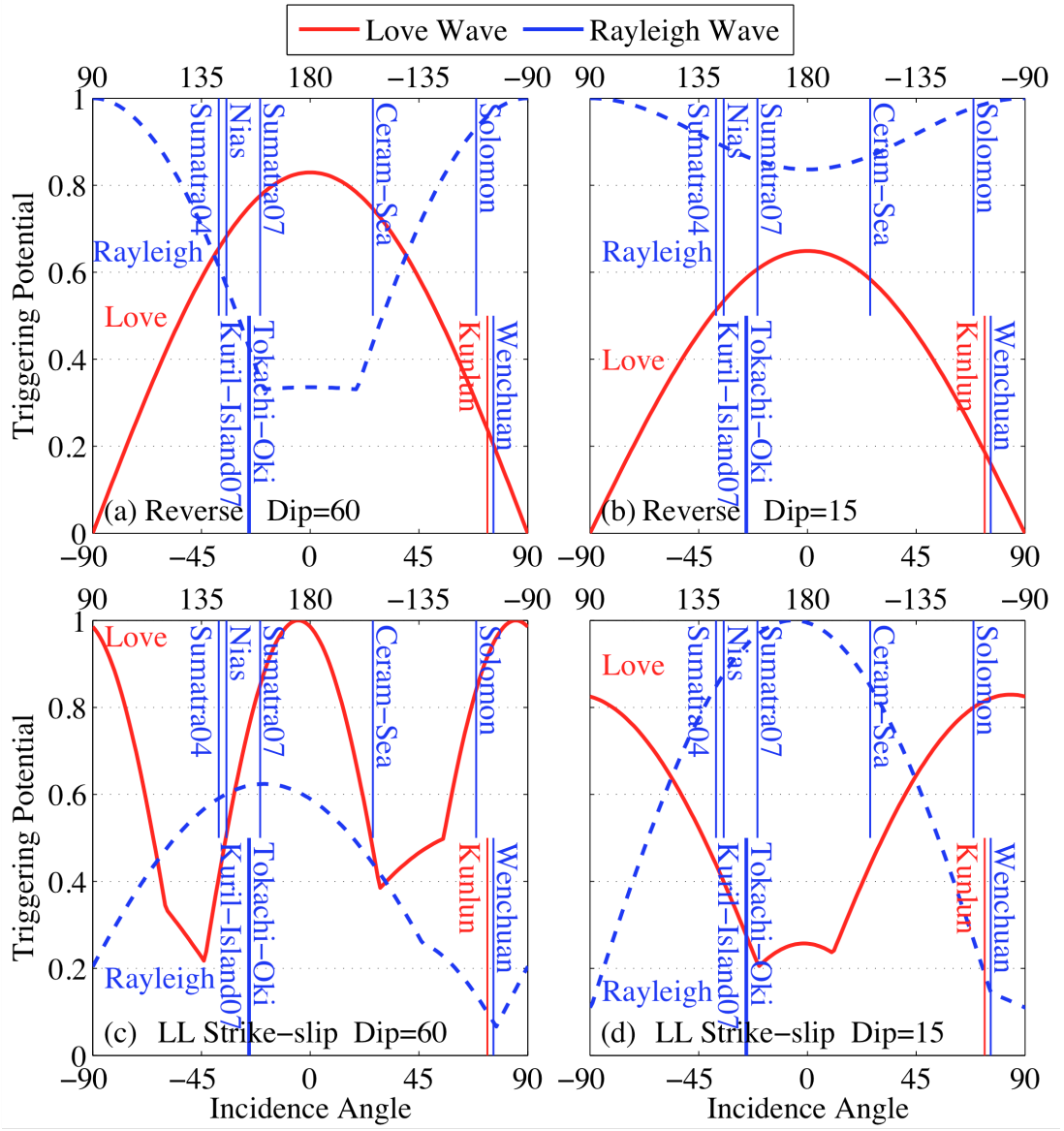

Figure 2.15 (a)–(b) Triggering potential of the reverse fault model dipping at 60° and 15° (Figure 2.14b). **(c)–(d)** Triggering potential of the left-lateral (LL) strike-slip fault

model dipping at 60° and 15° (Figure 2.14c). The triggering potentials of the Love (red solid line) and Rayleigh (blue dashed line) waves are calculated with 20-s period surface waves at a depth of 20 km assuming the coefficient of friction μ=0.2 and comparable displacement amplitudes at the surface for both Love and Rayleigh waves. The vertical solid lines mark the incidence angle of the 9 triggering earthquakes. The red and blue colors mark the events that show triggering with the Love and Rayleigh waves, respectively.

Here we compared the triggering potential between the four models (Figure 2.15) and the observations. The observations are based on the comparison between the tremor bursts and displacement seismograms (panel b of Figures 2.4–2.12) and are also summarized in Figure 2.14a. In general, the triggering potential of the models shown in Figure 2.15a–c are not consistent with the observations. For instance, both high-angle dip-slip models in Figure 2.15a and 2.15c suggest that Love waves (red solid line) have higher triggering potential in fault-parallel direction (around 0 and 180 degrees), which is opposite to the observations (i.e. the 1998 Ceram-Sea, 2003 Tokachi-Oki, 2004 Sumatra, 2005 Nias, 2007 Kuril-Island, and 2007 Sumatra earthquakes show predominate Rayleigh wave triggering). In fault-normal direction (around 90 and –90 degrees), the model of Figure 2.15c is consistent with the Love wave triggering of the 2001 Kunlun earthquake, but not for the same case shown in Figure 2.15a. As for the model with low-angle reverse faulting (Figure 2.15b), the Rayleigh wave (blue dashed line) has highest triggering potential for all incidence angles, which is not consistent with the observations.

On the other hand, the model of Figure 2.15d (LL faulting on the low-angle fault) has 77.8% (7 out of 9) of triggering earthquakes that are consistent with the observations. In detail, 1 out of 3 of earthquakes in fault-normal direction show Love wave triggering (i.e. the 2001 Kunlun earthquake in red color). In fault-parallel direction, all 6 events are

triggered by Rayleigh wave. However, not all triggering events are consistent with this model prediction. For example, the 2007 Solomon and 2008 Wenchuan earthquakes correlate better with Rayleigh waves. We additionally tested different dipping angles of this model and found similar triggering potential within 15 and 45 degrees. Hence, we suggest that the low to median dipping angle of LL strike-slip fault model (Figure 2.14c and 2.15d) better explains the observations.

2.5.3 Frequency

In this section we quantified the triggering threshold in terms of frequency by computing the amplitude spectra of surface waves for all 45 teleseismic earthquakes recorded at TPUB. The analysis procedure generally follows that of Peng *et al*. (2009) and is briefly described here. We first cut the instrument-corrected velocity seismograms within the apparent velocity of 5 to 2 km/s to include most of the surface waves. Next, we compute the corresponding spectra for both the transverse and vertical components and smooth the resulting spectra with a sliding window of 10 points. Figure 2.16 shows the velocity spectra for the 9 triggering (color lines), 1 possibly triggering (black line) and 35 non-triggering (gray lines) earthquakes in the transverse (a) and vertical (b) components. The surface wave spectra of these triggering earthquakes are mainly peaked in the frequency range from 10 to 50 s (0.02–0.1 Hz), and appear to be on the top of those non-triggering earthquakes, although there is no clear separation between these triggering and non-triggering groups (Peng *et al.*, 2009).

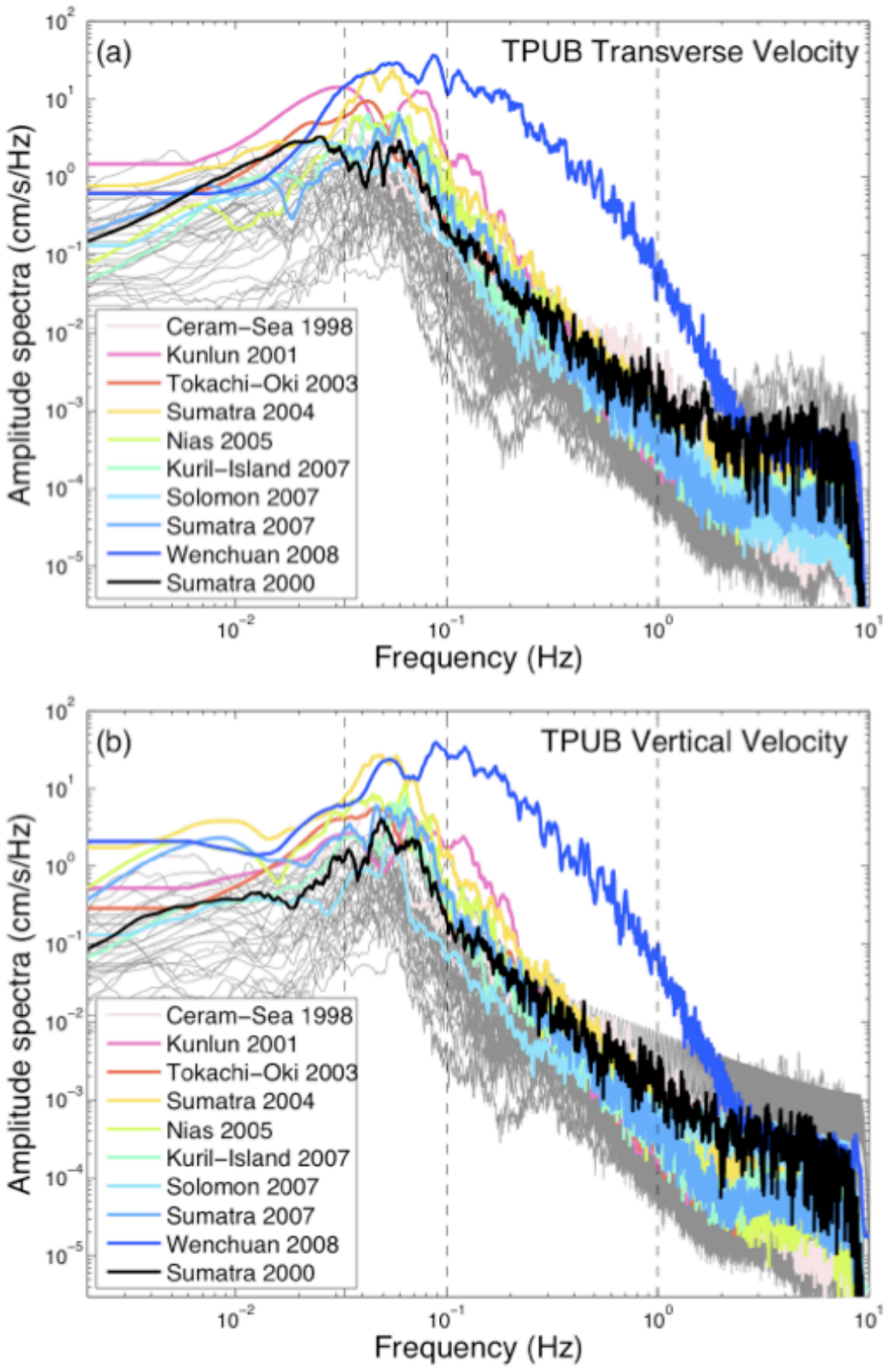

Figure 2.16 Velocity spectra for 9 triggering earthquakes (color lines), one possible triggering earthquake (in black line), and non-triggering earthquakes (gray lines) in the

transverse **(a)** and vertical **(b)** components at the broadband station TPUB. The vertical dashed lines mark the frequencies corresponding to 0.033 Hz (30 s), 0.1 Hz (10 s), and 1 Hz (1 s).

Previous studies have suggested that the surface waves longer than 30 s are more efficient in triggering tremor (Guilhem *et al.*, 2010) and earthquakes (Brodsky and Prejean, 2005). To better quantify the relationship between the frequency contents of the surface waves and triggered tremor, we filtered the displacement seismograms into long-period (>30 s), intermediate-period (30–10 s), and short-period (10–1 s) ranges, then compared them with tremor bursts for all 9 triggering events. Figure 2.17 shows three representative examples of such comparisons in different frequency ranges. For the Kunlun triggering case, the tremor bursts appears to be initiated by or show better correlation with the long-period Love or Rayleigh waves. For the Nias and the Tokachi-Oki cases, the tremor bursts do not show a clear correlation with the long-period Love wave, but are modulated later by the intermediate-period Rayleigh waves. Such a difference could be partially caused by the excitations of long- or intermediate-periods surface waves due to different styles of mainshock faulting. Nevertheless, here we show that intermediate-period surface waves could trigger/modulate tremor and long-period signals are not always needed.

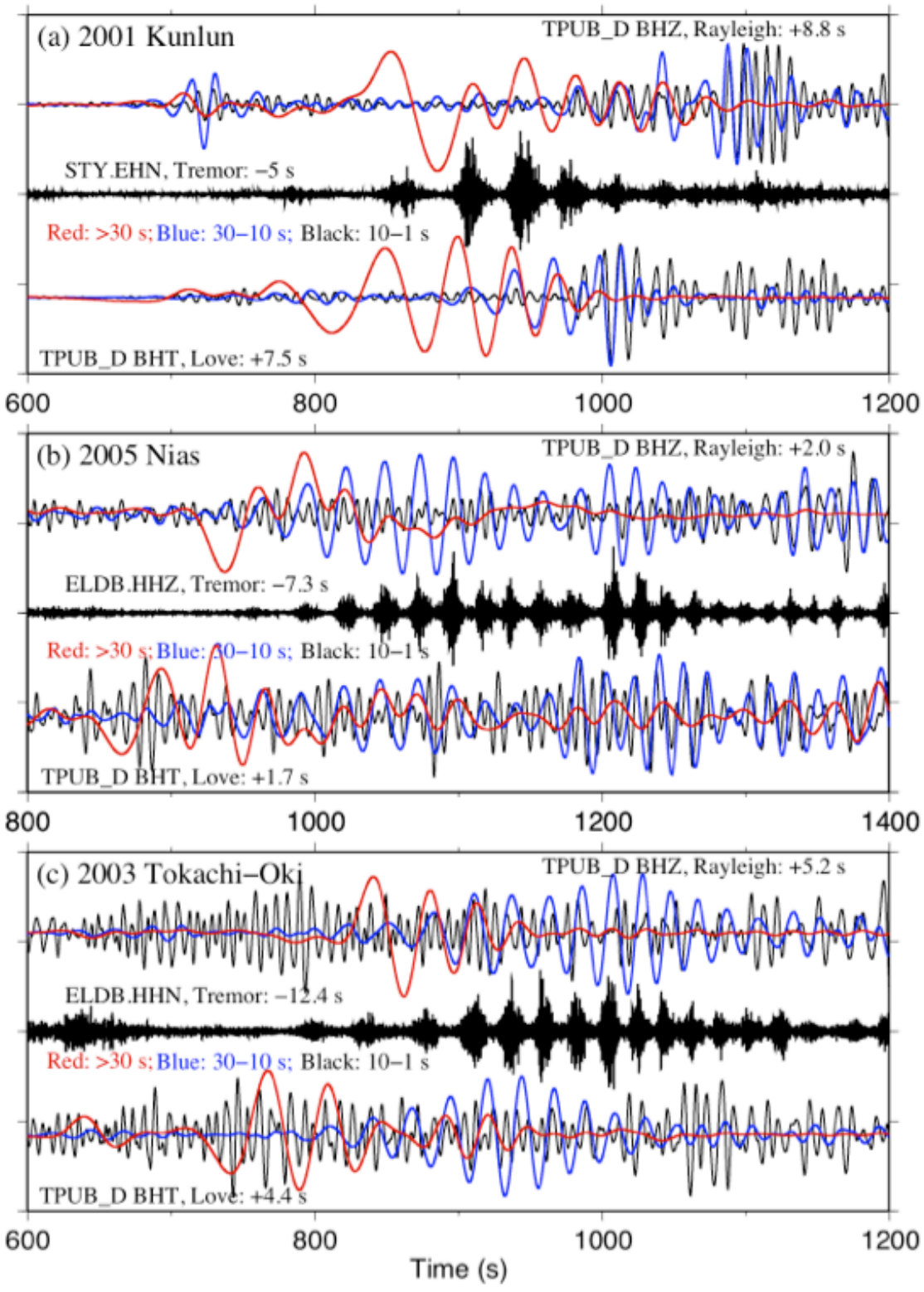

Figure 2.17 Comparisons between tremor and different periods of surface waves for the (a) 2001 Kunlun, **(b)** 2005 Nias, and **(c)** 2003 Tokachi-Oki earthquakes. The long-period

(>30 s), intermediate-period (30–10 s), and short-period (10–1 s) surface waves are marked as red, blue, and black colors, respectively. All displacement seismograms have been normalized to the same scale and time-shifted back to the tremor source region.

To test this statement further, we evaluate the triggering potential by measuring the PGVs from long-, intermediate-, and short-periods surface waves. As shown in Figure 2.18b-c, the PGVs from the intermediate-period surface waves appear to better separate the triggering/non-triggering cases than the long- or short-period surface waves. This is different than the results of Guilhem *et al.* (2010), who found that long-period surface waves (>30 s) better separate the triggering/non-triggering groups around Parkfield. It is worth noting that the intermediate-period (30–10 s) signals in this study include the predominant 20-s surface waves (i.e. spectral peaks in Figure 2.16). Hence, the apparent associations between the triggered tremor and intermediate-period surface waves could also be explained by the amplitude difference in different frequency bands.

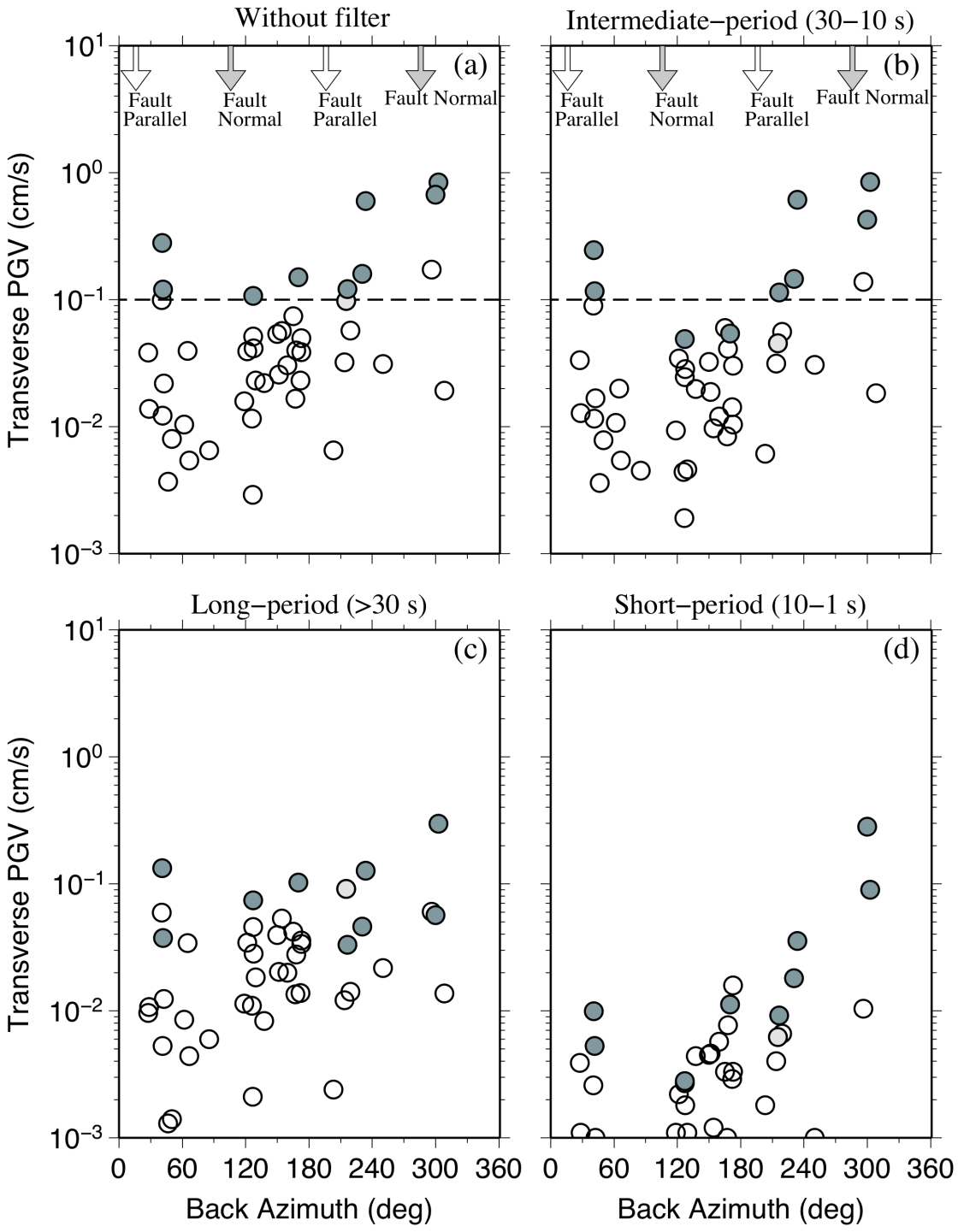

Figure 2.18 PGV versus back azimuth in transverse component for different frequency bands: **(a)** without filter, **(b)** intermediate-period (30–10 s), **(c)** long-period (>30 s), and **(d)** short-period (10–1 s) ranges. Other notations are the same as in Figure 2.2.

2.5.4 Testing of the "Clock-advance" Model and Background Noise Level

Assuming tremor occurs on the fault patches that are close to failure, Gomberg (2010) proposed the "clock-advance" model to explain the phenomenon of triggered tremors. In this model, triggered tremor can be considered as a sped-up occurrence of ambient tremor under fast loading from the passing surface waves. Because the rate of altered failure (i.e. triggered tremor) is directly proportional to the background (i.e. ambient tremor) rate and the amplitude of the triggering wave, we would expect to see higher likelihood of triggering with greater ambient rate, and larger amplitude of triggered tremor signals with larger amplitude of triggering waves (Miyazawa and Brodsky, 2008). Gomberg (2010) used four observations of triggered tremor in Cascadia (Rubinstein *et al.,* 2009) and found that they could not be simply explained by the "clock-advance" model.

Because the ambient tremor observation around our study region is still in the developing stage (Chao *et al.*, 2010), here we only quantified the relationship between the surface wave amplitude and the amplitude of triggered tremor. We measured the median amplitudes of 2–8 Hz band-pass-filtered envelope functions recorded at two horizontal components of station TPUB during the surface waves for all triggering and non-triggering events. In addition, we calculated the median background noise levels for individual event from the envelope functions during the 600 s time period before the occurrence of each mainshock. The median, rather than the maximum or average values in the 2–8 Hz envelope functions are used here to avoid potential contaminations from impulsive local earthquakes or other transient high-frequency noises. We found a relatively strong correlation (with a correlation coefficient of 0.90) for the nine triggering

and one possible-triggering events between the triggered tremor amplitudes and surface waves amplitudes (Figure 2.19a). Such a correlation is generally consistent with the "clock-advance" model (Gomberg, 2010). In comparison, there is no clear correlation between maximum surface waves amplitude and 2–8 Hz energy during the surface waves for the 35 non-triggering events (with a correlation coefficient of 0.06). The median noise level for all events (shadow area) is about 20 nm/s, which is a factor of 2 below the minimum tremor amplitude of ~40 nm/s observed in this study (Figure 2.19a).

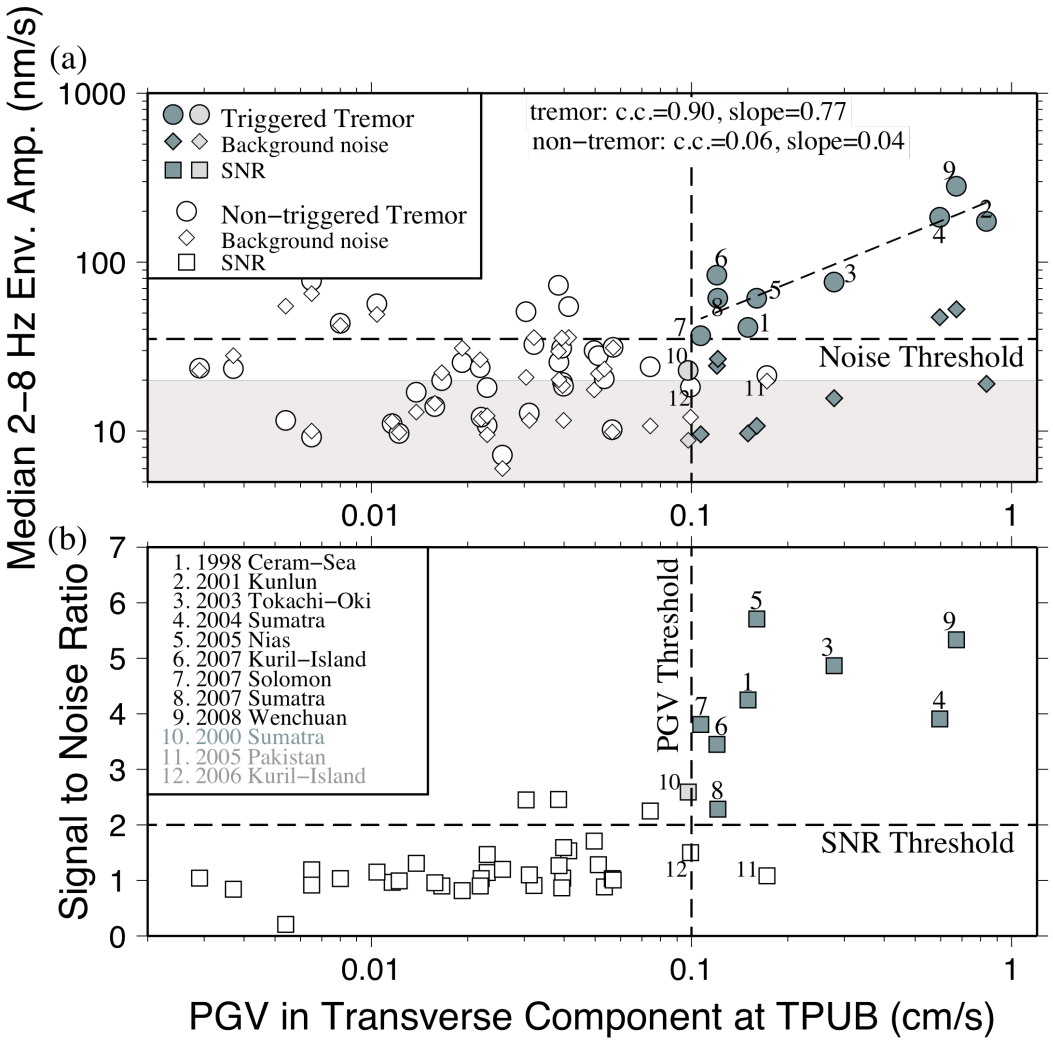

Figure 2.19 Maximum surface wave amplitude (horizontal axis) versus **(a)** median amplitude of the 2–8 Hz band-pass-filtered envelope functions during the surface waves and **(b)** signal to noise ratio (SNR) measured at station TPUB. The background noise

level of each event is calculated from a 600-s time window before the occurrence of each mainshock. The data points associated with the 9 tremor triggering, 1 possible triggering, and 35 non-tremor triggering events are marked as solid, gray and open symbols. The vertical dashed lines show the apparent triggering amplitude threshold of ~0.1 cm s^{-1}. The horizontal dashed line in (a) marks the apparent triggering background noise threshold of ~35 nm s^{-1}. The light gray background shows the median noise level for all events. The horizontal dashed line in (b) marks the SNR of 2.

Figure 19b shows the SNRs for all events. In general, the SNRs of the 9 triggering events and 1 possible-triggering event are greater than 2, but do not show a simple linear relationship with the surface wave amplitudes. This is likely because the background noise levels for these events vary significantly. For the 35 non-triggering events, only 3 events (i.e. the 2001 January 1 Mw7.5, the 2006 April 20 Mw7.6 and 2007 January 21 Mw7.5 earthquakes) have SNR larger than 2. The high-frequency signals during surface waves of these events do not have the characteristics of triggered tremor (i.e. modulated high-frequency bursts that are coherent among nearby stations), and hence the sources of such high-frequency signals are unclear to us at this stage. In addition, we note that the amplitudes of two non-triggering events with PGVs larger than the aforementioned threshold of 0.1 cm s^{-1} have SNR less than 2. It is possible that these events could have triggered tremors with amplitudes smaller than the level of background noise, which prevent them from being identified as tremor triggering events. Nevertheless, it is reasonable to assume that a SNR of 2 is needed for the triggered tremor to be visually identified in this study. This number is close to the aforementioned median noise level of 20 nm/s, and the minimum tremor amplitude of ~40 nm/s. In other words, we suggest that the background noise level could play an important role in determining the smallest triggered tremor observed in this study.

2.6 Discussions and Conclusions

In this study we have identified 9 teleseismic earthquakes that triggered clear tremors beneath the CR. In general, tremors from the southern CR are located between the CLF and the LVF (Peng and Chao, 2008; Tang *et al.*, 2010) below the seismogenic zone (Figure 2.1b) and above the Moho depth calculated by receiver functions (Tang *et al.*, 2011). The 9 tremor locations in the south (Figures 1 and 3) were close to the tremor source triggered by the 2001 Mw7.8 Kunlun earthquake (Peng and Chao, 2008). In addition, those locations are roughly centered around those of the LFEs triggered by the 2005 Nias earthquake (Tang *et al.*, 2010), although the hypocentral depth of 15–25 km for most events shown in this study is on the top of the LFEs distributed between 12–38 km (Figure 2.1b). Such a difference could be mainly caused by the envelope-based technique in this study with only the *S*-wave information, and the LFE-based technique in Tang *et al.* (2010) with both the *P* and *S* arrivals, which provides better constraints on the depth and tends to place the hypocenters at larger depth than other techniques (Kao *et al.*, 2009; La Rocca *et al.*, 2010). Other 5 tremor locations are distributed around the northern CR (Figure 1a). However, the tremor locations in that region have larger uncertainties (see Table S2.3) due to lack of sufficient seismic recordings. Further studies are needed to better constrain the hypocentral locations in the northern CR.

The apparent triggering threshold obtained in this study is about ~0.1 cm s^{-1} PGVs, which corresponds to the peak dynamic stress of 7–8 KPa (Figure 2.2). This number is slightly higher than the 2–3 KPa threshold found in a similar study of triggered tremor along the Parkfield section of SAF in central California (Peng *et al.*, 2009). However, we

found that the triggering threshold could be partially controlled by the background noise level (Figure 2.19). This is consistent with our recent study by comparing triggered tremor in three regions in California (Chao *et al.*, 2012a). Hence, the subtle difference between Taiwan and Parkfield could be related to the use of surface stations in Taiwan and more sensitive and less noisy borehole stations at Parkfield. In addition, we found a positive relationship between the amplitudes of the triggering surface waves and the amplitudes of the triggered tremor, which are consistent with the prediction by the "clock-advance" model (Gomberg, 2010). Therefore, we suggest that surface waves with relatively smaller amplitudes could also have the potential of triggering weaker tremors, although they may not be easily observed if their amplitudes are near or below the background noise level. In addition to the amplitudes, we also found that the incidence angles (Figures 2.2 and 2.15) and the frequency contents (Figures 2.16–2.18) could also play some roles in controlling the triggering potential. In particular, we found that the intermediate-period (30–10 s) surface waves appear to dominate the triggering potential. This is slightly different than the previous observations of long-period (>30 s) surface waves being the most important in triggering tremor (Guilhem *et al.,* 2010) and microearthquakes (Brodsky and Prejean, 2005). We suggest that long-period waves are helpful, but are not required in long-range triggering.

We found that both Love and Rayleigh waves are capable of triggering tremors in the CR (Figures 2.4–2.12). In particular, tremors show better correlations with Rayleigh waves for strike-parallel incidence (Figure 2.14a). Only one case shows Love-wave triggering for strike-normal incidence (Figure 2.4). These observations are consistent

with those by Velasco *et al.* (2009), and can be qualitatively explained by left-lateral shear slip on an low-angle detachment fault (Figure 2.14c). This is the same model originally proposed by Peng and Chao (2008), but is inconsistent with the distributions of triggered LFEs (Figure 2.1b) that are interpreted to occur on the high-angle reverse CLF (Tang *et al.*, 2010). Because the tremor locations (and especially the depth) obtained from this study have large uncertainties, we could not use them to further constrain the fault-dipping angle. Systematic relocations of tremors (Chao *et al.*, 2012d) and LFEs (Wang and Cochran, 2009), together with the focal mechanisms (Ide *et al.*, 2007) and polarization analysis (Miyazawa and Brodsky, 2008; Wech and Creager, 2007) of the triggered and ambient tremors are needed to better understand the fault motions that are responsible for generating tremor signals beneath the CR.

2.7 Supplement Tables

Table S2.1

Online version:

http://kevinchao.com/KChao/papers/Chao_etal_GJI_2012_Table_S1.txt

```
#  1          2   3  4  5  6    7      8          9        10     11   12      13      14      15      16     17   18   19
#  evid       yr  mo dy hr mi   sec    lon        lat      depth  mag  dist    BAZ    PGV_BHT PGV_BHZ signal  noise Q Comments
199803250312 1998 03 25 03 12 25.0700  149.52701 -62.87700 10.00 8.10  9884.26 167.20  0.0166 0.0331   19.90  22.10 0
199811291410 1998 11 29 14 10 31.9600  124.89101  -2.07100 33.00 7.70  2841.88 170.09  0.1500 0.1410   28.70   9.10 1 Ceram_Sea
199908170001 1999 08 17 00 01 39.1300   29.86400  40.74800 17.00 7.70  8421.36 308.38  0.0192 0.0123   25.50  31.00 0
199909301631 1999 09 30 16 31 15.6900  -96.93101  16.05900 60.60 7.50 14048.63  46.69  0.0037 0.0031   23.40  27.90 0
199911261321 1999 11 26 13 21 15.5700  168.21400 -16.42300 33.00 7.50  6784.12 125.90  0.0116 0.0083   11.10  11.40 0
200005040421 2000 05 04 04 21 16.2100  123.57301  -1.10500 26.00 7.60  2716.18 172.87  0.0497 0.0401   29.90  17.50 0
200006041628 2000 06 04 16 28 26.1700  102.08701  -4.72100 33.00 7.90  3693.58 215.35  0.0977 0.0595   22.80   8.80 0 Sumatra_00
200006181444 2000 06 18 14 44 13.3100   97.45300 -13.80200 10.00 7.90  4813.83 213.89  0.0322 0.0382   32.50  35.80 0
200011160454 2000 11 16 04 54 56.7400  152.16901  -3.98000 33.00 8.00  4559.99 127.32  0.0511 0.0248   28.00  21.90 0
200011160742 2000 11 16 07 42 16.9300  153.10201  -5.23300 30.00 7.80  4730.01 127.73  0.0413 0.0670   54.60  35.70 0
200011172101 2000 11 17 21 01 56.4900  151.78101  -5.49600 33.00 7.80  4644.48 129.37  0.0230 0.0124   10.80   9.50 0
200101010657 2001 01 01 06 57  4.1700  126.57900   6.89800 33.00 7.50  1921.85 159.73  0.0304 0.0156   50.90  20.80 0
200101131733 2001 01 13 17 33 32.3800  -88.66000  13.04900 60.00 7.70 14887.09  41.41  0.0122 0.0094    9.70   9.80 0
200106232033 2001 06 23 20 33 14.1300  -73.64101 -16.26500 33.00 8.40 18331.80  65.04  0.0396 0.0263   19.40  18.60 0 Peru
200107070938 2001 07 07 09 38 43.5200  -72.07700 -17.54300 33.00 7.60 18545.79  66.64  0.0054 0.0050   11.60  55.10 0
200110190328 2001 10 19 03 28 44.4600  123.90701  -4.10200 33.00 7.50  3049.28 172.89  0.0385 0.0107   25.60  20.20 0
200111140926 2001 11 14 09 26 10.0100   90.54101  35.94600 10.00 7.80  3214.65 302.70  0.8350 0.2680   65.20  18.00 1 Kunlun
200203052116 2002 03 05 21 16  9.1300  124.24901   6.03300 31.00 7.50  1947.99 167.96  0.0398 0.0188   18.40  11.60 0
200209081844 2002 09 08 18 44 23.7100  142.94501  -3.30200 13.00 7.60  3807.74 137.65  0.0220 0.0174   12.10  11.80 0
200210101050 2002 10 10 10 50 20.5700  134.29701  -1.75700 10.00 7.60  3140.11 150.06  0.0535 0.0207   20.40  23.30 0
200211032212 2002 11 03 22 12 41.5180 -147.45290  63.51410   4.20 7.90  7812.45  28.43  0.0138 0.0134   17.00  13.00 0 Denali
200301220206 2003 01 22 02 06 34.6100 -104.10400  18.77000 24.00 7.60 13292.22  50.04  0.0080 0.0067   43.60  42.20 0
200307152027 2003 07 15 20 27 50.5300   68.38200  -2.59800 10.00 7.60  6338.22 250.35  0.0311 0.0348   12.80  11.60 0
200309251950 2003 09 25 19 50  6.3600  143.91000  41.81500 27.00 8.30  2980.21  40.94  0.2790 0.1600   56.50  14.80 1 Tokachi_Oki
200311170643 2003 11 17 06 43  6.8000  178.65001  51.14600 33.00 7.80  5810.11  42.51  0.0219 0.0255   23.70  26.40 0
200411112126 2004 11 11 21 26 41.1500  124.86800  -8.15200 10.00 7.50  3506.31 171.96  0.0230 0.0548   18.10  12.30 0
200412231459 2004 12 23 14 59  4.4100  161.34500 -49.31200 10.00 8.10  8992.29 154.38  0.0565 0.0221   10.20   9.90 0
200412260058 2004 12 26 00 58 53.4500   95.98200   3.29500 30.00 9.00  3452.46 233.83  0.5960 0.6860  198.20  41.70 1 Sumatra_04
200503281609 2005 03 28 16 09 36.5300   97.10800   2.08500 30.00 8.60  3453.15 230.64  0.1600 0.1760   46.40  10.20 1 Nias_Sumatra
200509090726 2005 09 09 07 26 43.7300  153.47401  -4.53900 90.00 7.70  4708.35 126.61  0.0029 0.0023   23.60  22.80 0
200510080350 2005 10 08 03 50 40.8000   73.58801  34.53900 26.00 7.60  4707.62 296.23  0.1720 0.0566   21.30  19.80 0 Pakistan
200604202325 2006 04 20 23 25  2.1500  167.08900  60.94900 22.00 7.60  5479.28  27.83  0.0384 0.0684   72.80  29.60 0
200605031526 2006 05 03 15 26 40.2900 -174.12300 -20.18700 55.00 8.00  8550.78 118.86  0.0158 0.0252   14.00  14.60 0 Tonga
200607170819 2006 07 17 08 19 26.6800  107.41901  -9.28400 20.00 7.70  3877.25 203.24  0.0065 0.0083   77.70  65.20 0
200611151114 2006 11 15 11 14 13.5700  153.26601  46.59200 10.00 8.30  3896.18  40.38  0.0992 0.0653   18.20  12.10 0 Kuril_06
200701130423 2007 01 13 04 23 21.1600  154.52400  46.24300 10.00 8.10  3961.58  41.64  0.1200 0.1040   65.50  23.00 1 Kuril_07
200701211127 2007 01 21 11 27 45.0600  126.28201   1.06500 22.00 7.50  2532.36 165.26  0.0743 0.0286   24.10  10.70 0
200704012039 2007 04 01 20 39 56.3800  157.04401  -8.46000 10.00 8.10  5291.57 127.31  0.1070 0.0342   65.80  22.60 1 Solomon
200708152340 2007 08 15 23 40 57.8900  -76.60300 -13.38600 39.00 8.00 17893.43  61.88  0.0104 0.0123   56.70  49.10 0 Peru
200709121110 2007 09 12 11 10 26.8300  101.36700  -4.43800 34.00 8.40  3710.63 216.73  0.1210 0.1170   49.40  25.60 1 Sumatra_07
200709122349 2007 09 12 23 49  3.7200  100.84100  -2.62500 35.00 7.90  3578.94 219.41  0.0569 0.0704   31.40  31.10 0
200711141540 2007 11 14 15 40 50.4700  -69.86900 -22.20400 40.00 7.70 18930.91  85.62  0.0065 0.0073    9.20  10.00 0
200805120628 2008 05 12 06 28  1.5700  103.32201  31.00200 19.00 7.90  1912.00 300.22  0.6710 0.7130  290.80  50.70 1 Wenchuan
200901031943 2009 01 03 19 43 50.6500  132.88500  -0.41400 17.00 7.60  2937.08 151.50  0.0257 0.0166    7.20   6.00 0
200903191817 2009 03 19 18 17 40.9100 -174.65900 -23.04600 34.00 7.60  8668.23 121.61  0.0393 0.0619   30.90  35.50 0
# Earthquake parameters of the 45 teleseismic events analyzed in this study.
# The earthquake catalog information (origin time, location, and magnitude)
# is obtained from the Advanced National Seismic System (ANSS) catalog.
# The epicentral distance and back-azimuth (BAZ) is computed relative to
# the broadband station TPUB (stlo: 120.63, stla: 23.3005).
# The peak ground vertical (PGV_BHZ) and transverse (PGV_BHT) velocity are
# measured from the broadband recording by station TPUB, and are in the unit
# of cm/s. The median amplitude of signal and noise are in the unit of nm/s.
# The quality (Q) 1 marks events that trigger tremor around southern Central Range of Taiwan
# 0 marks those that do not.
```

Table S2.2

Online version:

http://kevinchao.com/KChao/papers/Chao_etal_GJI_2012_Table_S2.txt

```
Table S2-a
# Velocity model used to locate tremor sources in the southern Central Range

# This is the same velocity model used by Tang et al. (GRL, 2010) to locate LFEs in the same region
# Vp  Vp/Vs Vs  dep_range
 3.82 1.74 2.20  0.0  2.0
 4.93 1.68 2.93  2.0  4.0
 5.51 1.70 3.24  4.0  6.0
 5.63 1.70 3.31  6.0  9.0
 5.83 1.76 3.31  9.0 13.0
 5.99 1.75 3.42 13.0 17.0
 6.06 1.75 3.46 17.0 21.0
 6.13 1.75 3.50 21.0 25.0
 6.25 1.71 3.65 25.0 30.0
 6.54 1.73 3.78 30.0 35.0
 7.03 1.75 4.02 35.0 50.0
 8.00 1.74 4.60 50.0 70.0
 8.34 1.73 4.82 70.0 80.0
# The units of Vp, Vp/Vs, and Vs are in km/s
# The unit of depth_range is in km

Table S2-b
# Velocity model used to locate tremor sources in the northern Central Range
 3.88 1.81 2.14  0.0  2.0
 4.50 1.70 2.65  2.0  4.0
 4.89 1.68 2.91  4.0  6.0
 5.18 1.69 3.07  6.0  9.0
 5.65 1.69 3.34  9.0 13.0
 5.88 1.69 3.48 13.0 17.0
 6.07 1.70 3.57 17.0 21.0
 6.36 1.71 3.72 21.0 25.0
 6.62 1.73 3.83 25.0 30.0
 6.96 1.73 4.02 30.0 35.0
 7.36 1.73 4.25 35.0 50.0
 7.91 1.73 4.57 50.0 70.0
 8.14 1.73 4.71 70.0 80.0
# The units of Vp, Vp/Vs, and Vs are in km/s
# The unit of depth_range is in km
```

Table S2.3

Online version:

http://kevinchao.com/KChao/papers/Chao_etal_GJI_2012_Table_S3.txt

```
# 1          2   3  4  5  6  7       8          9       10   11      12   13    14    15      16      17   18      19  20   21   22   23   24   25   26  27      28          29   30   31      32        33
# evid       yr  mo dy hr mi sec     lon.       lat.    dep  mag     stn  dist  BAZ   PGV_BHT PGV_BHZ sig  noi     t_s t_e  tlon tlat tdep err1 err2 err3 RMS     event_name  R/L cor_R cor_L  Lo_win    Ra_win
19981129141O 1998 11 29 14 10 31.9600 124.89101 -2.07100 33.00 7.70 TPUB 2841.88 170.09 0.1500 0.1410 41.2  9.7     820 1000 120.80 23.10 20.0 0.17 0.85 N/A 1.6981      Ceram_Sea   1.54 0.28 -0.07  690_850   800_1050
20011114092G 2001 11 14 09 26 10.0100  90.54101 35.94600 10.00 7.80 TPUB 3214.65 302.70 0.8350 0.2680 174.6 19.1    850 1100 120.85 23.10 23.0 0.03 0.00   6 1.2027      Kunlun      0.21 0.36 0.03  800_1000  900_1300
20011114092G 2001 11 14 09 26 10.0100  90.54101 35.94600 10.00 7.80 TPUB 3214.65 302.70 0.8350 0.2680 174.6 19.1    850 1100 121.50 24.35 36.0 0.07 0.05   6 1.2728      Kunlun_N    N/A  N/A  N/A    N/A       N/A
20030925195O 2003 09 25 19 50 6.3600 143.91000 41.81500 27.00 8.30 TPUB 2980.21  40.94 0.2790 0.1600 76.4  15.7    750 1300 120.80 22.95 20.0 0.62 0.38 N/A 4.2554  Tokachi_Okt 0.56 0.39 -0.24  700_1000 800_1150
20030925195O 2003 09 25 19 50 6.3600 143.91000 41.81500 27.00 8.30 TPUB 2980.21  40.94 0.2790 0.1600 76.4  15.7    800 1100 121.71 24.48 20.0   x    x  x0 0.0000  Tokachi_Okt_N N/A  N/A  N/A    N/A       N/A
20041226005S 2004 12 26 00 58 53.4500  95.98200  3.29500 30.00 9.00 TPUB 3452.46 233.83 0.5960 0.6860 184.6 47.2    900 1600 120.95 23.15 20.0 0.27 0.20 N/A 4.4013  Sumatra_04  1.28 0.23 -0.44  850_1000  1000_1400
20041226005S 2004 12 26 00 58 53.4500  95.98200  3.29500 30.00 9.00 TPUB 3452.46 233.83 0.5960 0.6860 184.6 47.2    950 1600 121.53 24.51 20.0   x    x  x0 0.0000  Sumatra_04_N N/A  N/A  N/A    N/A       N/A
20050328160S 2005 03 28 16 09 36.5300  97.10800  2.08500 30.00 8.60 TPUB 3453.15 230.64 0.1600 0.1760  61.1 10.7    950 2000 120.85 23.15 14.0 0.00 0.05   6 1.1710      Nias        2.53 0.48 0.39  850_1100  1000_1300
20070113040S 2007 01 13 04 23 21.1600 154.52400 46.24300 10.00 8.10 TPUB 3961.58  41.64 0.1200 0.1040  83.8 24.3    1100 2000 120.85 23.10 30.0 0.08 0.25 N/A 1.4808  Kuril_07    0.64 0.23 0.11  950_1250  1150_1350
20070401203S 2007 04 01 20 39 56.3800 157.04401 -8.46000 10.00 8.10 TPUB 5291.57 127.31 0.1070 0.0342  36.6  9.6    1300 1500 121.00 23.00 20.0 0.65 0.27 N/A 5.8681  Solomon     1.89 0.23 0.13  1200_1350 1350_1500
20070401203S 2007 04 01 20 39 56.3800 157.04401 -8.46000 10.00 8.10 TPUB 5291.57 127.31 0.1070 0.0342  36.6  9.6    1350 1500 121.30 24.15 20.0   x    x  N/A 5.4564  Solomon_N   N/A  N/A  N/A    N/A       N/A
20070912111O 2007 09 12 11 10 26.8300 101.36700  -4.43800 34.00 8.40 TPUB 3710.63 216.73 0.1210 0.1170  61.0 26.7    1000 1800 120.85 23.20 19.0 0.02 0.15   6 1.3669  Sumatra_07  2.37 0.35 0.04  900_1100  1000_1300
20070912111O 2007 09 12 11 10 26.8300 101.36700  -4.43800 34.00 8.40 TPUB 3710.63 216.73 0.1210 0.1170  61.0 26.7    1000 1500 121.90 24.70 20.0 0.15 0.03 N/A 0.9113  Sumatra_07_N N/A  N/A  N/A    N/A       N/A
20080512062S 2008 05 12 06 28  1.5700 103.32201 31.00200 19.00 7.90 TPUB 1912.00 300.22 0.6710 0.7130 280.6 52.6    600  800 120.85 23.10 22.0 0.03 0.05   4 0.6300  Wenchuan    0.77 0.50 0.20  550_700   650_800
# note:
# general information for 9 tremor-triggering teleseismic earthquakes
# 1          2   3     4   5   6     7         8          9       10   11
# evid       yr  mo    dy  hr  mi    sec       lon.       lat.    dep  mag
# event_id   year month day hour minute second  longitude  latitude depth  magnitude
#
# Other parameters measured at TPUB
# 12         13  14                15                    16
#
# stn        17  18    PGV_BHT     PGV_BHZ
#            dist  BAZ
#               sig   noi
# station  distance back-azimuth transverse_PGV(cm/s)  vertical_PGV(cm/s)  signal(nm/s)  noise(nm/s)
#
# tremor information
# 19         20          21        22        23        24        25        26        27        28
# t_s        t_e         tlon      tlat      tdep      err1      err2      err3      RMS       event_name
# tremor_start_time  tremor_end_time tremor_lon tremor_lat tremor_dep error_lon error_lat error_dep RMS(sec)  location_from_south_or_north
#
# surface wave measurements for R/L, cor_R, and cor_L
# 29         30          31        32        33
#
# R/L        Lo_win      cor_R     cor_L     Ra_win
#
# amp_ratio_of_Ra/Lo  correlation_between_Ra_and_tremor  correlation_between_Lo_and_tremor  Love_windows  Rayleigh_window
```

CHAPTER 3 (Chao *et al.*, 2012a)

COMPARISONS OF TRIGGERED TREMOR IN CALIFORNIA

Summary

We conduct a visual inspection of deep nonvolcanic tremor triggered by large teleseismic earthquakes around the Calaveras fault in northern California (NC) and the San Jacinto fault in southern California (SC). Out of the 42 large (Mw ≥7:5) earthquakes between 2001 and 2010, only the 2002 Mw 7.9 Denali fault earthquake triggered clear tremor in these two regions. This is in marked contrast with the Parkfield–Cholame section of the San Andreas fault in central California (CC), where 12 earthquakes have triggered tremor in that region. The amplitude of the triggered tremor correlates with that of the triggering surface waves in CC and is consistent with the clock-advance model. The lack of widespread triggered tremor in NC and SC is not simply a consequence of their different background noise levels from CC, but rather reflects different background tremor rates in these regions.

3.1 Introduction

Deep tremor has been recorded along many major plate boundary faults, indicating that they are more common than previously thought (Peng and Gomberg, 2010; Beroza and Ide, 2011, and references therein). While most tremor occurs spontaneously with or following slow-slip events (Rogers and Dragert, 2003; Obara *et al*., 2004), tremor can also be triggered by large distant earthquakes and is known as "triggered tremor" (Miyazawa and Mori, 2006; Rubinstein *et al*., 2007). Although triggered and ambient

(i.e., not triggered) tremor share many similarities (Shelly *et al*., 2011), the fundamental mechanism of triggered tremor and their relationship with slow-slip events remains unclear (Beroza and Ide, 2009).

Gomberg (2010) proposed a clock-advance model assuming that triggered tremor occurs on the same patch of ambient tremor and that their duration time is advanced by the passing surface waves. In this model, the perturbed seismicity rate *r* is proportional to the background rate r_0, and a function is used to describe how the failure time of a fault patch is advanced by the perturbing stress. Hence, the model predicts that larger triggering waves would result in larger triggered tremor signals and that triggered tremor is more abundant when r_0 is larger. Both Rubinstein *et al*. (2009) and Gomberg (2010) examined triggered tremor in Cascadia and inferred that the tremor-triggering potential is higher during an episodic tremor-and-slip (ETS) event or intensive tremor sequence, which is consistent with the predictions of the clock-advance model. However, Gomberg (2010) examined the relationship between the amplitudes of the triggering waves and triggered tremor for four observations in Cascadia (Rubinstein *et al*., 2009), and the obtained results do not match the predictions of the clock-advance model. In comparison, Chao *et al*. (2012d) found a positive relationship between the amplitudes of surface waves from nine teleseismic earthquakes and those of triggered tremor beneath the Central Range in Taiwan. Miyazawa and Brodsky (2008) observed an exponential relationship between the triggered tremor amplitude and the dynamic stress at the source region in southwest Japan. Those diverse observations suggest more studies are needed to

understand the relationship between the triggering wave, triggered tremor, and background tremor rate.

An ideal region to examine the relationship between triggering waves and tremor characteristics is the Parkfield–Cholame section of the San Andreas fault (SAF) in central California (CC), where many triggered (Gomberg *et al*., 2008; Peng *et al*., 2008; Ghosh *et al*., 2009; Peng *et al*., 2009; Guilhem *et al*., 2010; Shelly *et al*., 2011) and ambient (Nadeau and Dolenc, 2005; Nadeau and Guilhem, 2009) tremors have been recorded. In comparison, in northern California (NC) and southern California (SC), the only clear case of teleseismically triggered tremor reported so far is by the 2002 Mw 7.9 Denali fault earthquake (Gomberg *et al*., 2008; Fabian *et al*., 2009; Wang and Cochran, 2009). It is not yet clear whether such a difference is caused by different observational capabilities (e.g., different instrumentation, background noise level) or different conditions that favor tremor generation in these regions.

In this study, we conduct a systematic search in NC and SC for tremor triggered by large teleseismic events between 2001 and 2010. We focus on the regions around the central segment of the Calaveras fault (CF) in NC (Fig. 3.1a) and the Anza segment of the San Jacinto fault (SJF) in SC (Fig. 3.1b), where tremor was triggered by the Denali fault earthquake (Gomberg *et al*., 2008). A total of 12 tremor-triggering events in CC (Peng *et al*., 2009; Peng *et al*., 2010; Shelly *et al*., 2011) were used for comparison with the results in NC and SC in the same time period. In addition, we measure the background noise level and quantify the triggering threshold in each region. Finally, we

explore possible reasons that explain the lack of triggered tremor observations in NC and SC.

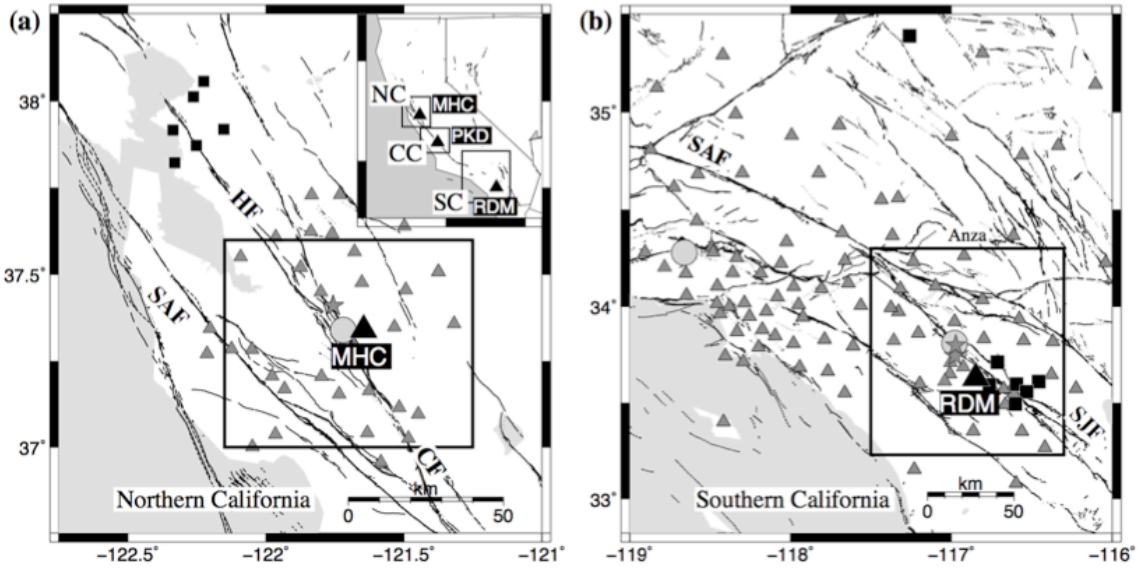

Figure 3.1 (a) Map of the study region in northern California (NC). Small triangles, short-period stations belonging to the Northern California Seismic Network (NCSN); black squares, the borehole stations in the Northern Hayward Fault Network (NHFN); large black triangle, broadband station MHC; black lines, the active faults of Calaveras fault (CF), San Andreas fault (SAF), and Hayward fault (HF); gray circle, location of the tremor triggered by the 2002 Mw 7.9 Denali fault earthquake (Gomberg *et al*., 2008). The two local earthquakes used to demonstrate the path or site effects (Fig. S4) are close to each other and are marked by a dark gray star. The insert indicates the study region in NC, central California (CC), and southern California (SC). The broadband stations MHC, PKD, and RDM are marked by small black triangles in NC, CC, and SC, respectively. **(b)** Study region in southern California. Black lines, active faults of San Jacinto fault (SJF) and SAF; gray triangles, broadband stations belonging to the Caltech (CI) and Anza (AZ) network; black squares, borehole stations belong to the Plate Boundary Observatory (PBO); gray circles, previously determined tremor locations triggered by the Denali earthquake (Gomberg *et al*., 2008). The dark gray stars mark two local earthquakes used to demonstrate the path or site effects (Fig. S3.4).

3.2 Data and Analysis Procedure

In this study, we first selected 42 earthquakes from the Advanced National Seismic System (ANSS) earthquake catalog between 2001 and 2010; all had moment magnitude Mw ≥ 7:5, hypocentral depth < 100 km, and epicentral distance >1000 km from the broadband station PKD in CC (Table S3.1). Except for time range, the other search criteria are the same as used in Peng *et al*. (2009). Next, we acquired seismic data spanning five hours before and after the origin time of each teleseismic event at all available stations in NC and SC. In CC, we used the results from the 31 earthquakes analyzed in Peng *et al*. (2009) and requested the seismic data for 11 additional events since June 2008.

Following Peng *et al*. (2009), we visually identified triggered tremor as bursts of high-frequency (2–8 Hz), nonimpulsive signals that are coherent among many nearby stations and correlate with the timing of the surface waves from the teleseismic earthquakes (e.g., Fig. 3.2). We used the following criteria to identify triggered tremor. First, the high-frequency tremor bursts were associated with the periods of surface waves and were recorded by at least five surrounding stations within 100 km of the potential triggered tremor source. Second, the move-out patterns (i.e. later arrivals with increasing distances) of tremor bursts (Fig. 3.2) were used to further confirm the positive triggering cases. Figure 3.2 shows a case in which triggered tremor was identified in NC and SC after the 2002 Mw 7.9 Denali fault earthquake. Figure 3.3 demonstrates one nontriggering example without coherence signals by the 2007 Mw 8.1 Kuril Island earthquake in NC and SC. Figure 3.4 shows another example in which triggered tremor

could not be identified following the 2010 Mw 8.8 Chile earthquake. In this case, we used a higher frequency band of 10 Hz, high-pass-filtered in NC and SC, respectively, in order to remove potential contamination of earthquake signals from the Coso geothermal fields triggered by the Chile mainshock (Peng *et al*., 2010; Fig. S3.1).

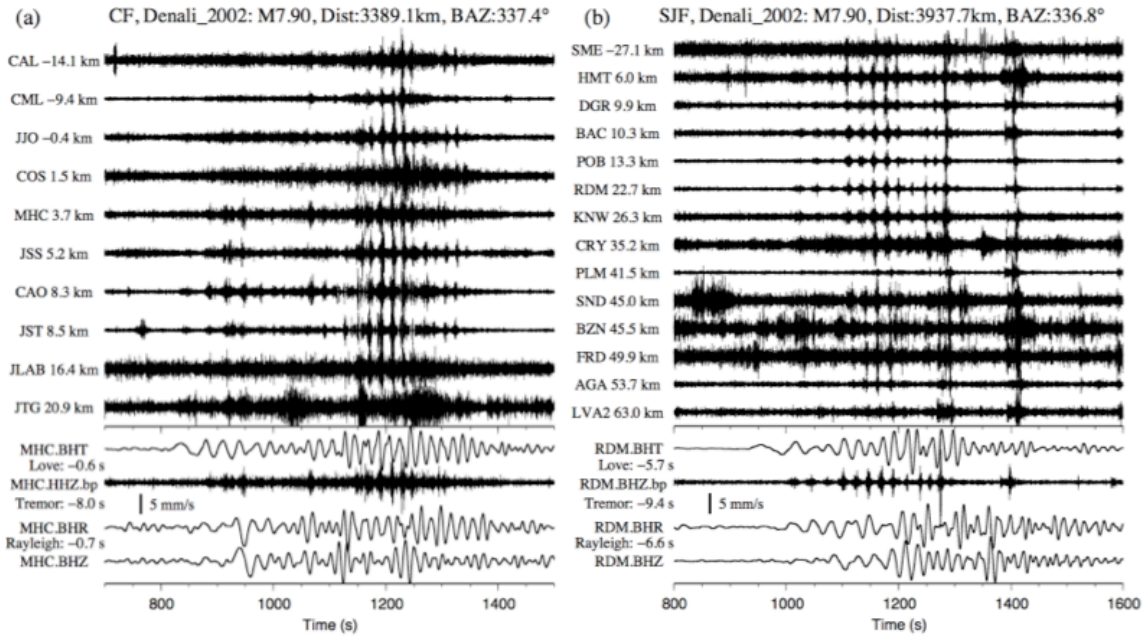

Figure 3.2. (a) Top: 2–8-Hz band-pass-filtered vertical seismograms showing the move-out of tremor along the Calaveras fault (CF) in northern California (NC) triggered by the 2002 Mw 7.9 Denali fault earthquake. The seismograms are plotted along the strike of the CF, with northwest at the top and southeast on the bottom. The along-strike distance to the tremor source and the station names are marked by the seismograms. The event name and the occurrence year, its magnitude (M), and the epicenter distance (Dist) and back azimuth (BAZ) relative to the broadband station are shown above the siesmograms. Bottom: A comparison between the instrument-corrected transverse (BHT), radial (BHR), and vertical (BHZ) velocity seismograms and the 2–8-Hz band-pass-filtered seismogram recorded at the broadband station MHC. The zero time corresponds to the origin time of the mainshock. The velocity seismograms have been time-shifted back to the tremor sources. The adjusted times of Love waves (in the T component), Rayleigh waves (in the R and Z components), and tremor are marked below the station names. The thick vertical bar marks the amplitude scale of surface waves. **(b)** Top: 2–8-Hz band-pass-filtered vertical seismograms showing the move-out of tremor triggered by the Denali fault earthquake along the San Jacinto fault (SJF) in the Anza network in southern California (SC). The seismograms are plotted along the strike of the SJF, with northwest at the top and southeast on the bottom. Bottom: A comparison between the velocity and the 2–8-Hz band-pass-filtered seismograms recorded at the broadband station RDM. Other notations are the same as in Figure 3.2a.

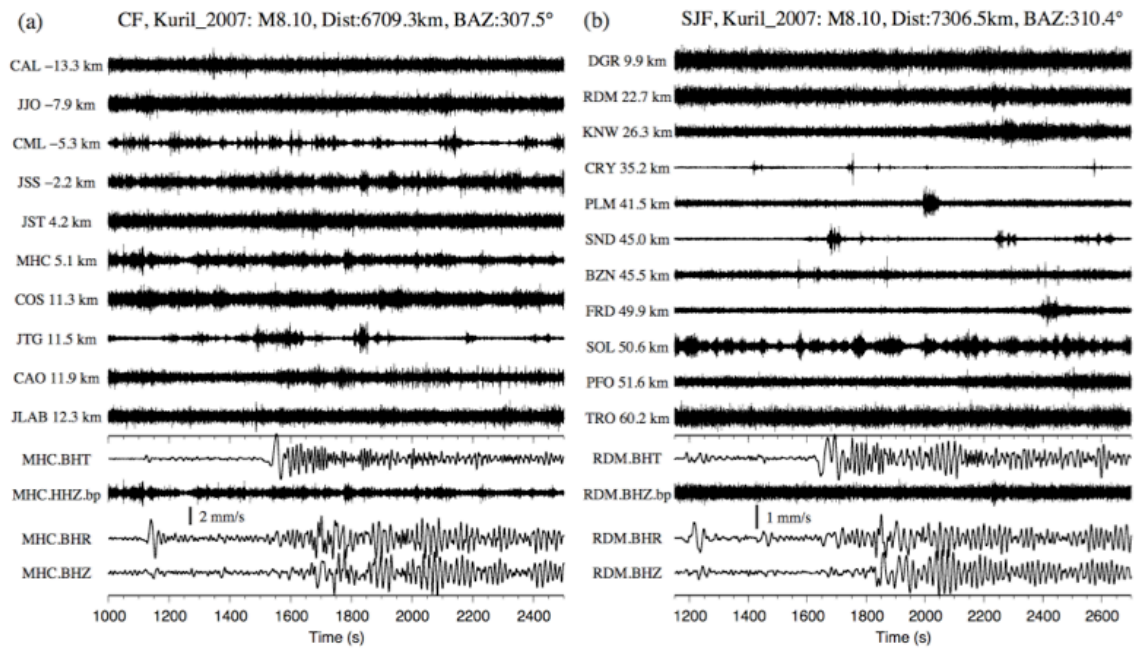

Figure 3.3 2–8-Hz band-pass-filtered seismograms showing no tremor triggered by the 2007 Mw 8.1 Kuril Island earthquake at **(a)** the Calaveras fault (CF) in NC and at **(b)** the San Jacinto fault (SJF) in SC. Other notations are the same as in Figure 3.2.

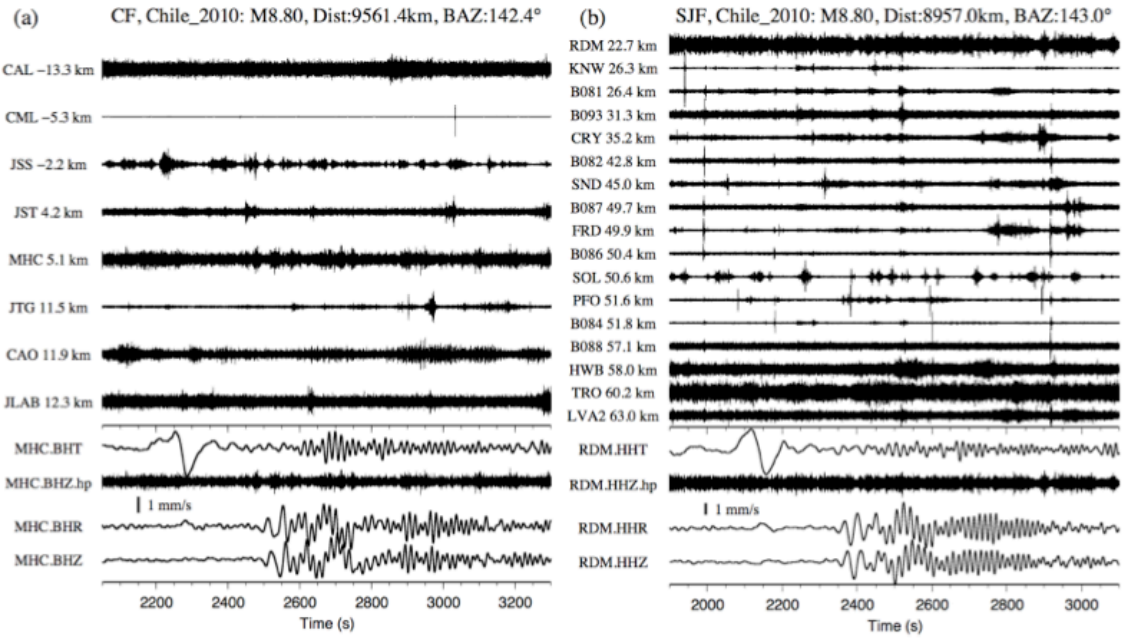

Figure 3.4 10-Hz high-pass-filtered seismograms showing no tremor triggered by the 2010 Mw 8.8 Chile earthquake at **(a)** the Calaveras fault (CF) in NC and at **(b)** the San Jacinto fault (SJF) in SC. Other notations are the same as in Figure 3.2.

3.3 Triggered Tremor in California

Among all 42 events, the 2002 Mw 7.9 Denali fault earthquake is the only event that has triggered tremor in NC and SC (Fig. 3.2), which is in marked contrast with the observations of 12 telesesmic earthquakes that triggered tremor (including the Denali fault event) in CC. This perhaps is not surprising because the Denali fault earthquake produced the largest peak ground velocity (PGV) at all regions (Fig. 3.5). However, the 2007 Mw 8.1 Kuril Island earthquake also triggered tremor in CC (Peng *et al*., 2009) but not in NC and SC (Fig. 3.3). Similarly, the 2010 Chile earthquake triggered clear tremor in CC (Peng *et al*., 2010) but did not trigger any tremor in NC or SC (Fig. 3.4). Although there were some high-frequency spikes at a few stations during the timing of the surface waves, these signals are not coherent at nearby stations and hence are not classified as triggered tremor.

Tremor triggered by the Denali fault earthquake has been analyzed in several previous studies (Gomberg *et al*., 2008; Peng *et al*., 2008; Peng *et al*., 2009). Here we used the tremor locations triggered by the Denali fault earthquake along the CF in NC (121.72° W, 37.34° N, 15 km in depth) and the SJF in SC (116.98° W, 33.81° N, 14 km in depth; Gomberg *et al*., 2008) and shifted the tremor bursts and nearby surface waves back to the tremor source region to further examine their relationships. In both regions, the tremor was initiated in the first few cycles of the Love waves when it propagated to the southwest (positive value in Fig. 3.2) and then further intensified during the large-amplitude Rayleigh waves. This is consistent with the observations along the Parkfield–

Cholame section of the SAF in CC (Peng *et al*., 2008; Peng *et al*., 2009), suggesting a similar triggering mechanism among these regions.

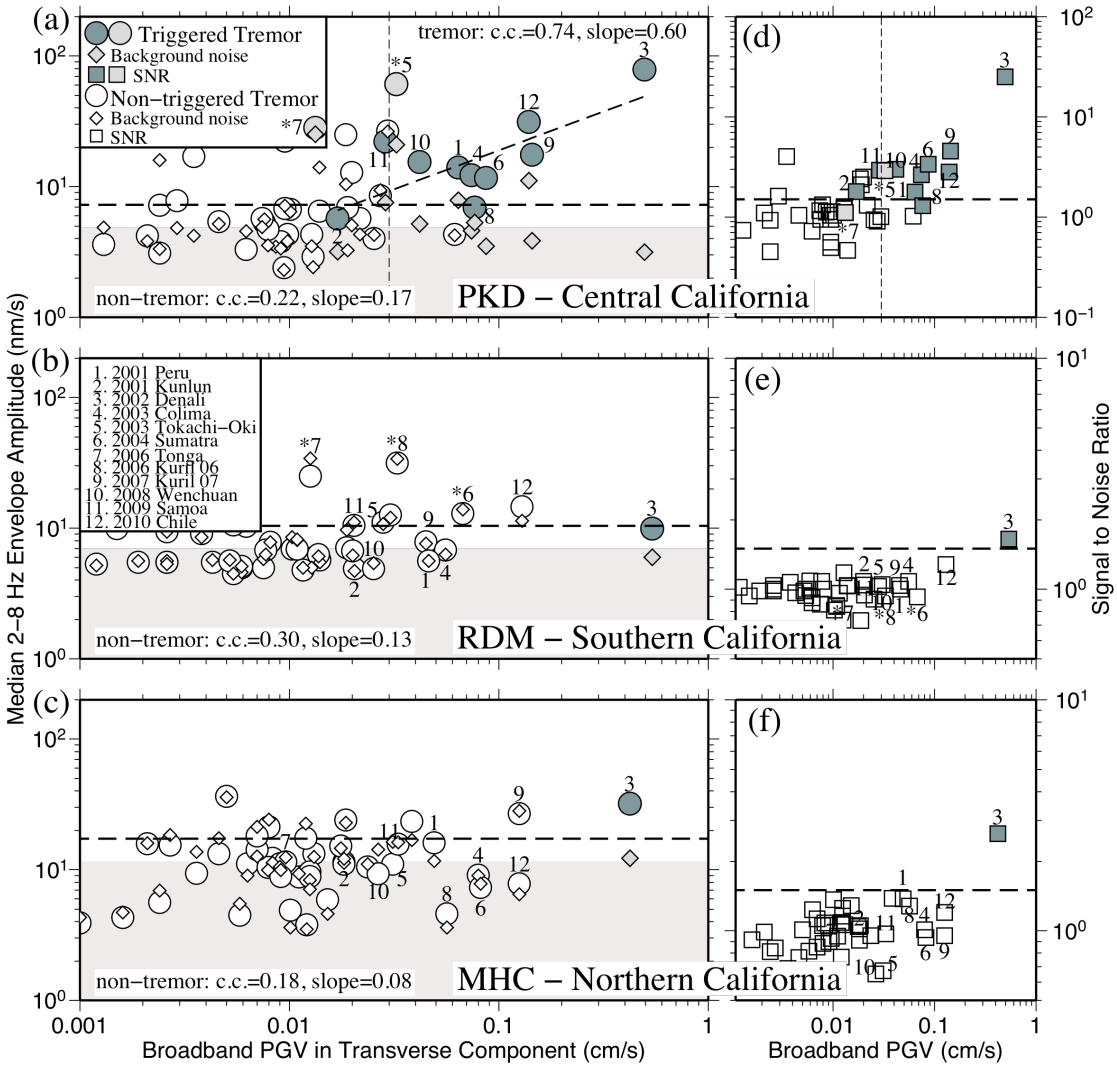

Figure 3.5 Maximum peak ground velocity (PGV) of surface wave (horizontal axis) in transverse component versus median amplitude (vertical axis) of the 2–8 Hz three-component band-pass-filtered envelope functions **(a–c)** during the surface waves and **(d–f)** signal-to-noise ratio (SNR) at broadband stations PKD, RDM, and MHC in central California (CC), southern California (SC), and northern California (NC), respectively. The event numbers preceded by an asterisk (*) indicate the measurement is from the nearby station FROB in CC and DNR in SC (Table S3.1). The tremor-triggering and nontriggering events were marked by shaded and open symbols, respectively. A total of 42 earthquakes were selected among the three regions. The numbers mark the

measurements of 12 triggering events in CC. The background noise level of each event is calculated from a 600-s time window before the arrival of the predicted P-wave. The correlation coefficient (c.c.) and slope of the fitting line between the median tremor amplitudes and the PGVs for tremor and nontremor in each region are marked in (a–c). The light gray background shows the median noise level for all events. The horizontal dotted lines in (a–c) mark the 1.5 times of the median noise level in each region. The vertical dotted lines in (a, d) show the apparent triggering amplitude threshold of 0.03 cm/s in CC (Peng *et al*., 2009). The horizontal dotted lines in (d–f) marks the 1.5 of the SNR.

3.4 Triggering Waves, Triggered Tremor, and Background Noise Level

To quantify the relationship between amplitudes of triggering waves and triggered tremor, we compared the PGV of teleseismic waves with the median amplitudes of the high-frequency signals during the arrival of large-amplitude surface waves, and preevent noise (Chao *et al*. 2012d) recorded at the broadband stations PKD, RDM, and MHC in the CC, SC, and NC regions, respectively (Fig. 3.5). We computed the median amplitudes of both triggered tremor signals and nontriggering records from the three-component 2–8-Hz band-pass-filtered envelope functions, as well as the median amplitudes of noise during the 600-s before the predicted P-wave (or first PKP-type-wave) arrival. We adopted median, rather than mean or maximum amplitude to suppress the impulsive signals generated by local earthquakes or other nontremor sources. In the cases when the signals during the surface waves were not well recorded at the three aforementioned stations, we measured the PGVs and amplitudes from nearby broadband stations instead (marked with asterisks in Fig. 3.5a,b; Table S3.1).

For the 10 (i.e., excluding two measurements from nearby stations) tremor-triggering events recorded at PKD in CC (Fig. 3.5a), we found a positive correlation between the median tremor amplitudes and the PGVs of the Love waves measured from the transverse

component. The fitting line has a slope of 0.6 in log–log scale (correlation coefficient is 0.74), and the corresponding p-value equals 0.0144. The result indicates a 1.44% chance for the correlation between the x axis and y axis to be random, suggesting that the correlation is significant at more than 95% confidence level. In comparison, we found no evident correlation for the nontriggering events between PGVs of teleseismic surface waves and the median amplitudes of band-pass-filtered seismograms (with slope of 0.17, correlation coefficient of 0.22, and p-value of 0.2427). We measured the PGVs from the transverse components mainly because the tremor around the SAF shows higher correlations with the fault-parallel shear stresses induced by the Love waves (Peng *et al*., 2009; Hill, 2010). A similar positive correlation is shown by the PGVs measured from the vertical component (Fig. S3.2). We also corrected for the effects of geometrical spreading and attenuation with a constant Q of 100 (Fig. S3.3), based primarily on the triggered tremor locations reported in Peng *et al*. (2009) (Table S3.2). For the triggered tremor since 2009 (namely the 2009 Mw 8.1 Samoa and 2010 Mw 8.8 Chile earthquakes), we used the centroid location from the triggered low-frequency earthquakes (Shelly *et al*., 2011) during the arrival time of large-amplitude surface waves (Table S3.2). Figure S3.3 shows that their correlations remain largely unchanged with and without corrections, mainly because the majority of the triggered tremor occurred near Cholame and their hypocentral distances to station PKD are similar.

Figure 3.5 shows that the median background noise levels for all events are 4.85, 6.95, and 11.5 nm/s in CC, SC, and NC, respectively. The smallest amplitude of the triggered tremor in CC is 5.7 nm/s (associated with the 2001 Kunlun earthquake), which

is close to 1.5 times the median background noise level. We found that a signal-to-noise ratio (SNR) of 1.5 provides a reasonable threshold to separate most triggering events from nontriggering ones in the three regions (Fig. 3.5d–f). For events with lower SNR, the high-frequency tremor amplitude during the surface waves can be very close to the background noise level, which might interfere with the identification of possible triggered tremor.

3.5 Discussions and Conclusions

In this study we have systematically examined deep tremor triggered by large teleseismic earthquakes between 2001 and 2010 in three tectonically active regions along the SAF system. Our results revealed a marked difference in triggering behavior in California. In CC, 12 out of 42 large teleseismic events triggered tremor along the Parkfield–Cholame segment of the SAF. In comparison, only the 2002 Denali fault earthquake has triggered tremor around the CF in NC and the SJF in SC. In these two regions, the tremor was initiated by the Love waves and then intensified during the large-amplitude Rayleigh waves. In addition, tremor in this case occurred only when the particle velocity of the Love wave is to the southwest (positive value in Fig. 3.2), which produced right-lateral shear stress along the fault strike. The process is similar to that observed in CC (Peng *et al*., 2008; Peng *et al*., 2009). These observations suggest that triggered tremor in NC and SC was also the result of shear failure at depth driven by dynamic stresses from large-amplitude surface waves. Finally, the tremor amplitude has a positive correlation with the PGVs of the triggering waves in CC, further supporting the clock-advance model (Gomberg, 2010).

Because the PGVs of the triggering waves observed at three regions are similar, the associated dynamic stresses and deformation should be essentially the same. Hence, the variable triggering behavior observed in these regions could be largely attributed to background noise levels, background tremor rates, or frictional properties of the fault. As shown in Figure 3.5, the background noise levels measured at three broadband stations in each region are somewhat different. Station PKD in CC has the lowest background noise, while station MHC in NC has the highest. It is worth noting that the Parkfield–Cholame section of the SAF has high-quality and low-noise borehole sensors that are part of the High Resolution Seismic Network (HRSN). They are helpful in identifying triggered tremor with relatively weak signals in CC. However, the Plate Boundary Observatory (PBO) borehole stations were installed in SC after 2006. Although these stations have similar qualities to HRSN, they did not record any triggered tremor associated with the 23 teleseismic earth-quakes (six of them triggered tremor in CC). For example, the 2010 Chile earthquake produced the second largest PGV but only triggered tremor in CC (Peng *et al*., 2010), despite the fact that SC is slightly closer to the Chile mainshock and has larger PGV.

If we extrapolate the positive relationship between the PGVs and amplitudes of triggered tremor in CC to NC and SC, the maximum tremor amplitudes would be associated with the Denali fault event (Fig. 3.5b,c). In addition, the corresponding triggered tremor amplitudes for smaller PGVs in NC and SC would be much lower than the background noise levels. Hence, even if tremor was triggered by teleseismic events

other than the Denali fault earthquake in NC and SC, the tremor amplitude would be overwhelmed by the noise amplitude. In this case, the signals would not be coherent among different stations and would not be possibly identified by our visual inspection. In addition, if the preevent noise level in CC is set to be that of NC, 6 out of the 12 observed triggering cases would become invisible. This indicates that at least some difference in observations of triggering behavior is due to the background noise levels. Recent studies have shown that additional triggered tremor could be identified in NC and SC based on waveform matched filter techniques (Aguiar *et al*., 2009; Brown, 2010). However, further analysis (A. Aguiar and J. Brown, personal comm., 2011) also revealed that the Denali fault earthquake was the only teleseismic earthquake that has triggered tremor in these regions. These results suggest that while additional triggered tremor may exist in NC and SC, their amplitudes are smaller and hence closer to or hidden by the background noises. In other words, it will require more advanced signal processing techniques to identify such signals if they exist.

It is worth noting that the maximum difference in the background noise levels at these regions is less than a factor of 3, which cannot explain a factor of 10 difference in the amplitude of tremor triggered by the Denali fault earthquake. To further demonstrate this, we compared the spectra during the surface waves of the Denali fault earthquake and the preevent background noises in three regions (Fig. 3.6a). While the shape of the surface wave spectra in the frequency range of 0.01–0.2 Hz (5–100 s) are quite similar, the high-frequency signals (>2 Hz) are different in these regions. Hence, some differences were apparently caused by the different background noise. For example, station RDM

appeared to record high background noise at frequencies of >10 Hz. However, even after we removed the contribution from the preevent noise (assuming the noise spectra is stationary; Fig. 3.6b), we still found a factor of ~10 difference (Fig. 3.6c) in the spectra in the frequency range of tremor observation (2–8 Hz). The result again suggests that the background noise level likely contributes to, but is not the primary cause of, the different triggering behaviors.

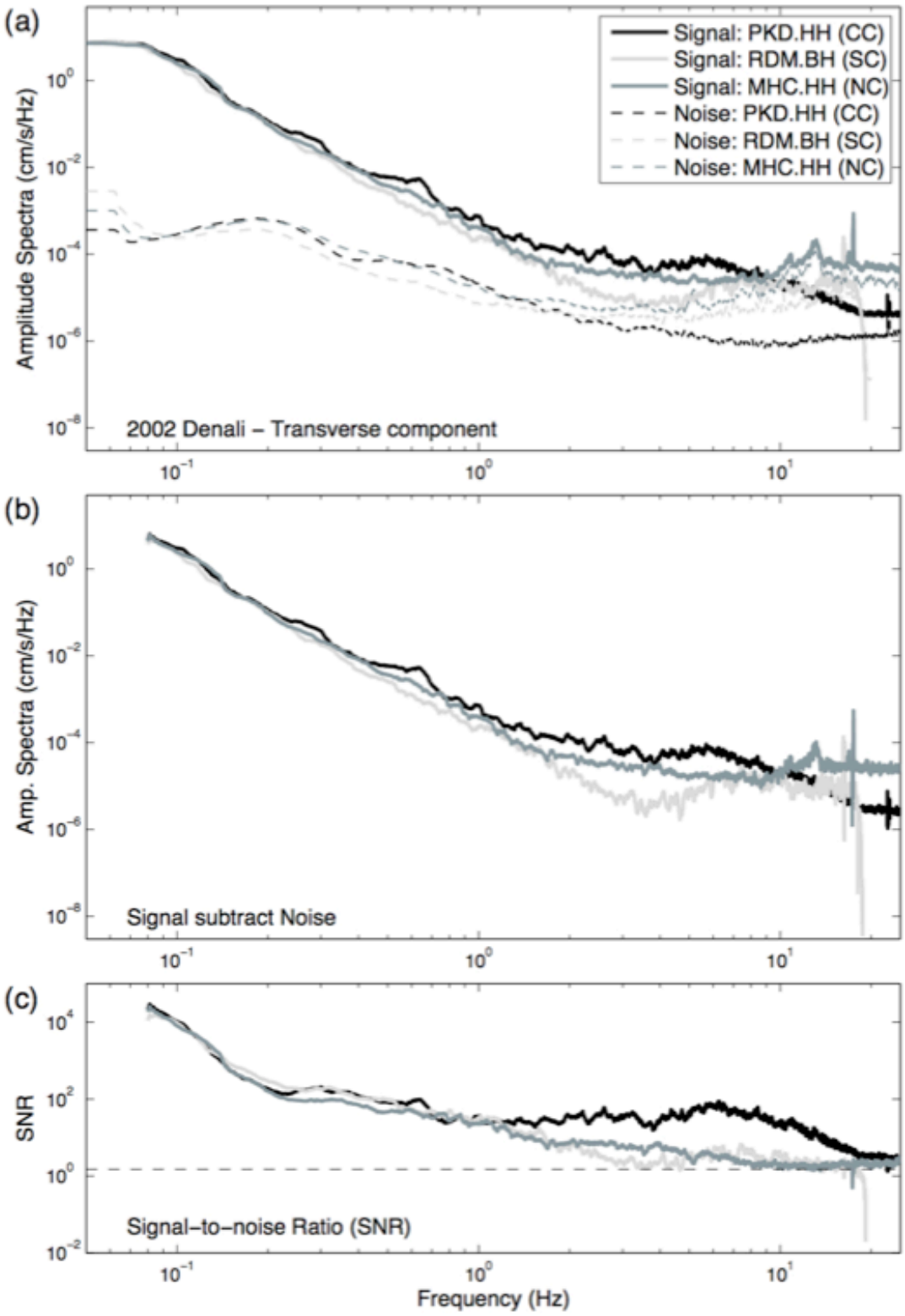

Figure 3.6 (a) Comparison of signal (solid line) and noise (dotted line) spectra in transverse velocity component at stations PKD in central California (CC), RDM in

southern California (SC), and MHC in northern California (NC) for the 2002 Denali fault earthquake. The BH- channel (40-Hz sampling rate) data at RDM are used for computing the noise spectra due to lack of long-enough HH-channel (100-Hz sampling rate) data before the P-wave. **(b)** The spectral difference after subtracting the noise from the signal spectra. **(c)** The signal-to-noise ratio (SNR) spectra.

In addition to background noise, the differences in tremor amplitudes could also be due to the path or site effects. For example, it is possible that in the frequency band of 2–8 Hz, the path and site effect in CC could amplify higher ground motions than in SC and NC. Because we did not have accurate path and site information in these regions, we randomly chose two microearthquakes in each region from the magnitude range of 1.5–2 within 10 km from the tremor source of the Denali fault earthquake in three regions (Table S3.3). These events were used as an empirical Green's function to demonstrate the path and site effects. The computed stress drops in CC and SC are compatible (Allmann and Shearer, 2007; Shearer *et al*., 2006). Hence, we assumed that these events have similar source spectra. We computed the S-wave spectra for 10 s, starting 1 s before the S-wave arrivals, and the noise spectra for 10 s before the P-wave arrivals. Figure S3.4 shows that the S-wave spectra around 2 Hz are compatible in three regions. The spectra at station RDM is higher for frequency $f > 10$ Hz, which is either due to the high background noise level or site amplification effects. In summary, the path and site effects also cannot completely explain the difference in tremor amplitudes for the frequency range of 2–8 Hz in these regions.

In addition to the amplitude of the triggering surface wave, another important parameter that controls the rate and amplitude of the triggered events is the unperturbed or background tremor rate (Gomberg 2010). Ambient tremor is very active in CC

(Nadeau and Dolenc, 2005; Nadeau and Guilhem, 2009; Shelly *et al*., 2011), while ambient tremor has not been detected with current instrumentation (J. P. Ampuero, personal comm., 2011). So far there have been no ambient tremor reports in NC. The fact that the ambient tremor activities in CC occur hourly to daily (Nadeau and Guilhem, 2009) indicates that many tremor patches could be on the verge of slipping and hence are prone to be triggered by the next coming large-amplitude surface waves. On the contrary, the lack of widespread ambient tremor in NC and SC suggests that either fewer tremor patches are ready to be triggered or that the patches need higher (longer) loading stress in order to reach their failure stage. Hence, the lack of widespread triggering of tremor in NC and SC is likely related to the low or absent background tremor rate in these regions.

The exact reason for different triggering and ambient tremor rates in these regions is still not clear (Peng and Gomberg, 2010; Beroza and Ide, 2011). Ellsworth (2008) suggested that triggered tremor in CC and NC might be associated with serpentinized fossil oceanic crust in these regions. However, such inference is rather speculative at this stage. Systematic searches for triggered and ambient tremor elsewhere, along with detailed analysis of the geophysical and material properties at tremor depth, are needed to further identify essential factors for tremor generation.

3.6 Data and Resources

Seismograms used in this study were downloaded from the Northern California Earthquake Data Center (http://www.ncedc.org/, last accessed May 2011) and the Southern California Earthquake Data Center (http://www.data.scec.org/, last accessed May 2011).

3.7 Supplement Tables and Figures

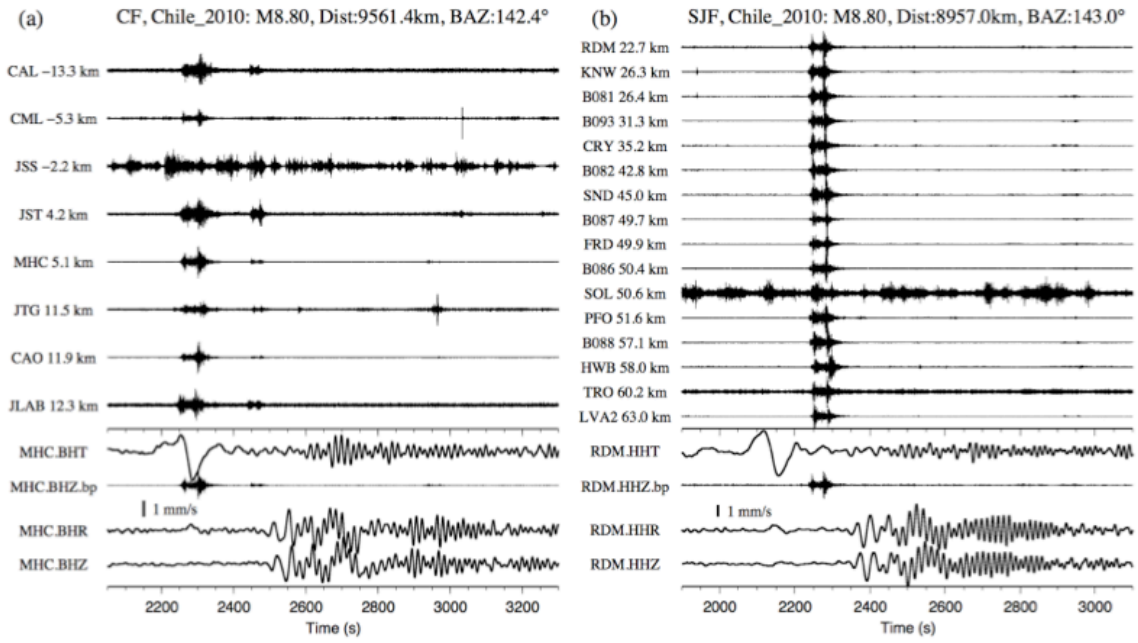

Figure S3.1 (a) (Top) 2-8 Hz band-pass-filtered vertical seismograms showing the triggered earthquake signals in Coso by the 2010 Mw8.8 Chile earthquake at the Calaveras Fault (CF) in Northern California (NC). The seismograms are plotted along the strike of the CF, with northwest at the top and southeast on the bottom. The along-strike distance to the tremor source in NC triggered by the 2002 Mw 7.9 Denali Fault earthquake, and the station names are marked by the seismograms. The event name and the occurrence year, its magnitude (M), and the epicenter distance (Dist) and back azimuth (BAZ) relative to the broadband station are shown on the top. (Bottom) A comparison between the instrument-corrected transverse (T), radial (R), and vertical (Z) velocity seismograms and the 2-8 Hz band-pass-filtered seismograms recorded at the broadband station MHC. The zero time corresponds to the origin time of the mainshock. The velocity seismograms have been time-shifted back to the tremor sources. The adjusted times of Love waves (in T component), Rayleigh waves (in R and Z components), and tremor are marked below the station names. The thick vertical bar

marks the amplitude scale of surface waves. **(b)** (Top) 2-8 Hz band-pass-filtered vertical seismograms showing the triggered earthquake signals in Coso by the 2010 Mw8.8 Chile earthquake at the San Jacinto fault (SJF) in the Anza network in Southern California (SC). The seismograms are plotted along the strike of the SJF to the tremor source in SC triggered by the 2002 Mw 7.9 Denali Fault earthquake, with northwest at the top and southeast on the bottom. (Bottom) A comparison between the velocity and the 2-8 Hz band-pass-filtered seismograms recorded at the broadband station RDM. Other notations are the same as in Figure S1a.

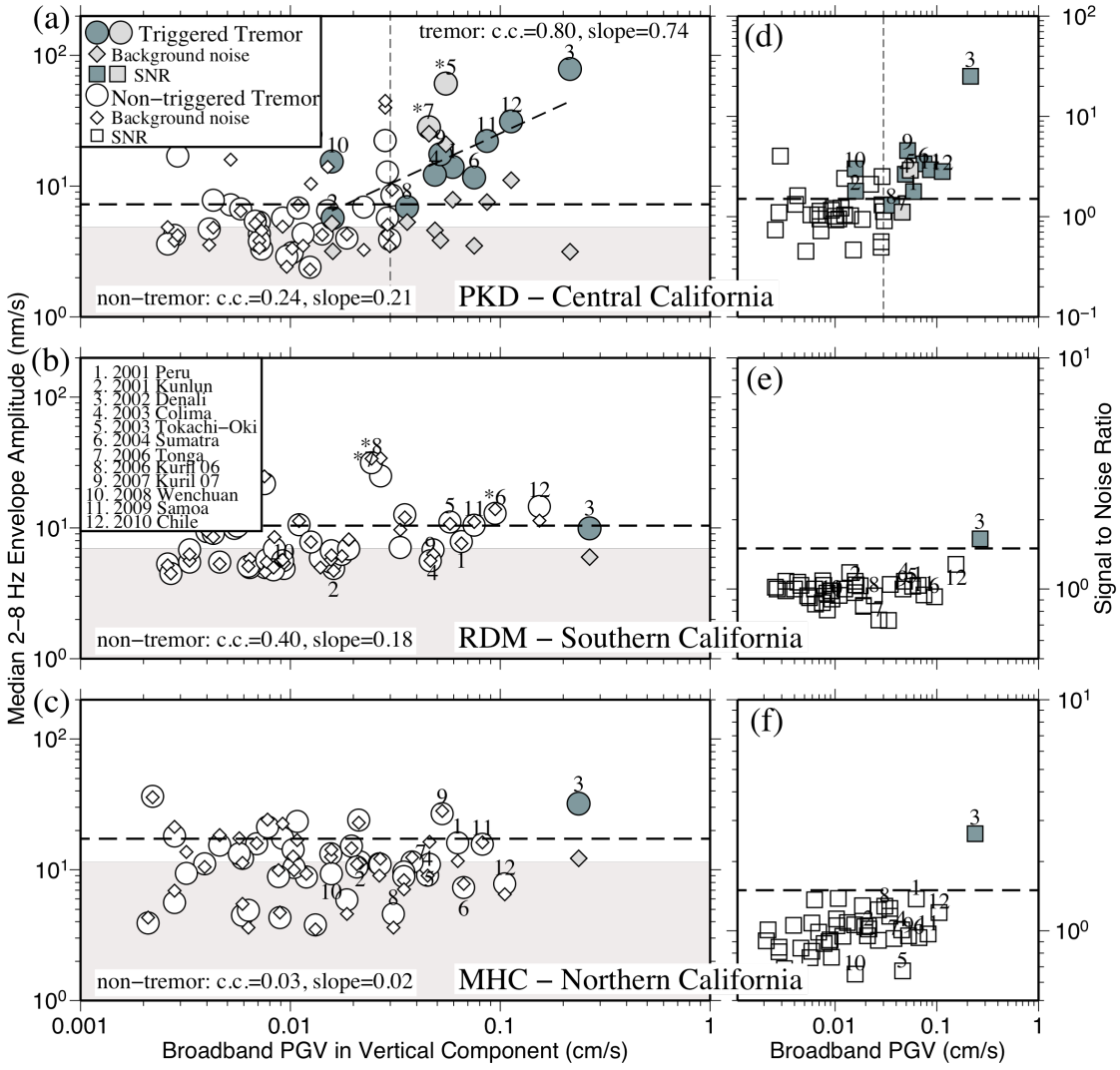

Figure S3.2 Maximum peak ground velocity (PGV) of surface wave (horizontal axis) in vertical component versus median amplitude (vertical axis) of the 2-8 Hz 3-components band-pass-filtered envelope functions during the surface waves **(a-c)** and signal to noise

ratio (SNR) **(d-f)** at broadband stations PKD, RDM, and MHC in Central California (CC), Southern California (SC), and Northern California (NC), respectively. The event number with star symbol (*) indicates the measurement is from the nearby station FROB in CC and DNR in SC (Table S3.1). The tremor-triggering and non-triggering events were marked by shaded and open symbols, respectively. A total of 42 earthquakes were selected among the three regions. The numbers mark the measurements of 12 triggering events in CC. The background noise level of each event is calculated from a 600-s time window before the arrival of the predicted P-wave. The correlation coefficient (c.c.) and slope of the fitting line between the median tremor amplitudes and the PGVs for tremor and non-tremor in each region are marked in (a-c). The light gray background shows the median noise level for all events. The horizontal dotted lines in (a-c) mark the 1.5 times of the median noise level in each region. The vertical dotted lines in (a, d) show the apparent triggering amplitude threshold of 0.03 cm s-1 in CC (Peng *et al*., 2009). The horizontal dotted lines in (d-f) marks the 1.5 of SNR.

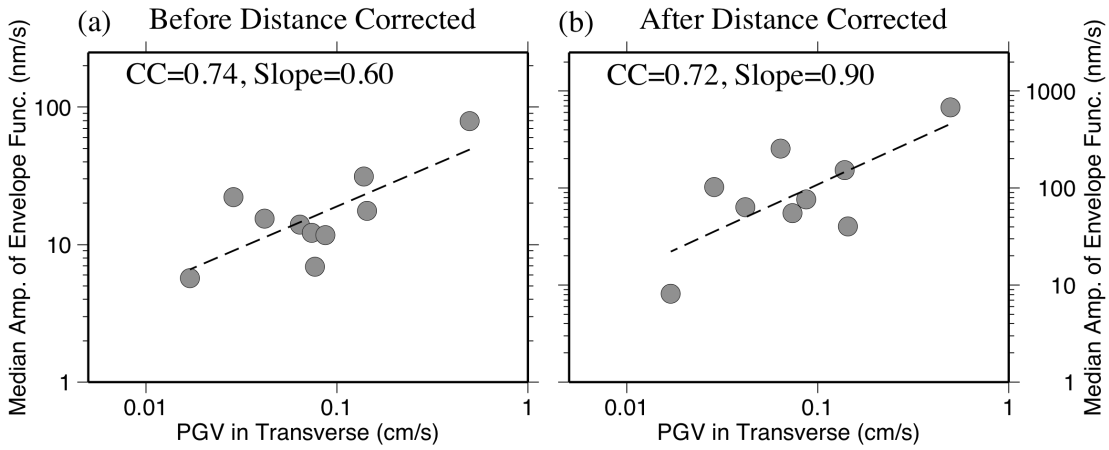

Figure S3.3 Tremor amplitude versus PGV in Central California (CC) before **(a)** and after **(b)** distance correction.

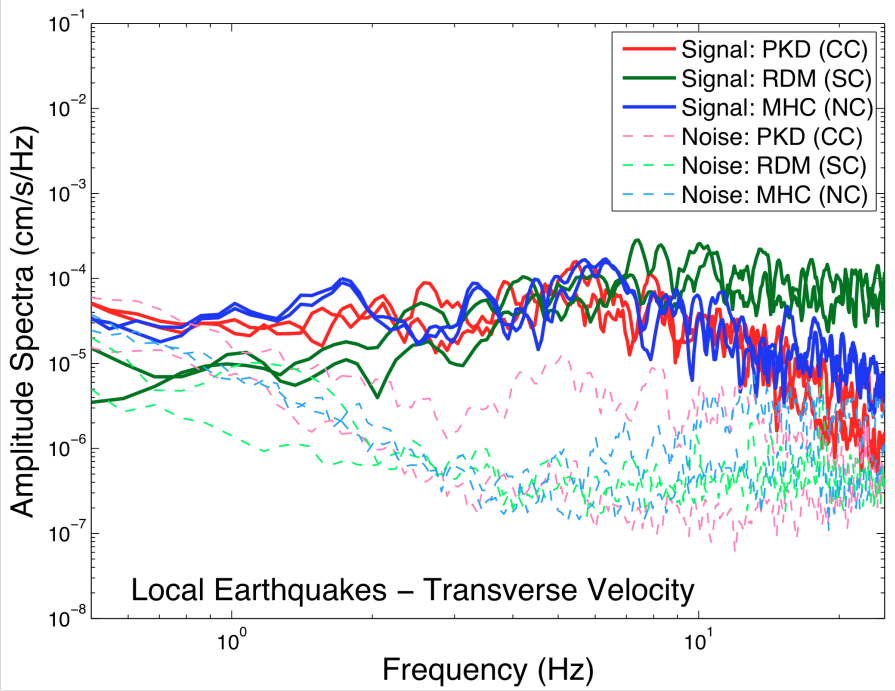

Figure S3.4 S-wave spectra of local earthquakes (thick lines) and the corresponding noise spectra (dotted lines) recorded at stations PKD, RDM, and MHC in Central California (CC), Southern California (SC), and Northern California (NC), respectively.

Table S3.1 List of the information and measured parameters for all 42 teleseismic earthquakes used in this study. See the title within the file for the details of each field. Online version: http://www.seismosoc.org/publications/BSSA_html/bssa_102-2/2011151-esupp/Table_S1.txt

```
#  1          2   3  4  5  6    7      8          9        10     11   12      13      14      15      16     17   18   19
#  evid       yr  mo dy hr mi   sec    lon        lat      depth  mag  dist    BAZ    PGV_BHT PGV_BHZ signal  noise Q Comments
199803250312 1998 03 25 03 12 25.0700  149.52701 -62.87700 10.00 8.10  9884.26 167.20  0.0166 0.0331   19.90  22.10 0
199811291410 1998 11 29 14 10 31.9600  124.89101  -2.07100 33.00 7.70  2841.88 170.09  0.1500 0.1410   28.70   9.10 1 Ceram_Sea
199908170001 1999 08 17 00 01 39.1300   29.86400  40.74800 17.00 7.70  8421.36 308.38  0.0192 0.0123   25.50  31.00 0
199909301631 1999 09 30 16 31 15.6900  -96.93101  16.05900 60.60 7.50 14048.63  46.69  0.0037 0.0031   23.40  27.90 0
199911261321 1999 11 26 13 21 15.5700  168.21400 -16.42300 33.00 7.50  6784.12 125.90  0.0116 0.0083   11.10  11.40 0
200005040421 2000 05 04 04 21 16.2100  123.57301  -1.10500 26.00 7.60  2716.18 172.87  0.0497 0.0401   29.90  17.50 0
200006041628 2000 06 04 16 28 26.1700  102.08701  -4.72100 33.00 7.90  3693.58 215.35  0.0977 0.0595   22.80   8.80 0 Sumatra_00
200006181444 2000 06 18 14 44 13.3100   97.45300 -13.80200 10.00 7.90  4813.83 213.89  0.0322 0.0382   32.50  35.80 0
200011160454 2000 11 16 04 54 56.7400  152.16901  -3.98000 33.00 8.00  4559.99 127.32  0.0511 0.0248   28.00  21.90 0
200011160742 2000 11 16 07 42 16.9300  153.10201  -5.23300 30.00 7.80  4730.01 127.73  0.0413 0.0670   54.60  35.70 0
200011172101 2000 11 17 21 01 56.4900  151.78101  -5.49600 33.00 7.80  4644.48 129.37  0.0230 0.0124   10.80   9.50 0
200101010657 2001 01 01 06 57  4.1700  126.57900   6.89800 33.00 7.50  1921.85 159.73  0.0304 0.0156   50.90  20.80 0
200101131733 2001 01 13 17 33 32.3800  -88.66000  13.04900 60.00 7.70 14887.09  41.41  0.0122 0.0094    9.70   9.80 0
200106232033 2001 06 23 20 33 14.1300  -73.64101 -16.26500 33.00 8.40 18331.80  65.04  0.0396 0.0263   19.40  18.60 0 Peru
200107070938 2001 07 07 09 38 43.5200  -72.07700 -17.54300 33.00 7.60 18545.79  66.64  0.0054 0.0050   11.60  55.10 0
200110190328 2001 10 19 03 28 44.4600  123.90701  -4.10200 33.00 7.50  3049.28 172.89  0.0385 0.0107   25.60  20.20 0
200111140926 2001 11 14 09 26 10.0100   90.54101  35.94600 10.00 7.80  3214.65 302.70  0.8350 0.2680   65.20  18.00 1 Kunlun
200203052116 2002 03 05 21 16  9.1300  124.24901   6.03300 31.00 7.50  1947.99 167.96  0.0398 0.0188   18.40  11.60 0
200209081844 2002 09 08 18 44 23.7100  142.94501  -3.30200 13.00 7.60  3807.74 137.65  0.0220 0.0174   12.10  11.80 0
200210101050 2002 10 10 10 50 20.5700  134.29701  -1.75700 10.00 7.60  3140.11 150.06  0.0535 0.0207   20.40  23.30 0
200211032212 2002 11 03 22 12 41.5180 -147.45290  63.51410  4.20 7.90  7812.45  28.43  0.0138 0.0134   17.00  13.00 0 Denali
200301220206 2003 01 22 02 06 34.6100 -104.10400  18.77000 24.00 7.60 13292.22  50.04  0.0080 0.0067   43.60  42.20 0
200307152027 2003 07 15 20 27 50.5300   68.38200  -2.59800 10.00 7.60  6338.22 250.35  0.0311 0.0348   12.80  11.60 0
200309251950 2003 09 25 19 50  6.3600  143.91000  41.81500 27.00 8.30  2980.21  40.94  0.2790 0.1600   56.50  14.80 1 Tokachi_Oki
200311170643 2003 11 17 06 43  6.8000  178.65001  51.14600 33.00 7.80  5810.11  42.51  0.0219 0.0255   23.70  26.40 0
200411112126 2004 11 11 21 26 41.1500  124.86800  -8.15200 10.00 7.50  3506.31 171.96  0.0230 0.0548   18.10  12.30 0
200412231459 2004 12 23 14 59  4.4100  161.34500 -49.31200 10.00 8.10  8992.29 154.38  0.0565 0.0221   10.20   9.90 0
200412260058 2004 12 26 00 58 53.4500   95.98200   3.29500 30.00 9.00  3452.46 233.83  0.5960 0.6860  198.20  41.70 1 Sumatra_04
200503281609 2005 03 28 16 09 36.5300   97.10800   2.08500 30.00 8.60  3453.15 230.64  0.1600 0.1760   46.40  10.20 1 Nias_Sumatra
200509090726 2005 09 09 07 26 43.7300  153.47401  -4.53900 90.00 7.70  4708.35 126.61  0.0029 0.0023   23.60  22.80 0
200510080350 2005 10 08 03 50 40.8000   73.58801  34.53900 26.00 7.60  4707.62 296.23  0.1720 0.0566   21.30  19.80 0 Pakistan
200604202325 2006 04 20 23 25  2.1500  167.08900  60.94900 22.00 7.60  5479.28  27.83  0.0384 0.0684   72.80  29.60 0
200605031526 2006 05 03 15 26 40.2900 -174.12300 -20.18700 55.00 8.00  8550.78 118.86  0.0158 0.0252   14.00  14.60 0 Tonga
200607170819 2006 07 17 08 19 26.6800  107.41901  -9.28400 20.00 7.70  3877.25 203.24  0.0065 0.0083   77.70  65.20 0
200611151114 2006 11 15 11 14 13.5700  153.26601  46.59200 10.00 8.30  3896.18  40.38  0.0992 0.0653   18.20  12.10 0 Kuril_06
200701130423 2007 01 13 04 23 21.1600  154.52400  46.24300 10.00 8.10  3961.58  41.64  0.1200 0.1040   65.50  23.00 1 Kuril_07
200701211127 2007 01 21 11 27 45.0600  126.28201   1.06500 22.00 7.50  2532.36 165.26  0.0743 0.0286   24.10  10.70 0
200704012039 2007 04 01 20 39 56.3800  157.04401  -8.46000 10.00 8.10  5291.57 127.31  0.1070 0.0342   65.80  22.60 1 Solomon
200708152340 2007 08 15 23 40 57.8900  -76.60300 -13.38600 39.00 8.00 17893.43  61.88  0.0104 0.0123   56.70  49.10 0 Peru
200709121110 2007 09 12 11 10 26.8300  101.36700  -4.43800 34.00 8.40  3710.63 216.73  0.1210 0.1170   49.40  25.60 1 Sumatra_07
200709122349 2007 09 12 23 49  3.7200  100.84100  -2.62500 35.00 7.90  3578.94 219.41  0.0569 0.0704   31.40  31.10 0
200711141540 2007 11 14 15 40 50.4700  -69.86900 -22.20400 40.00 7.70 18930.91  85.62  0.0065 0.0073    9.20  10.00 0
200805120628 2008 05 12 06 28  1.5700  103.32201  31.00200 19.00 7.90  1912.00 300.22  0.6710 0.7130  290.80  50.70 1 Wenchuan
200901031943 2009 01 03 19 43 50.6500  132.88500  -0.41400 17.00 7.60  2937.08 151.50  0.0257 0.0166    7.20   6.00 0
200903191817 2009 03 19 18 17 40.9100 -174.65900 -23.04600 34.00 7.60  8668.23 121.61  0.0393 0.0619   30.90  35.50 0
# Earthquake parameters of the 45 teleseismic events analyzed in this study.
# The earthquake catalog information (origin time, location, and magnitude)
# is obtained from the Advanced National Seismic System (ANSS) catalog.
# The epicentral distance and back-azimuth (BAZ) is computed relative to
# the broadband station TPUB (stlo: 120.63, stla: 23.3005).
# The peak ground vertical (PGV_BHZ) and transverse (PGV_BHT) velocity are
# measured from the broadband recording by station TPUB, and are in the unit
# of cm/s. The median amplitude of signal and noise are in the unit of nm/s.
# The quality (Q) 1 marks events that trigger tremor around southern Central Range of Taiwan
# 0 marks those that do not.
```

Table S3.2 List of triggered tremor locations used in this study.
Online version:
http://www.seismosoc.org/publications/BSSA_html/bssa_102-2/2011151-esupp/Table_S2.txt

```
##############################################
# Triggered tremor locations
##############################################
# in central California (CC)
# 2001 to 2008, from Peng et al, JGR 2009
200106232033 -121.09 36.42 24.0
200111140926 -121.12 36.42 19.0
200111140926 -120.57 36.02 31.0
200211032212 -120.84 36.36 15.0
200211032212 -120.28 35.68 24.0
200301220206 -120.27 35.69 16.0
200301220206 -120.22 35.60 24.0
200301220206 -120.26 35.60 20.0
200309251950 -120.53 36.19 24.0
200309251950 -120.56 36.09 60.0
200309251950 -120.27 35.70 23.0
200309251950 -120.28 35.59 30.0
200412260058 -120.82 36.30 25.0
200412260058 -120.23 35.60 25.0
200701130423 -120.62 36.12 26.0
200701130423 -120.72 36.19 23.0
200805120628 -120.28 35.69 22.0
200805120628 -120.30 35.70 23.0
200805120628 -120.31 35.72 23.0
200805120628 -121.09 36.41 24.0
200805120628 -120.28 35.70 21.0
# 2009 to 2010, from LFE catalog by David Shelly
200909290634 -120.26 35.69 23.4
201002270634 -120.25 35.68 24.0
##############################################
# in southern California (SC)
# from Gomberg et al, Science, 2008
200211032212 -116.98 33.81 14.0
##############################################
# in nothern California (NC)
# from Gomberg et al, Science, 2008
200211032212 -121.72 37.34 15.0
##############################################
```

Table S3.3 List of local earthquakes used in Figure S3.4.
Online version:
http://www.seismosoc.org/publications/BSSA_html/bssa_102-2/2011151-esupp/Table_S3.txt

```
# yy/mm/dd hr/mi/sec   mag  dep   lon     lat     dist(CC)
2006/02/04 04:58:19.83 1.85  7.0 -120.327 35.730  6.99
2006/03/18 09:20:26.38 1.94 11.5 -120.356 35.744  9.89
# yy/mm/dd hr/mi/sec   mag  dep   lon     lat     dist(SC)
2009/08/20 12:38:17.10 1.54 15.3 -116.978 33.743  7.43
2009/11/15 22:39:13.03 1.59 13.9 -116.973 33.798  1.48
# yy/mm/dd hr/mi/sec   mag  dep   lon     lat     dist(NC)
2008/04/20 19:22:07.33 1.70  8.2 -121.757 37.410  8.40
2008/06/27 03:53:29.55 1.70  8.6 -121.756 37.410  8.40
# note:
# dist: the epicentral distance to the tremor location triggered
# by the 2002 Denali earthquake (Gomberg et al., Science, 2008)
```

CHAPTER 4 (Chao *et al*., 2012b)

GLOBAL SEARCH OF TRIGGERED TREMOR FOLLOWING THE 2011 MW9.0 TOHOKU-OKI EARTHQUAKE

Summary

The 2011 Mw9.0 Tohoku-Oki, Japan earthquake triggered deep tectonic tremor and shallow microearthquakes in many places around the world. Here we conduct a systematic survey of triggered tremor in regions where ambient or triggered tremor has been previously identified. We find triggered tremor in the following regions: South-Central Alaska, the Aleutian Arc, Shikoku in southwest Japan, the North Island of New Zealand, the Parkfield-Cholame section of the San Andreas Fault in central California, the San Jacinto Fault in southern California, Taiwan, and the Vancouver Island. The only exceptions are the Calaveras Fault in northern California, Costa Rica, and Guerrero, Mexico. Such a widespread triggering of tremor occurs as a result of large amplitude surface waves (minimum peak value of ~0.1 cm/s) and the associated dynamic stresses (at least ~10 kPa), which appears to be one of the most important factors in controlling the triggering threshold. The incident angles of the teleseismic surface waves also affect the triggering potentials of the Love and Rayleigh waves, and we find that both Love and Rayleigh waves contribute to triggering tremor in many regions. Triggered tremor generally locates around regions where previous ambient and/or triggered tremor have been identified, further supporting the notion that triggered and ambient tremor share similar mechanisms but with different driving forces. We find a positive relationship between the amplitudes of the triggering waves and those of the triggered tremor, which

is consistent with the prediction of the clock-advance model. Our systematic survey suggests that the timing and amplitude of the triggered tremor could be somewhat predictable, if we know the amplitude and period of the surface waves and the associated time-varying dynamic stresses.

4.1 Introduction

Following the first observation of deep non-volcanic tremor at the Nankai subduction zone in southwest Japan (Obara, 2002), tremor has been observed worldwide in different tectonic settings (Beroza and Ide, 2011; Peng and Gomberg, 2010, and references therein). Tremor occurs spontaneously (also known as ambient tremor) or accompanying slow-slip events (Rogers and Dragert, 2003), locates mostly below the brittle-ductile transition zone, and has extended source duration and non-impulsive arrivals that lack of high-frequency content as compared with regular earthquakes in the brittle upper crust. In addition, tremor can be instantly triggered by the dynamic stresses from regional or teleseismic earthquakes (Gomberg *et al*., 2008; Miyazawa and Mori, 2006; Rubinstein *et al*., 2007). Many recent studies suggest that triggered and ambient tremor share many similar characteristics. For instance, triggered tremor is mostly located in regions where ambient tremor is found (Peng and Gomberg, 2010), and their spectra shapes are similar (Peng *et al*., 2008; Rubinstein *et al*., 2007). In addition, at least part of the triggered tremor consists of many low-frequency earthquakes (LFEs) that also occur during ambient tremor (Peng *et al.*, 2010a; Shelly *et al.*, 2011).

Peng and Gomberg (2010) summarized observations around the world and suggested that teleseismically induced dynamic stresses on the order of several kilopascals (kPa) are capable of triggering tremor. However, triggering threshold appears variable in different regions. For example, the apparent triggering threshold is about 2-3 kPa at the Parkfield-Cholame section of the San Andreas Fault (SAF) (Peng *et al*., 2009), but is about 8-10 kPa beneath the Central Range (CR) in Taiwan (Chao *et al*., 2012d). It is still not clear whether such a difference is caused by different instrumentation or different tremor behavior.

Different models exist for the relationship between triggered and ambient tremor. Gomberg (2010) proposed a clock-advance model where triggered tremor is considered to be sped-up ambient tremor while the perturbed stress from surface waves reaches the failure threshold of the tremor patch. In particular, the instantaneous perturbed rate is proportional to the background rate and a function describes how the perturbing stress changes the failure time of a fault patch (Gomberg, 2010). Gomberg (2010) also examined the relationship between the amplitudes of the triggering waves and triggered tremor for 4 observations in Cascadia (Rubinstein *et al*., 2009), and found that the results did not match the predictions of the clock-advance model. In comparison, Chao *et al*. (2012d) found a positive relationship between the amplitudes of surface waves from 9 teleseismic earthquakes and those of triggered tremor beneath the CR in Taiwan. In addition, Chao *et al.* (2012a) compared triggered tremor observed in the Parkfield-Cholame section of the SAF with the San Jacinto Fault (SJF) in southern California and the Calaveras Fault (CF) in northern California. They suggested that the abundant

triggered tremor observations in Parkfield and the relative lack of triggered tremor observations in the other two regions could be related to their different background tremor rates. Those results suggest that further studies are needed to better understand the relationship between the triggering surface wave, triggered tremor, and background tremor rate.

The 2011 Mw9.0 Tohoku-Oki, Japan earthquake triggered widespread shallow earthquakes and deep tremor activities at many places around the world (Chao *et al*., 2011; Gonzalez-Huizar *et al*., 2012; Hill *et al*., 2012; Miyazawa, 2011; Rubinstein *et al*., 2011; Wang *et al*., 2011). These observations provide a new opportunity to test the prediction of the clock-advance model (Gomberg, 2010), and to better understand the triggering mechanisms and conditions for tremor generation. In this study, we systematically examine triggered tremor during the surface waves of the Tohoku-Oki mainshock in many regions where ambient or triggered tremor have been previously observed (Figure 4.1). These include Alaska (Peterson and Christensen, 2009), Aleutian Arc (Peterson *et al*., 2011), Nankai in southwest Japan (Obara, 2002), the north island of New Zealand (Fry *et al*., 2011; Ide, 2012), the Parkfield-Cholame section of the SAF in central California (Nadeau and Dolenc, 2005; Peng *et al*., 2009), the CF in northern California and the SJF in southern California (Chao *et al*. 2012a; Gomberg *et al*., 2008), Taiwan (Chao *et al*., 2012d)., and Cascadia (Gomberg *et al*., 2010; Rubinstein *et al*., 2009). In the following sections, we first show the observations and locations of triggered tremor in each region. Then, we calculate the dynamic stresses of surface waves at

different tectonic settings and estimate their triggering potentials. Finally, we discuss the prediction of the clock-advance model and the implications of our observations.

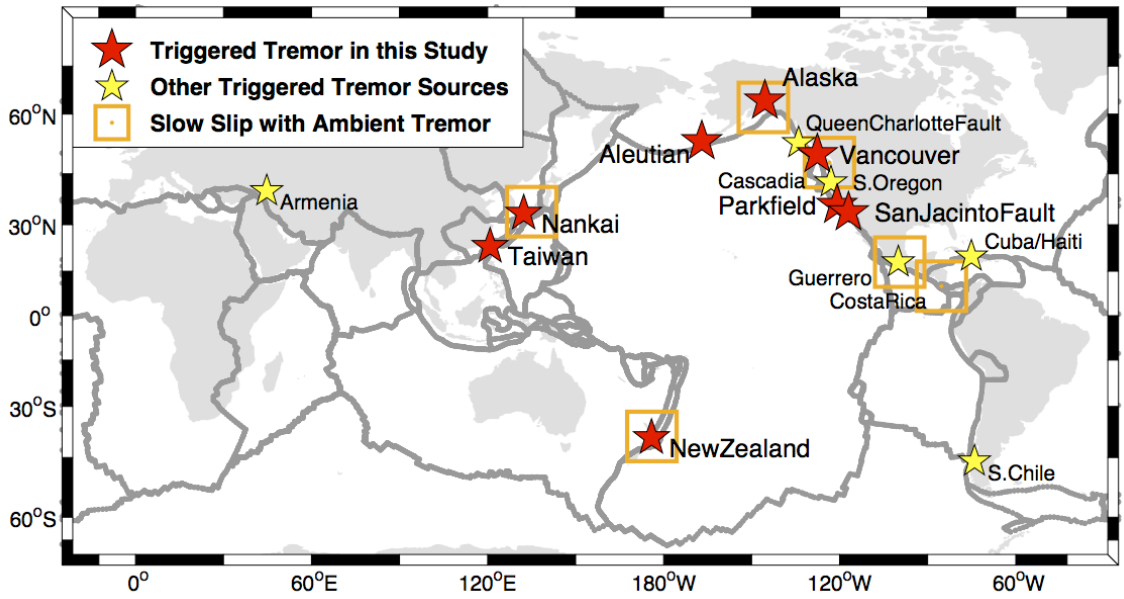

Figure 4.1 A summary map of triggered and ambient tremor locations around the world. The red stars show the study regions of triggered tremor following the 2011 Mw9.0 Tohoku-Oki Japan earthquake. The yellow stars mark the newly identified regions with triggered tremor reported by recent studies (e.g., Gonzalez-Huizar *et al.*, 2012; Peng *et al.*, 2012; Rubinstein *et al.*, 2011; Zigone *et al.*, 2012). Regions where episodic tremor and slow-slip events have been observed are marked as squares.

4.2 Data and Analysis Procedure

The analysis procedure generally follows those used in previous studies (Chao *et al.*, 2012d; Peng *et al.*, 2009) and is briefly described here. We download three-component broadband and short-period seismograms in each region (see Data and Resources), cut the data 1000 s before and 9000 s after the origin time of the Tohoku-Oki mainshock, remove the mean of the signals, and generate either band-pass or high-pass

filtered seismograms. We also remove the instrument response to obtain velocity and displacement seismograms and compare them with the high-frequency signals. In each region, we visually inspect potential tremor as high-frequency non-impulsive signals with no clear P- and S-wave arrivals and modulated by the passing surface waves of the Tohoku-Oki mainshock. We require that the tremor signals are coherent for at least three nearby stations, and that the SNR for tremor is higher than 1.5 (Chao *et al*., 2012a; Chao *et al*., 2012d). We also compute the spectrogram of seismic data recorded at selected stations (Peng *et al*., 2011) and use them to help determine the suitable frequency range (2-8 Hz band-pass filter or 4, 5 Hz high-pass filter) and component (i.e., E, N, or Z) that produce the most clear tremor signals.

Once a tremor sequence is identified, we locate each tremor burst by a conventional envelope cross-correlation method (Obara, 2002; Peng and Chao, 2008). Specifically, we search for the location that corresponds to the minimum root-mean-square (RMS) between the theoretical and observed travel time differences for all possible station pairs (See Appendix A for detailed analysis procedures). The error is estimated from the c-square distribution within 68% confidence level (Chao *et al.*, 2012d; Shearer, 1999). Because the depth is normally not well constrained by using such method (Chao *et al.*, 2012d), we fix the tremor depth to be at 25 km along the SAF, SJF, and Taiwan, 35 km in the relatively young subduction zones (e.g., SW Japan, Cascadia), and 45 km in the relatively old subduction zones (e.g., Aleutian and Alaska, New Zealand). These numbers are mainly based on previous studies in each region. In regions where tremor appears to come from multiple locations, we divide the seismic data into several

groups and locate them separately. The detailed tremor location information for all regions can be found in Table S4.1.

4.3 Triggered Tremor Observations

In this section, we describe the characteristics of triggered tremor in 8 regions, namely Nankai, Taiwan, Aleutian Arc and Alaska, Cascadia, Central and Southern California, and New Zealand. In addition, we also include some regions where ambient or triggered tremor have been found in previous studies, but no triggered tremor was found during the Tohoku-Oki mainshock (e.g., the CF in Northern California, Costa Rica, and Guerrero in Mexico), and regions where the Tohoku-Oki mainshock has triggered tremor, but were not analyzed in this study (e.g., Cuba). We sort these regions according to their distances relative to the epicenter of the Tohoku-Oki mainshock. We measure the peak ground velocities (PGVs) for the Love and Rayleigh waves shown in the instrument-corrected transverse and vertical component seismograms, respectively. In addition, we compute the expected PGV at each station based on the surface wave magnitude Ms equation (Lay and Wallace, 1995; van der Elst and Brodsky, 2010):

$$\log_{10} A_{20} = Ms - 1.66\log_{10}\Delta - 2 \tag{4.1}$$

where Δ is the epicentral distance in degrees, and A_{20} is the peak surface wave displacement at 20 s. We use the surface wave magnitude Ms=8.4 for the Tohoku mainshock based on the empirical estimation (Geller, 1976; Stein and Wysession, 2003).

We also assume a predominant period (T) of 20 s for the surface waves and convert the peak displacement (A_{20}) to peak velocity ($\dot{u}$) with the equation $\dot{u} \approx 2\pi A_{20}/T$ (Aki and Richards, 2002). Finally, we estimate the corresponding dynamic stress ($\Delta\sigma$) based on equation (4.2), using a nominal shear rigidity (G) of 35 GPa and a phase velocity (v) of 4.1 km/s and 3.5 km/s for Love and Rayleigh waves, respectively:

$$\Delta\sigma = G\dot{u}/v \tag{4.2}$$

As shown in Figure 4.2, the epicentral distance controls the PGVs and the associated dynamic stresses for all the regions examined in this study. In addition, the measured PGVs are larger than 0.1 cm/s, which corresponds to the dynamic stress of ~10 KPa.

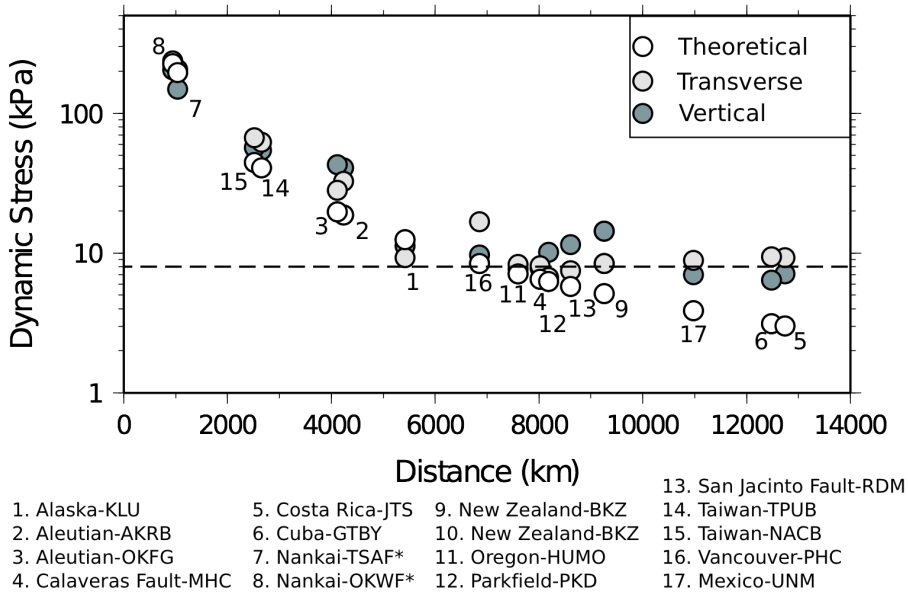

Figure 4.2 Theoretical and observed dynamics stress in each region versus epicentral distance to the Tohoku-Oki mainshock. The number marks different region and the

seismic station used for measuring the peak ground velocity (PGV). The observed dynamics stress is calculated from the PGV of surface wave in transverse and vertical component from the broadband and strong-motion (with * symbol) stations (Tables S4.2).

4.3.1 Nankai, Japan

Widespread ambient tremor activities in the Nankai subduction zone have been well studied since 2002 (Ide, 2010; Obara, 2002; Obara, 2011). While ambient tremor occurs along most of the Nankai trough (Obara *et al*., 2010), triggered tremor is mostly found at certain regions such as Shikoku, Kii, and Tokai (Miyazawa and Mori, 2005; Miyazawa and Mori, 2006; Miyazawa and Brodsky, 2008). Here we only focus on the Shikoku region because the regions of Kii and Tokai are close to the Tohoku-Oki epicenter (i.e., less than 800 km) such that the early aftershock signals from the Tohoku-Oki rupture zone may interfere with the locally triggered tremor signals.

We find at least two tremor sources in Shikoku during the passing surface waves of the Tohuku-Oki mainshock. For the source in western Shikoku, the first tremor burst occurred during the arrivals of Love and Rayleigh waves between 350 s and 450 s (Figure 4.3). Additional tremor bursts with smaller amplitudes continued until 800 s (Figure S4.1). In central Shikoku, clear tremor bursts are mainly associated with Rayleigh wave between 350 s and 500 s and smaller amplitude tremor bursts last until 700 s (Figure S4.1). A detailed analysis of the relationship between the triggered tremor and surface waves in this region can be found in Enescu *et al*. (2012).

We also compare the triggered tremor sources with the ambient tremor locations (Obara *et al*., 2010) one month before and after the Tohoku-Oki earthquake within 50 km from the epicenter of triggered tremor sources. As shown in Figure 4.3a, the hourly ambient tremor locations generally occurred in the down-dip directions as compared with triggered tremor. Even if we do not fix the triggered tremor depth to be 35 km, the change of best-fitting horizontal location is within ±0.02°, which would still place the triggered tremor to be slightly in the up-dip edge of the ambient tremor zone. In addition, ambient tremor activities in both regions show slightly different temporal patterns before and after the Tohoku-Oki mainshock. In the western Shikoku, ambient tremor is not active before the Tohoku-Oki mainshock, but the tremor activity has significantly increased after the mainshock (Figure 4.3c). In contrast, in the central Shikoku, the ambient tremor episodes are active before the Tohoku-Oki mainshock and did not show any significant changes after the mainshock (Figure 4.3d). We note that none of the large-amplitude triggered tremor identified in the first 800 s was shown in the ambient tremor catalog.

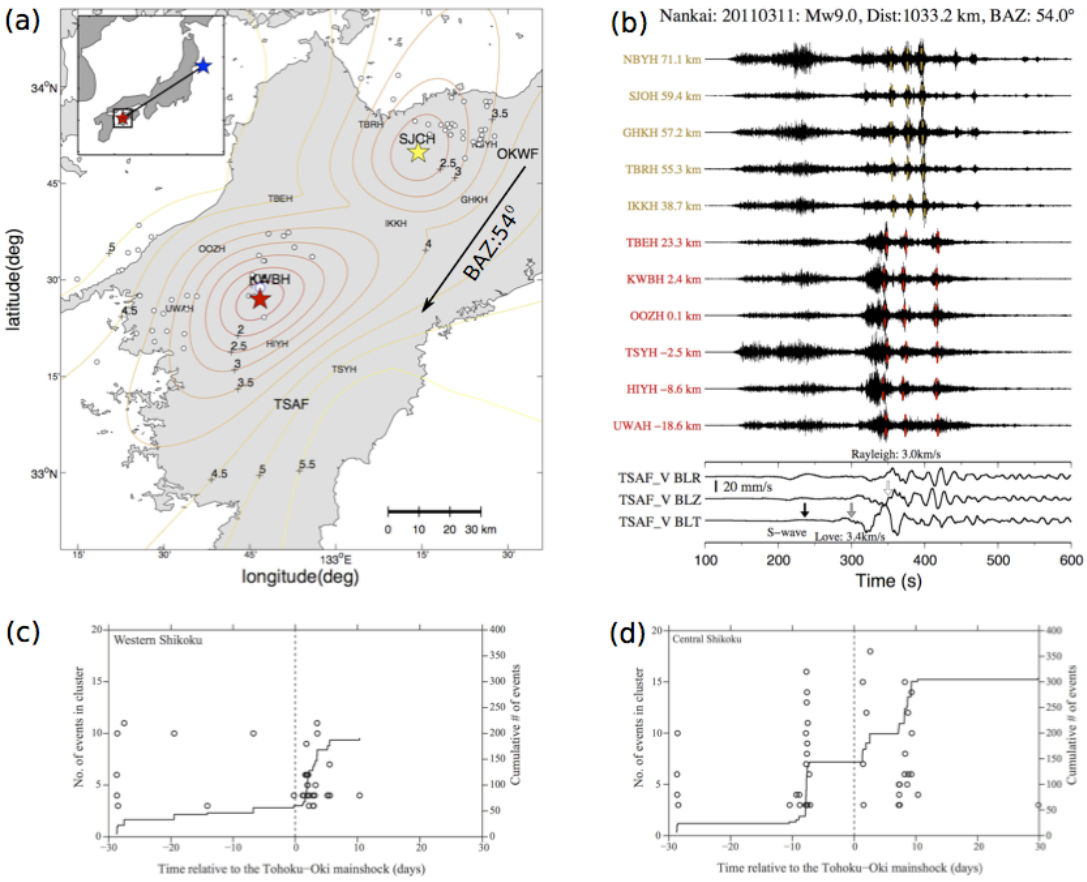

Figure 4.3 Triggered and ambient tremor activities in Shikoku, Nankai around the 2011 Mw9.0 Tohoku-Oki mainshock. **(a)** A map view of multiple sources of triggered tremor (stars) and seismic stations (marked with station name) in southwest Japan. The contour lines denote the root-mean-square (RMS) differences (in seconds) between the observed and predicted S-wave travel times of tremor bursts. The large circle indicates the location of tremor triggered by the 2008 Mw7.9 Wenchuan earthquake (Miyazawa *et al.*, 2008). The small white circles mark the ambient tremor locations (Obara *et al.*, 2010) one month before and after the Tohoku-Oki mainshock within 50 km from the epicenter of triggered tremor sources. The arrow marks the back-azimuth of the incoming surface waves from the Tohoku-Oki mainshock and the inset shows the great circle path between the mainshock and study region (square). **(b)** The 5 Hz high-pass filtered seismograms in E-component showing the moveout of triggered tremor at multiple source regions in Shikoku. The along-strike distance to the tremor source in western Shikoku (Tables S4.1) and the station names are marked to the left of the seismograms. The tremor bursts used to locate different tremor source are marked with vertical dotted lines and different colors. The bottom three traces show the instrument-corrected strong motion velocity (V) seismograms in radial (BLR), vertical (BLZ), and transverse (BLT) components at the F-net station TSAF. The study region, magnitude (M) of the 2011/03/11 Tohoku-Oki mainshock, and the epicenter distance (Dist) and back azimuth (BAZ) relative to the station TSAF are shown above the seismograms. The zero time corresponds to the origin time of the Tohoku-Oki mainshock. The arrow marks the predicted arrival of S-wave of

the mainshock. The thick vertical bar marks the amplitude scale of surface waves. **(c)** The ambient tremor activity in western Shikoku one month before and after the mainshock that are shown in (a). Each open circle (left y-axis) marks the number of events in each cluster in the ambient tremor catalog. The line (right y-axis) shows the cumulative number of event within each cluster. **(d)** The ambient tremor activity in central Shikoku.

4.3.2 Taiwan

Triggered tremor has been found in the southern CR of Taiwan, an arc-continent collision environment (Chao *et al.*, 2012d; Peng and Chao, 2008; Tang *et al.*, 2010). Triggered tremor was mainly located in the lower crust below the seismogenic zone and above the Moho, although it was still not clear whether it occurred on the low-angle detachment fault or high-angle thrust fault beneath the CR (Chao *et al.*, 2012d; Tang *et al.*, 2010). In addition, triggered tremor has been observed in the northern CR (Chao *et al.*, 2012d; Peng and Chao, 2008), but accurate tremor location and tremor-generation environment are still unclear due to lack of high-quality recordings of tremor among many nearby stations. Recently, Chao *et al*. (2012c) also found ambient tremor in the southern CR around the source regions of triggered tremor.

The Tohoku-Oki mainshock triggered at least three tremor activities in Taiwan (Figure 4.4). The best-fitting tremor location in southern CR is close to previous triggered tremor sources (Chao *et al.*, 2012d; Peng and Chao, 2008; Tang *et al.*, 2010). As shown in Figure 4.4b, the strongest tremor burst occurred during the Love waves starting at ~730 s and continued until 1000 s with the subsequent Rayleigh waves. Two possible weak tremor bursts occurred between 620 s and 680 s and were recorded at stations TPUB, ELD, and WTP during the S-wave and beginning of the Love waves. In northern

Taiwan, we identify two sources of triggered tremor around the previously identified triggered tremor regions (Chao *et al.*, 2012d). The first location is beneath the northern CR near the broadband station NACB (Figure 4.4a). Clear tremor burst started at ~600 s during the S-wave and beginning of the Love wave, and continued up to ~950 s during the subsequent Love and Rayleigh waves. Another source was further north near the coast and around station TWC, and the tremor bursts mainly occurred between 700 s and 800 s.

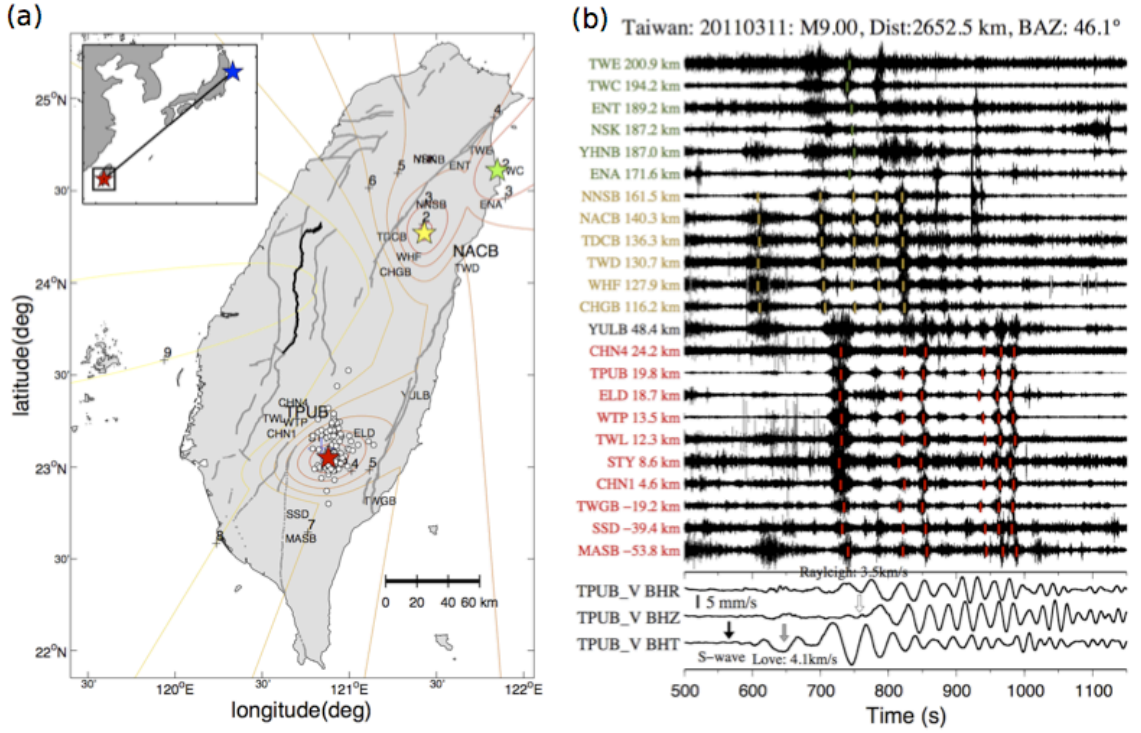

Figure 4.4 Triggered tremor observed in Taiwan. **(a)** A map view of multiple sources of triggered tremor in Taiwan during the Tohoku-Oki earthquake. The small circles mark the locations of ambient tremor from February to April 2010 (Chao *et al.*, 2012c). The gray and solid lines mark the active faults and the rupture zone of the 1999 Mw7.6 Chi-Chi earthquake. Other notations are the same as in Figure 4.3a. **(b)** The 5 Hz high-pass filtered seismograms in E-component showing the moveout of triggered tremor at multiple source regions in Taiwan. The seismograms are plotted along the strike of the Central Range. The bottom three traces show the instrument-corrected broadband velocity seismograms at station TW.TPUB. Other notations are the same as in Figure

4.3b.

4.3.3 Aleutian Arc and Alaska

Ambient tremor was found in South-Central Alaska (Peterson and Christensen, 2009) and the Aleutian arc (Brown *et al*., 2012; Peterson *et al*., 2011). In South-Central Alaska, ambient tremor episodes mostly occurred during slow-slip events (Peterson and Christensen, 2009). No slow-slip events have been observed in the Aleutian arc. In central Aleutian arc, the passing surface waves of the Tohoku-Oki mainshock generated multiple tremor sources near the Makushin, Akutan, and Shishaldin islands (Figure 4.5), close to the main ambient tremor sources from the previous study (Peterson *et al*., 2011). The first tremor source was on the island of Makushin during the arrival of Love wave between 1000 s and 1050 s. The second tremor patch was located between the Makushin and Akutan islands during the Rayleigh waves between 1050 s and 1400 s. The third tremor was triggered further northeast near the Shishaldin Island during the passing Rayleigh waves between 1050 and 1500 s.

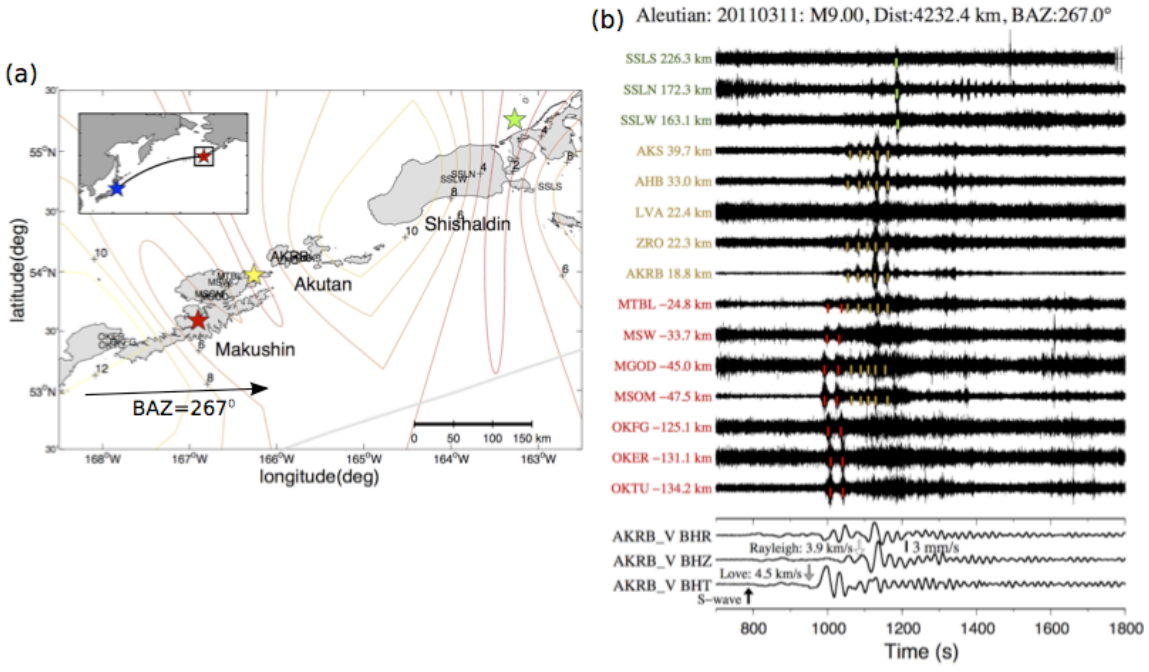

Figure 4.5 Triggered tremor observed in the Aleutian arc. **(a)** A map view of multiple sources of triggered tremor in central Aleutian during the Tohoku-Oki earthquake. The gray line marks the subduction trench. The names of three volcanic islands are marked. Other notations are the same as in Figure 4.3a. **(b)** The 5 Hz high-pass filtered seismograms in Z-component showing the moveout of triggered tremor at multiple source regions in Aleutian. The seismograms are plotted along the strike of the Aleutian arc. The bottom three traces show the instrument-corrected broadband velocity seismograms at station AV.AKRB. Other notations are the same as in Figure 4.3b.

Triggered tremor was identified in South-Central Alaska following the Tohoku-Oki earthquake (Flinchum and Brudzinski, 2011; Rubinstein *et al*., 2011). Here we examine the triggered tremor in more details. Small-amplitude tremor burst occurred at ~1300 s during the arrival of the Love waves (Figure 4.6). The subsequent Rayleigh waves triggered high-amplitude tremor bursts between 1400 s and 2200 s. Triggered tremor was located near station KLU east of the region where previous ambient tremor are found (i.e., around station SAW) (Peterson and Christensen, 2009). It is also possible that additional tremor might be triggered at the surrounding regions (e.g., noting different tremor signals at station RC01). However, we do not have enough station recordings to locate them accurately.

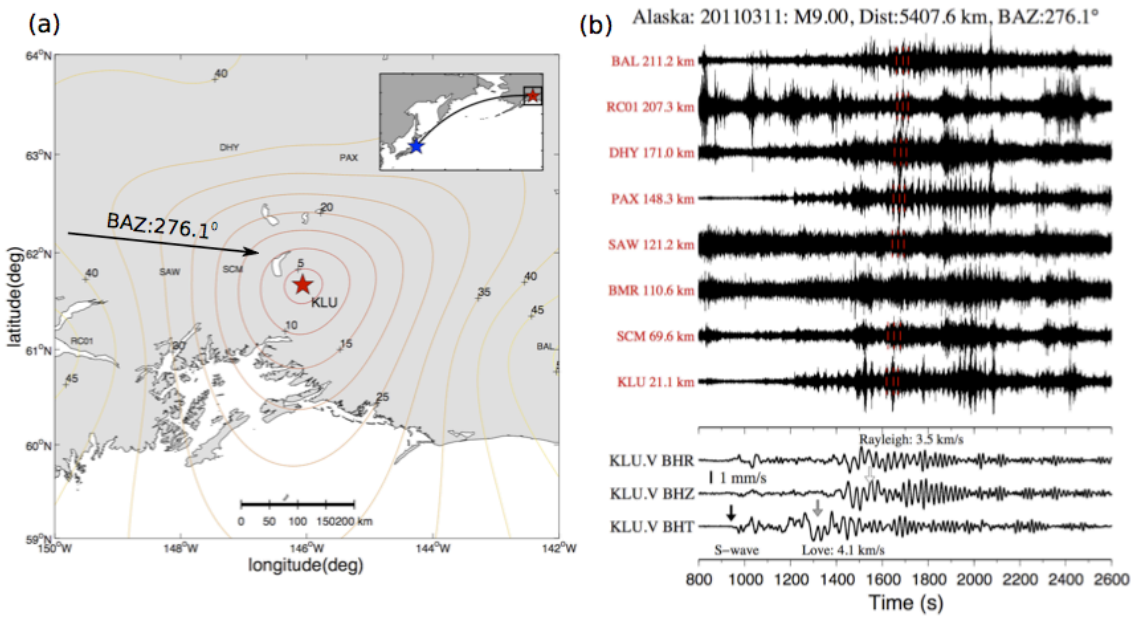

Figure 4.6 Triggered tremor observed in south-central Alaska. **(a)** A map view of single triggered tremor source in south-central Aleaska during the Tohoku-Oki earthquake. Other notations are the same as in Figure 4.3a. **(b)** The 5 Hz high-pass filtered seismograms in E-component showing the moveout of triggered tremor at multiple source regions in Aleutian. The seismograms are aligned with the epicentral distance relative to the best tremor source. The bottom three traces show the instrument-corrected broadband velocity seismograms at station AK.KLU. Other notations are the same as in Figure 4.3b.

4.3.4 Cascadia

The Cascadia subduction zone is one of the most well-studied regions that host episode tremor and slips (ETS) (Beroza and Ide, 2011; Gomberg *et al*., 2010). The ETS occur every ~15 months and last for about 2-3 weeks (Miller *et al*., 2002; Rogers and Dragert, 2003; Wech and Creager, 2011). Triggered tremor has also been observed in the Vancouver Island in northern Cascadia (Rubinstein *et al*., 2007; Rubinstein *et al*., 2009) and in the State of Washington in central Cascadia (Gomberg, 2010). Following the 2011 Tohoku-Oki earthquake, triggered tremor has been identified near the Vancouver Island (Rubinstein *et al*., 2011) and south Oregon (Gonzalez-Huizar *et al*., 2012). Figure 4.7

shows the location and waveforms of the Tohoku-Oki triggered tremor in northern Vancouver Island. The tremor occurred near station MAYB and was close to the source regions of previously identified triggered tremor sources (Rubinstein *et al*., 2007; Rubinstein *et al*., 2009). As was found in other regions, tremor first occurred during the arrival of Love wave at ~1600 s, and became further modulated by the subsequent Rayleigh waves.

We compare the ambient tremor activity (Kao and Shan, 2004; Kao *et al*., 2010) one month before and after the Tohoku-Oki mainshock (Figure 4.7c). Ambient tremor episodes are located at the down-dip section of the subduction interface as compared with the triggered tremor location (Figure 4.7a). The changes of depth between 32 and 37 km in Vancouver Island causes ±0.02° variations on triggered tremor locations. The ambient tremor in this region was sporadic with bursts of activities at 29 and 4 days before the occurrence of the Tohoku-Oki mainshock. There was a clear increase of tremor activities immediately following the Tohoku-Oki mainshock. Another ambient tremor episodes occurred about 9 days after the mainshock. In contrast, no clear triggered tremor was found in central Cascadia (Figure S4.2). In the southern Oregon, clear tremor bursts occurred during the surface wave recorded at station HUMO (Figure S4.3) (Gonzalez-Huizar *et al*., 2012). However, we did not find other nearby stations that record similar tremor signals. Hence, we do not locate this tremor source.

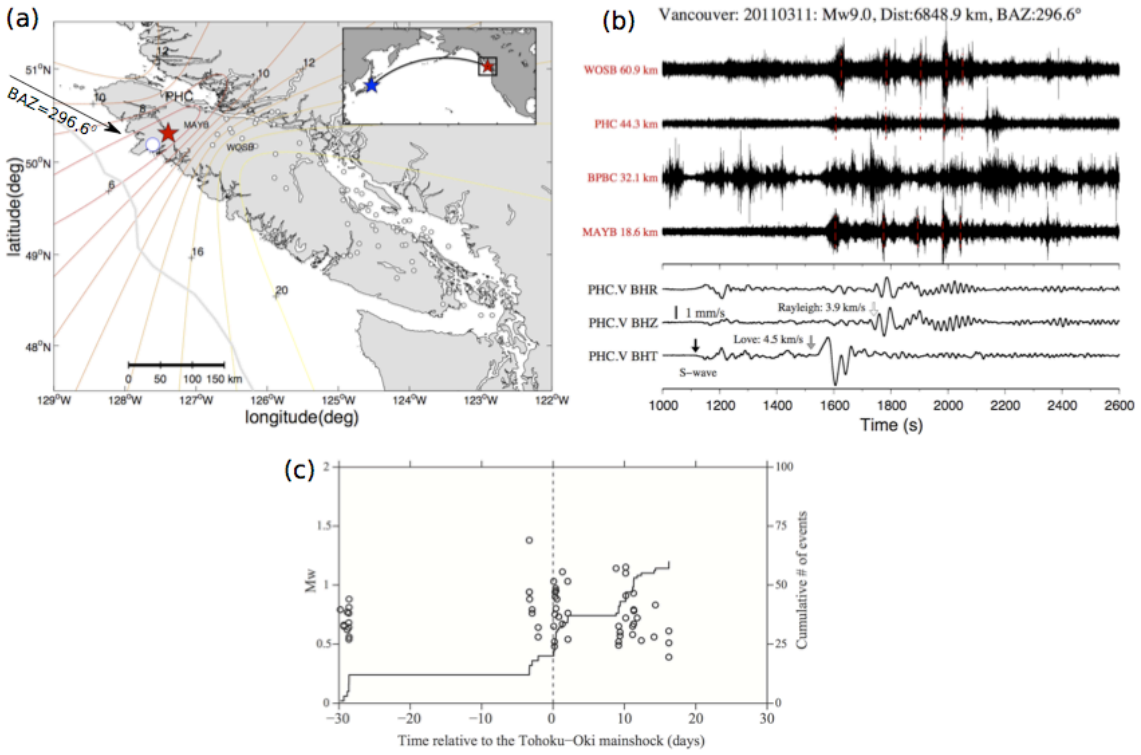

Figure 4.7 Triggered and ambient tremor in northern Vancouver Island around the Tohoku-Oki mainshock. **(a)** A map view of the triggered tremor source in northern Vancouver Island during the Tohoku-Oki earthquake. The large circle marks the location of tremor triggered by the 2002 Mw7.8 Denali, Alaska, earthquake (Rubinstein *et al.*, 2007). The small white circles mark the locations of ambient tremor one month before and after the Tohoku-Oki mainshock (Kao and Shan, 2004; Kao *et al.*, 2010). Other notations are the same as in Figure 4.3a. **(b)** The 5 Hz high-pass filtered seismograms in Z-component showing the moveout of triggered tremor for single tremor source. The seismograms are aligned with the epicentral distance relative to the best tremor source. The bottom three traces show the instrument-corrected broadband velocity seismograms at station CN.PHC. Other notations are the same as in Figure 4.3b. **(c)** The ambient tremor activity in the Vancouver Island one month before and after the Tohoku-Oki mainshock. The left y-axis shows the moment magnitude of each tremor, and the line shows the cumulative number of tremor.

4.3.5 Parkfield

The Parkfield-Cholame section of the SAF in central California is another region where ambient (Nadeau and Dolenc, 2005; Nadeau and Guilhem, 2009; Shelly *et al.*, 2009; Shelly and Hardebeck, 2010) and triggered (Gomberg *et al.*, 2008; Peng *et al.*,

2009; Peng *et al.*, 2010a; Shelly *et al.*, 2011) tremor have been well studied. Rather than locating the tremor with our envelope cross-correlation technique, we take advantage of the existing LFE catalog (Shelly and Hardebeck, 2010) and use the LFEs during the teleseismic waves to quantify spatio-temporal evolutions of triggered tremor. Hill *et al*. (2012) conducted a detailed analysis of the tremor around Parkfield triggered by the 2011 Tohoku-Oki mainshock. Here we briefly summarize their observations.

A clear tremor burst was first triggered at ~1300 s by the arrival of S wave and the tremor source was located in the creeping section of the SAF northwest of station PKD (Figure 4.8). A weak tremor burst was triggered by the SHSH wave (e.g., SH wave reflected by Earth's surface midway between the epicenter and Parkfield) at ~1600 s and was located beneath the hypocenter of the 2004 Mw6.0 Parkfield earthquake. Love wave triggered two majority tremor bursts at about 1800 s and 1950 s, respectively, and the sources were located mostly near Cholame. The subsequent Rayleigh waves also triggered multiple tremor sources scattered at both in the creeping section of the SAF and around Cholame. As was done in other regions, we further examine the ambient tremor activities 6 days before and after the Tohoku-Oki mainshock. As shown in Figure 4.8b, clear tremor episodes occurred 2, 4, and 6 days before the Tohoku-Oki mainshock. There is a clear increase of tremor activity during the teleseismic waves and the first few hours afterward. However, we find no significant changes of tremor activities a few days after the mainshock.

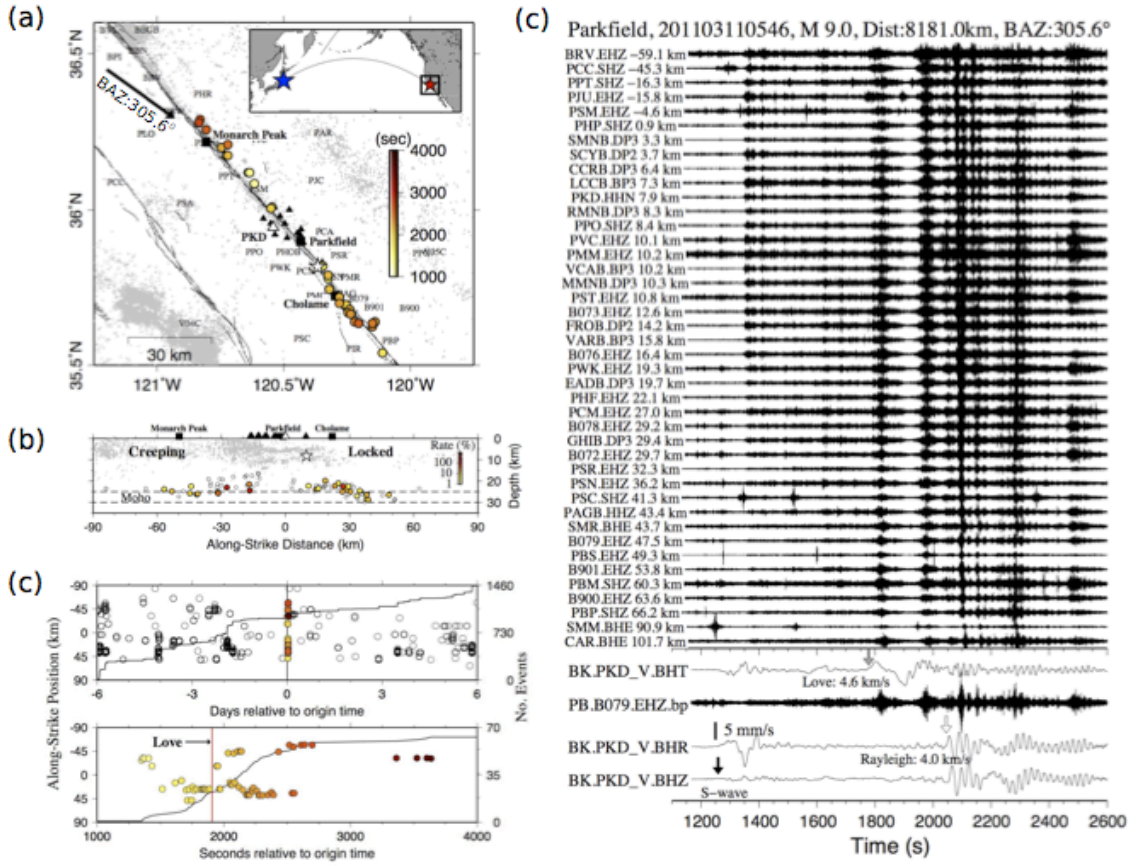

Figure 4.8 Triggered and ambient tremor along the Parkfield-Cholame section of the San Andreas Fault (SAF) around the Tohoku-Oki mainshock. **(a)** A map view of triggered tremor during the Tohoku-Oki mainshock. The tremor locations are marked as circles with color denoting the time since the mainshock. The black dots mark the background seismicity, and the lines denote active faults. Other notations are the same as in Figure 4.3a. **(b)** An along-fault cross-section view showing the depth profile of the 88 tremor locations. The color denotes the ratio between the number of tremor during the mainshock and that during the 6 days before the mainshock. **(c)** (top) Along-strike distances versus the occurrence times of tremor within 6 days of the Tohoku-Oki mainshock. (bottom) A zoom-in plot around the teleseismic waves of the mainshock. The vertical line marks the arrival time of large-amplitude Love waves. **(d)** The 2-8 Hz band-pass filtered seismograms showing the moveout of triggered tremor at multiple sources. The seismograms are plotted along the SAF strike. The bottom three traces show the instrument-corrected broadband velocity seismograms at station BK.PKD. Other notations are the same as in Figure 4.3b.

4.3.6 San Jacinto fault, southern California

In comparing with the abundant triggered tremor in central California, the 2002 Mw7.9 Denali Fault earthquake is the only teleseismic event that has triggered tremor along the SJF in southern California (Chao *et al*., 2012a; Gomberg *et al*., 2008). In addition, although several studies have attempted to identify ambient and additional triggered tremor in this region (Hillers and Ampuero, 2009), ambient tremor has not been detected with current instrumentation (J. P. Ampuero, personal comm., 2011).

Here we identify a possible tremor observation in SJF during the passing surface waves of the Tohoku-Oki earthquake. We first examine the spectrogram (Peng *et al*., 2011) of several recordings and determine that tremor signals are best shown in the horizontal component with the frequency range of 4-10 Hz. The first tremor burst occurred during Love wave at ~2050 s. Additional tremor bursts occurred between 2350 s and 2550 s during the later arriving Rayleigh waves (Figure 4.9). In addition, a local earthquake occurred at ~2240 s during the first few cycles of the Rayleigh waves. The triggered tremor is located in the Anza section of the SJF, at about ~36 km southeast from the tremor source triggered by the Denali Fault earthquake (Gomberg *et al*., 2008).

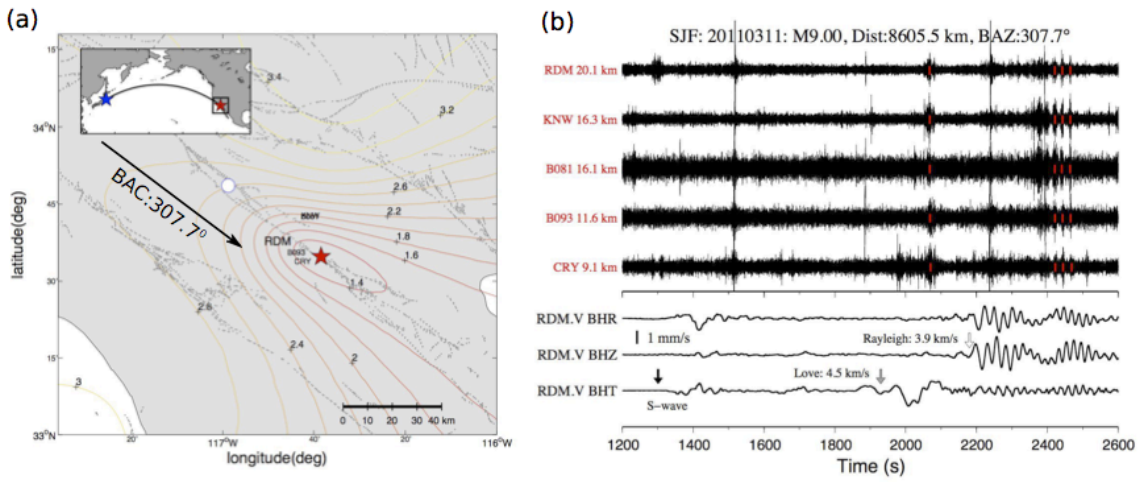

Figure 4.9 Triggered tremor observed at San Jacinto Fault (SJF) in southern California. **(a)** A map view of single triggered tremor source during the Tohoku-Oki earthquake. Other notations are the same as in Figure 4.3a. **(b)** The 4-10 Hz band-pass filtered seismograms in N-component showing the moveout of triggered tremor. The seismograms are aligned with the epicentral distance relative to the best tremor source. The bottom three traces show the instrument-corrected broadband velocity seismograms at station AZ.RDM. Other notations are the same as in Figure 4.3b.

4.3.7 North Island of New Zealand

The Hikurangi Subduction Margin, New Zealand marks the convergent plate boundary where the Hikurangi Plateau, part of the Pacific plate, subducts beneath the North Island at 2-6 cm/yr (Wallace *et al*., 2004). Numerous slow-slip events have been observed both in the up-dip and down-dip directions from the interseismically locked regions (McCaffrey *et al*., 2008; Wallace and Beavan, 2010). Delahaye *et al*. (2009) conducted a systematic search but failed to find any tremor signals associated with shallow slow-slip events at the northern Hikurangi margin. Instead, they found numerous reverse-faulting microearthquakes. Recently triggered (Fry *et al*., 2011) and ambient (Ide, 2012; Kim *et al*., 2011) tremor have been found in the North Island of New Zealand, near the regions of deep slow-slip events (Wallace and Beavan, 2010). The Tohoku-Oki

mainshock also triggered clear tremor bursts at stations BKZ and BHHZ (Figure 4.10), mostly during the passing Rayleigh waves between 2650 s and 2900 s. The tremor source is located at the southeast of Lake Taupo, which is about 60 km northeast of the tremor source triggered by the 2010 Mw8.8 Chile mainshock (Fry *et al*., 2011). In general, those triggered tremor sources are aligned parallel to the subduction zone trench and are around the ambient tremor sources (Ide, 2012).

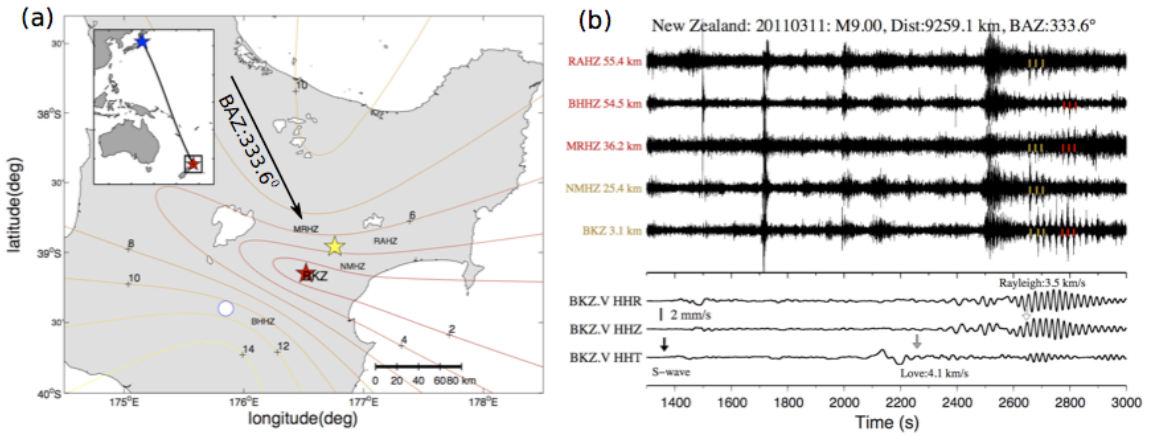

Figure 4.10 Triggered tremor observed in north Island of New Zealand. **(a)** A map view of triggered tremor during the Tohoku-Oki earthquake. Other notations are the same as in Figure 4.3a. **(b)** The 2-8 Hz band-pass filtered seismograms in E-component showing the moveout of triggered. The seismograms are aligned with the epicentral distance relative to the best tremor source by station BKZ. The bottom three traces show the instrument-corrected broadband velocity seismograms at station NZ.BKZ. Other notations are the same as in Figure 4.3b.

4.3.8 Other Regions

Ambient tremor and episodic slow-slip events have been found along the Middle-American Trench in Guerrero, Mexico (Payero *et al*., 2008) and in Costa Rica (Brown *et al*., 2009; Outerbridge *et al*., 2010; Walter *et al*., 2011). Triggered tremor was found in

Mexico triggered by the 2010 Mw8.8 Chile earthquake, but no clear triggered tremor has been identified during the 2011 Tohoku-Oki earthquake (Zigone *et al*., 2012). However, no triggered tremor has been found in Costa Rica (Swiecki and Schwartz, 2010), and the 2011 Tohoku-Oki earthquake also did not trigger any clear tremor in this region (Figure S4.4; Hernandez, S. personal comm. 2012). We also examine seismic recordings in the CF where the 2002 Denali Fault earthquake has triggered tremor (Chao *et al*., 2012a; Gomberg *et al*., 2008), but did not find any clear triggering during the Tohoku-Oki mainshock (Figure S4.5).

Gonzalez-Huizar *et al*. (2012) reported triggered tremor at station SAO in the creeping section of the SAF, station GNI in Armenia, and station GTBY in Cuba. Because station SAO is about 88 km away from the northwestern-most tremor on the creeping section of the SAF, it is not clear whether the recorded tremor signals originated from a new source region, or could be generated by the same source as shown in Figure 4.8. Only the 2011 Tohoku-Oki event has triggered tremor-like signals at station GNI, while the 2010 Mw8.8 Chile earthquake and its large aftershocks have triggered tremor in Cuba (Gonzalez-Huizar *et al*., 2012). Thus, we only include the Cuba case in the subsequent analysis.

4.4 Tremor Amplitudes and Dynamic Stress Changes

We quantify the relationship between tremor amplitudes and dynamic stress changes at all the regions that we have examined in this study. In regions with multiple

tremor sources (e.g., Japan, Taiwan, Aleutian), we measure the values for each tremor source separately. As mentioned before, the PGV is measured as the maximum peak on the transverse and vertical components of velocity seismograms within the apparent velocities of 5 to 2 km/s. To measure tremor amplitude, we follow our previous studies (Chao *et al.*, 2012a; Chao *et al.*, 2012d) and compute the median amplitude of triggered tremor from the two horizontal-component band-pass-filtered displacement seismograms during the large-amplitude surface waves. We use a fixed frequency range between 5-15 Hz so that the tremor amplitudes at different sites are comparable. The displacement seismograms were integrated from the band-pass-filtered velocity seismogram for the purpose of amplitude correction as described below. In regions where no triggered tremor was found, we measure the median amplitudes of 5-15 Hz band-pass-filtered seismograms during the surface-wave time period within the apparent velocities of 5-2 km/s. Finally, we compute the median amplitudes of the background noise during the 600-s before the P wave arrival of the mainshock.

We correct for the effects of geometrical spreading (Boore, 2003) and attenuation (Chao *et al*., 2012a; Shearer, 1999) with the following equation:

$$A = \left(A_0 / R\right) * \exp[(-2\pi \cdot f \cdot R)/(2 \cdot v_s \cdot Q)] \tag{4.3}$$

where A is the observed tremor amplitude at a station, A_0 is the corrected tremor amplitude from the tremor source, R is the hypocentral distance between station and tremor source, $1/R$ is the geometrical spreading function (for $R < 70$ km), f is the dominant frequency, V_s is shear wave velocity, and Q is a quality factor. Here we assume

a constant Q = 100 and average V_s = 3.9 km/s for lower crust (Shearer, 1999), and assume f = 5 Hz with the highest amplitude of triggered tremor (Rubinstein *et al*., 2007).

The median tremor amplitudes have a positive correlation with the dynamic stresses estimated from both Love and Rayleigh waves on the transverse and vertical components, respectively (Figure 4.11). The correlation coefficient in the log-log scale is more than 0.57 for 12 measurements both before and after the amplitude corrections. The corresponding two-tailed p value is 0.053, indicating that the correlation is significant at more than 95% confidence level. In comparison, the background noises do not show any correlations with the dynamic stresses. The measurements in two regions (Cuba and south Oregon) with triggered tremor but no tremor locations are not included in the fit. However, the triggered tremor amplitudes are roughly in the range of other measurements with similar dynamic stresses.

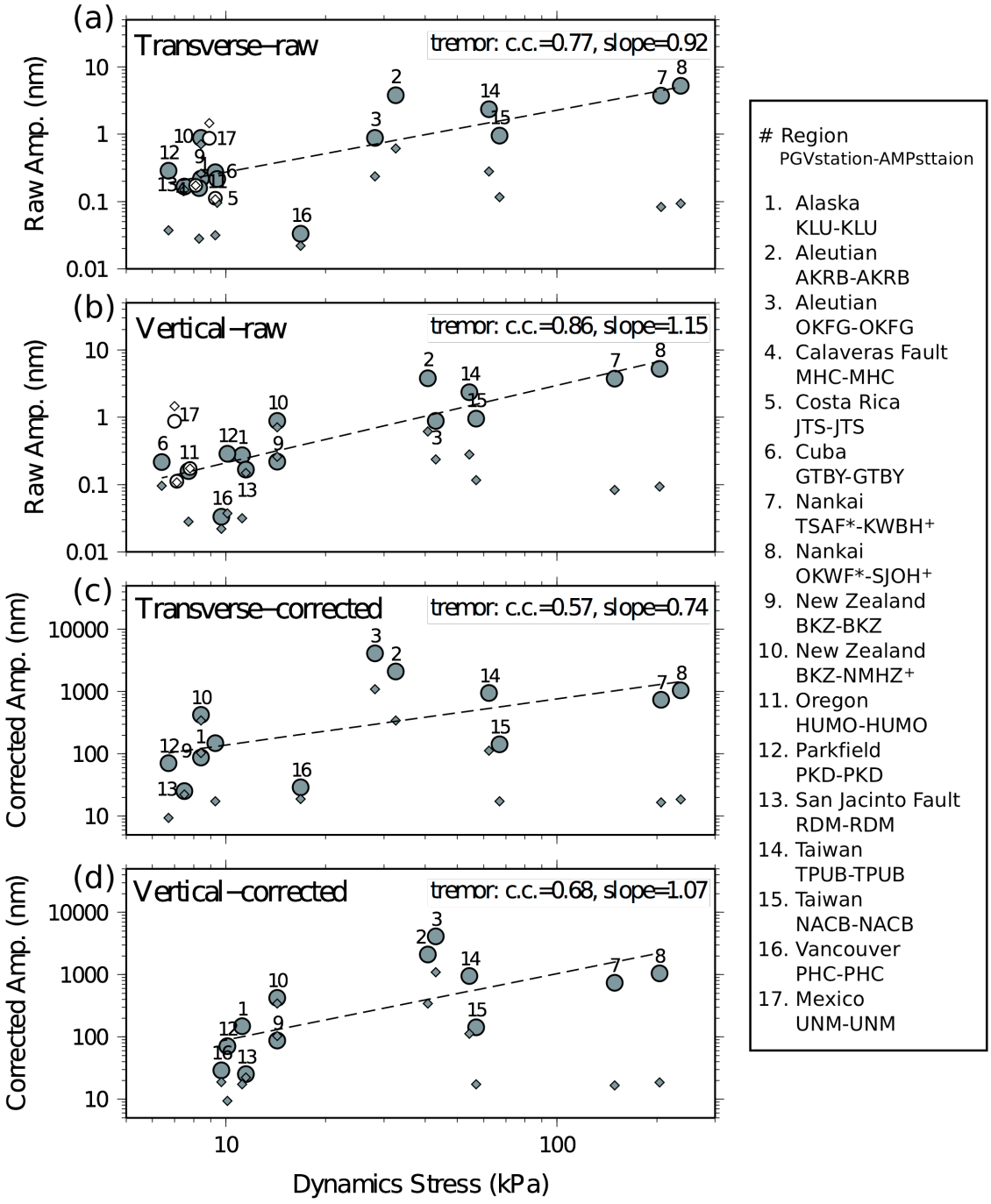

Figure 4.11 Median tremor amplitude measured from the 5–15 Hz two-horizontal-component band-pass-filtered envelope functions versus dynamic stress of surface wave for the Tohoku-Oki mainshock. Panels (a) and (b) show raw tremor amplitudes, and panels (c) and (d) show the amplitudes after correcting for geometrical spreading and attenuation. The tremor-triggering and non-triggering events were marked by shaded and open symbols, respectively. The background noise level is marked with diamond symbol and is calculated from a 600-s time window before the occurrence of the Tohoku-Oki

mainshock in each region. The number marks different region, the seismic station used for measuring the peak ground velocity (PGV), and the station used for measuring median amplitude of tremor and non-tremor signals. The station names marked with asterisk (*) and cross (+) indicate the strong motion (BL) and extremely short-period (EH) instruments. Others are measured from broadband stations (BH or HH, Table S4.2). The correlation coefficient (c.c.) and slope of the fitting line are calculated between the median tremor amplitudes and the PGVs for tremor with shaded circles.

4.5 Modeling of Tremor Triggering potential

We follow the modeling approach used by Hill (2008) and Gonzalez-Huizar and Velasco (2011) for triggered earthquakes to quantify the trigger potential of the surface wave from the Tohoku-Oki earthquake in the different tectonic environment presented in this study. We used two modeling approaches assuming that tremor was produced by a shear slip at nearby major plate-boundary faults following a simple Coulomb failure criterion. In the first approach, we compute the theoretic potentials of surface waves with fixed amplitude and frequency to trigger tremor in a fault plane with specific orientation and faulting mechanism. In the second approach, we use the time-dependent frequency and amplitude information of the triggering wave to model the time-dependent dynamic stresses or stress-grams.

In the first approach, we calculate the triggering potential of Love and Rayleigh waves with a predominant period of 20 s (see e.g. Hill, 2010). As briefly mentioned before, we group our study regions into three tectonic models. For the strike-slip faults (e.g., SAF and SJF), we use a vertical-dipping fault and set the tremor depth at 25 km. For the relatively young subduction zones (e.g., SW Japan and Cascadia), we use a shallow-dipping fault of 15° and set the tremor depth to be at 35 km. For the relatively

old subduction zones (e.g., Aleutian, Alaska and New Zealand), we use 25°-dipping angle to approximate the subduction-zone plate interface, and set the tremor depth to be at 45 km (e.g., Brown *et al*., 2012). Because the faulting style for tremor in Taiwan is still not clear (Chao *et al.*, 2012d; Tang *et al.*, 2010), we do not include the results from Taiwan in this analysis.

Figure 4.12 shows the triggering potentials for Love and Rayleigh waves for each of the simplified tectonic models. For the strike-slip faults (Figures 4.12 a and d), Love waves show a higher triggering potential than Rayleigh waves for the incident angles at the regions of interest. This means that we should expect more predominant tremor activity during the passing Love waves. This is generally consistent with the observation at Parkfield (e.g., Figure 4.8). However, Rayleigh wave triggered larger amplitude tremor than the Love wave (Gonzalez-Huizar *et al*., 2012). For the relatively young subduction zones (Figures 4.12 b and e), triggering potentials are of comparative magnitudes for Love and Rayleigh waves for the incident angles of interest. Thus, triggering tremor rate during Love waves should be similar to that expected during Rayleigh waves (e.g., Figure 4.7). Finally, for the relatively old subduction zones model (Figures 4.12 c and f), Rayleigh waves show a higher triggering potential. In this case, we expect higher amplitude of triggered tremor rates during the Rayleigh than during the Love waves. The triggered tremor observed in the Aleutian arc, Alaska, and New Zealand was mostly triggered during the Rayleigh waves (Figures 4.5, 4.6, 4.10), although Love waves also trigger slightly small amplitude tremor (e.g., Figure 4.5).

For this simple modeling the triggering potential for the Love and Rayleigh wave is calculated with a constant dominant period of 20 s and equal amplitude. In addition, the comparisons with the tremor amplitudes are qualitative. To obtain a more quantitative estimate of how dynamic stress triggers tremor, we need to know the precise amplitude and frequency of the triggering wave at the exact time when tremor pulse occurs. This can be done by time-shifting the triggered tremor and triggering waves back to the tremor source (e.g., Peng *et al*., 2009; Rubinstein *et al*., 2009). Therefore, precise triggered tremor locations and related fault plane orientations are required to produce an acceptable estimate of the triggering dynamic stress.

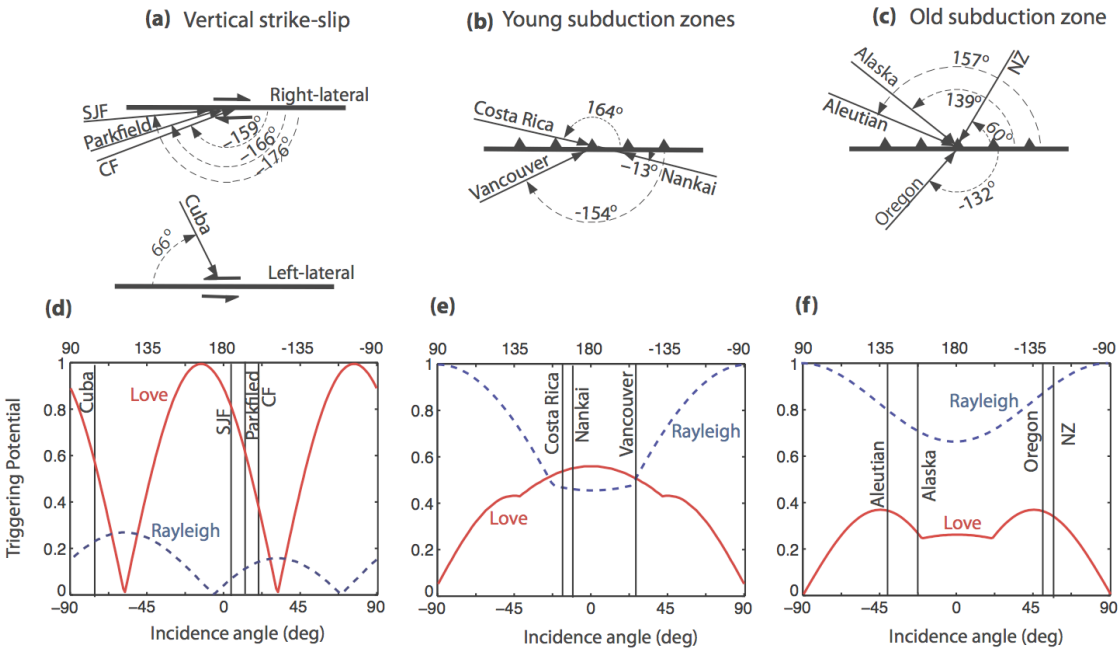

Figure 4.12 Surface wave potentials to trigger tremor for three simplified tectonic models. Panels (a) (b) and (c) show idealized maps for the tectonic models, and the arrows represent the incident angles of teleseismic waves on each of the regions. Panels (d), (e) and (f) show the triggering potential of the Love (solid lines) and Rayleigh (dash lines) waves as a function of the incident angles for the tectonic models in (a), (b) and (c), respectively. Vertical lines in triggering potential plots define the incident angle for each

of region where tremor was triggered.

We calculate the stress-grams for two representative tectonic regions with precise triggered tremor locations: The Parkfield-Cholame strike-slip section of the SAF, and the subduction zone in Western Shikoku, Japan (Figure 4.13). In both cases, individual dynamic stress tensors are calculated for triggering wave's amplitudes and frequencies as measured from consecutive peaks in the displacement seismograms. Then, the time-dependent stress values are interpolated to obtain a continuous stress-gram signal. For the SAF the stress-grams are calculated for a vertical strike-slip right-lateral fault with strike angle of 319° (Chao *et al*., 2012a), and a tremor source of 25 km depth. For the Western Shikoku we use a tremor source of 35 km depth for a thrust fault of strike and dip angles of 225° and 15°, respectively (Hill, 2010; Miyazawa and Brodsky, 2008) (Table S4.4). For both fault planes a coefficient of static friction $\mu = 0.2$ is used (Hill, 2010). This is justified by the inference of near-lithostatic pore pressure at tremor depth from tidal correlations at Parkfield (Thomas *et al*., 2009) and seismic tomography in other regions (Shelly *et al*., 2006). We shift the tremor signals back to the source region based on a 1D velocity model in each region, and use a constant phase velocity (4.1 km/s for the Love and 3.5 km/s for the Rayleigh wave) to shift the time-dependent triggering potentials or dynamic stress-gram back to the tremor source region. We also take a smoothed envelope function of the tremor signals and compute the cross-correlations with the stress-grams for the Love and Rayleigh waves and the sum traces separately.

In Western Shikoku (Figure 4.13a), the Love wave correlates better with the first two cycles of tremor bursts, but the later single tremor burst is not correlated well with the Love nor Rayleigh waves. At SAF (Figure 4.13b), tremor bursts are better correlated with the Love wave in the first 2 cycles of tremor burst, between 1800 s and 2000 s, then later associated with Rayleigh waves. In both cases, the CC values for the Love waves are higher than those for the Rayleigh waves, which are consistent with the higher triggering potential of the Love waves (Figure 4.12) and their larger amplitudes.

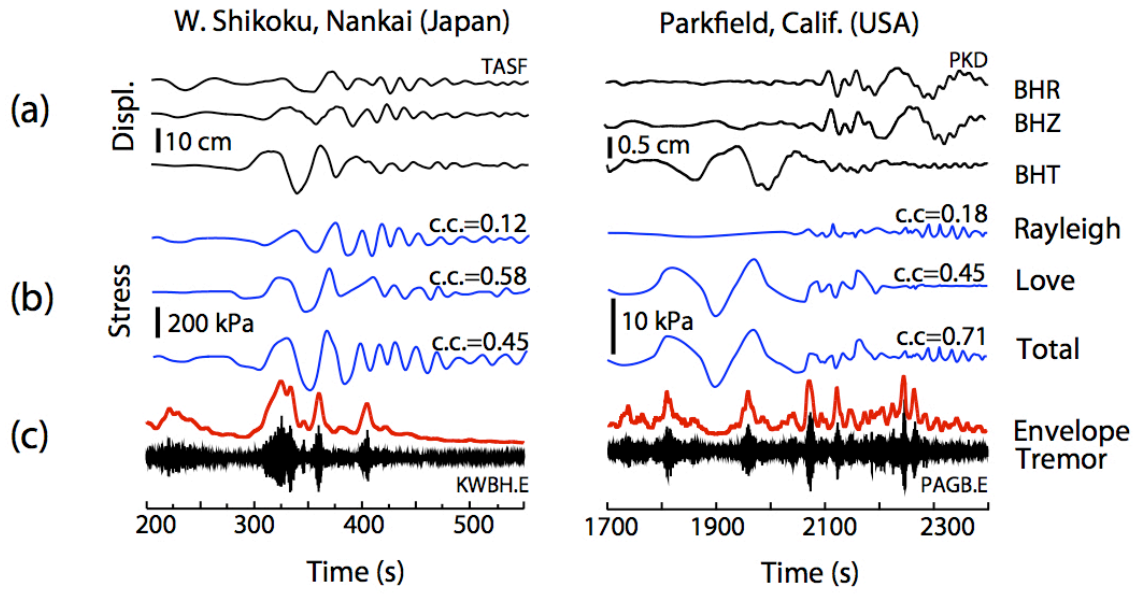

Figure 4.13 Time-dependent dynamic stress (stress-grams) as a measurement of the surface wave potential to trigger tremor in Shikoku, Japan and Parkfield, California. (a) Radial, vertical and transverse displacement components recorded by broadband seismic stations. (b) Dynamic stress caused by Love, Rayleigh and combined (total) ground displacement. (c) Triggered tremor and tremor's envelope signals as showed in high-pass filtered seismograms. The cross-correlation (c.c.) between dynamic stress and triggered tremor's envelope is shown in (b). All signals have been time shifted back to the triggered tremor source location.

4.6 Discussions and Conclusions

We conducted a global search of deep tremor triggered by the 2011 Mw9.0 Tohoku-Oki earthquake. Out of 12 regions where either ambient or triggered tremor has been previously observed, we have found tremor triggered by the Tohoku-Oki mainshock occurred in 8 regions (Figures 4.3-10). Such a widespread triggering of tremor by the Tohoku-Oki mainshock is perhaps not surprising because the associated dynamic stresses observed at all regions are at least 8 kPa (Figure 4.2), close or higher than the apparent triggering threshold found in previous studies (Chao *et al.*, 2012d; Peng *et al.*, 2009; Rubinstein *et al.*, 2009). The only exception is no clear evidence of tremor triggered by the Tohoku-Oki earthquake in the CF in northern California (Figure S4.5), Guerrero in Mexico (Zigone *et al*., 2012), and Nicoya Peninsula, Costa Rica (Hernandez, S. personal comm. 2012). While we have found several high-frequency signals recorded by the nearby broadband stations in the later two regions during the teleseismic surface waves (Figure S4.4), we did not have access to additional waveform data to verify the existence or lack of triggered tremor. In the CF, we did not identify coherent tremor-like signals in the band-pass-filtered seismograms (Figure S4.5). In comparison, small-amplitude tremor signals were observed in the surface broadband and borehole short-period recordings in the SJF in southern California (Figure 4.9). We cannot rule out the possibility that weak tremor was triggered in the CF, but were not detected because its amplitude is smaller than or near that of the background noise.

In places where ambient tremor has been previously found (e.g., SW Japan, Taiwan, Aleutian, Alaska, Cascadia, Parkfield, and New Zealand), triggered tremor was

generally found to be near the ambient tremor sources. In SW Japan, triggered tremor appeared to occur in the up-dip direction as compared with the location of most ambient tremor. Even if we perform a grid search in depth from 0 to 60 km, the horizontal locations only vary within ±0.02° in these regions, suggesting that fixing tremor depth would not affect the horizontal location significantly. Although we could explain such observations as depth-dependent behaviors of triggered and ambient tremor (e.g., Wech and Creager, 2011), the triggered and ambient tremor in SW Japan was located using different techniques. Hence, the apparent differences in the horizontal locations of triggered and ambient tremor could simply originate from the use of different location techniques, rather than reflecting genuine behavior differences.

Parkfield is the only region where triggered and ambient tremor was identified and located with the same technique (Shelly and Hardebeck, 2010). Shelly *et al*. (2011) summarized previous observations of triggered tremor in that region, and found that the shallowest (< 20 km) tremor families in the creeping section of the SAF were infrequently triggered. However, it is not clear whether such a difference is caused by depth-dependent tremor behavior, or variations in the tremor amplitudes, which may cause the weak tremor sources to be masked by concurrent strong tremor sources. We also examined the ratios between the number of tremor occurred during the teleseismic surface waves to the total number of tremor occurred within 6 days before the Tohoku mainshock (Figure 4.8b). Only the deep tremor (e.g., > 20 km) in the creeping section of the SAF were triggered, similar to the general patterns observed in Shelly *et al*. (2011). However, such pattern is not clear for the tremor sources near Cholame. Nevertheless, it

is evident that triggered and ambient tremor at Parkfield share the same LFE template families, suggesting that they originated from the same source but were driving by different forces (Shelly *et al*., 2011). Further systematic studies are needed to verify if there is any systematic difference in the locations between triggered and ambient tremor, and to identify the cause of possible depth-dependent tremor behaviors in the creeping section of the SAF.

We found a positive correlation between the amplitudes of triggered tremor and the amplitudes and the associated dynamic stresses of the teleseismic surface waves at all regions (Figure 4.11). This observation is generally consistent with the prediction of the aforementioned clock advance model (Gomberg, 2010) that larger triggering waves result in larger triggered tremor signals. For example, in SJF the PGV measured at station RDM during the Tohoku-Oki mainshock is ~0.12 cm/s, which is about 5 times lower than the PGV of 0.54 cm/s during the 2002 Denali Fault earthquake (Chao *et al*., 2012a). The median triggered tremor amplitude is ~0.2 nm/s and ~10 nm/s for the Tohoku-Oki and Denali Fault earthquake, respectively, again qualitatively consistent with the prediction of the clock advance model. This also suggests that in regions where the background tremor rate is low (e.g., SJF or CF in California) or the background seismic noise is high, larger triggering waves are needed to trigger tremor with amplitudes larger than the background noise level. While the correlation between the PGV and tremor amplitude is statistically significant, there is a large amount of scatter, and the scatter becomes larger after the tremor amplitude corrections. This is likely caused by the assumption of a constant Q, location errors, and/or other unknown path or site effects that modify the high-frequency

tremor amplitudes. In addition, we also did not take into account the difference in background tremor rate in each region.

Finally, we systematically modeled the triggering potentials of Love and Rayleigh waves using a simple Coulomb failure criterion (Hill, 2010). Our modeling results confirmed that both Love and Rayleigh waves play important roles in the triggering of tremor, and that their triggering potentials are partially controlled by the incident angles of incoming surface waves (Figure 4.12). We also computed the time-dependent Love and Rayleigh waves related stress changes, or stress-grams, and compared them with the tremor signals. We found that tremor pulses do not necessarily correlate with the picks in any of the three displacement components but with picks in the calculated triggering potential (Figure 4.13). In other words, neither the Love nor the Rayleigh waves by themselves are responsible for tremor triggering, but caused by the combination of the dynamic stresses from both surface waves. This observation indicates that it is important to take the contributions of both Love and Rayleigh waves into account for triggering tremor.

The fact that the tremor amplitude is controlled mainly by the triggering waves and the background tremor rate, indicate that one could predict the occurrence of triggered tremor in certain region right after the occurrence of major earthquakes and before the arrivals of surface waves. The amplitudes of the triggered tremor are ~10-100 nm/s, that is, equivalent to a magnitude 0-1 earthquake. Hence, although triggered tremor do not cause any damage, they can present a perfect cases to study the predictability of

earthquakes, like the micro-repeating earthquakes at Parkfield. (Zechar and Nadeau, 2012). This will be done in the follow-up works.

4.7 Data and Resources

Seismograms used in this study were downloaded from the following resources. (1) Alaska and Aleutian Arc: the Alaska Volcano Observatory (Network code: AV) distributed through the IRIS website (http://www.iris.edu/mda, last accessed March 2012). (2) Cascadia: the Canadian National Seismograph Network (CNSN, http://www.earthquakescanada.nrcan.gc.ca/stndon/AutoDRM/autodrm_req-eng.php, last accessed March 2012) operated by the Geological Survey of Canada (GSC), and the Pacific Northwest Regional Seismic Network (Network code: UW) distributed through the IRIS website (http://www.iris.edu/mda, last accessed March 2012). (3) Nankai subduction zone, Japan: the Hi-net (High Sensitivity Seismograph Network, http://www.hinet.bosai.go.jp/, permission required, last accessed March 2012) and F-net (Broadband Seismograph Network, http://www.fnet.bosai.go.jp/, permission required, last accessed March 2012) operated by the National Research Institute for Earth Science and Disaster Prevention (NIED), Japan. (4) New Zealand: the GeoNet - the New Zealand National Seismic Network (http://www.geonet.org.nz/, last accessed March 2012). (5) Others: Calaveras Fault (BK.MHC), Costa Rica (II.JTS), Cuba (CU.GTBY), Oregon (BK.HUMO) are from the Berkeley Digital Seismograph Network (Network code: BK), the Global Seismograph Network (Network code: II), the USGS Caribbean Network (Network code: CU) distributed through the IRIS website (http://www.iris.edu/mda, last accessed March 2012). (6) Parkfield: the Northern

California Earthquake Data Center (network codes: BP, NC, and PB, http://www.ncedc.org/, last accessed March 2012). (7) San Jacinto Fault: the Southern California Earthquake Data Center (network codes: AZ, CI and PB, http://www.data.scec.org/, last accessed March 2012). (8) Taiwan: the Broadband Array in Taiwan for Seismology (BATS, http://bats.earth.sinica.edu.tw/, last accessed March 2012) operated by the Institute of Earth Sciences (IES), Academia Sinica, and the short-period Central Weather Bureau Seismic Network (CWBSN, http://gdms.cwb.gov.tw/, permission required, last accessed March 2012) operated by the Taiwan Central Weather Bureau (CWB).

4.8 Supplement Figures and Tables

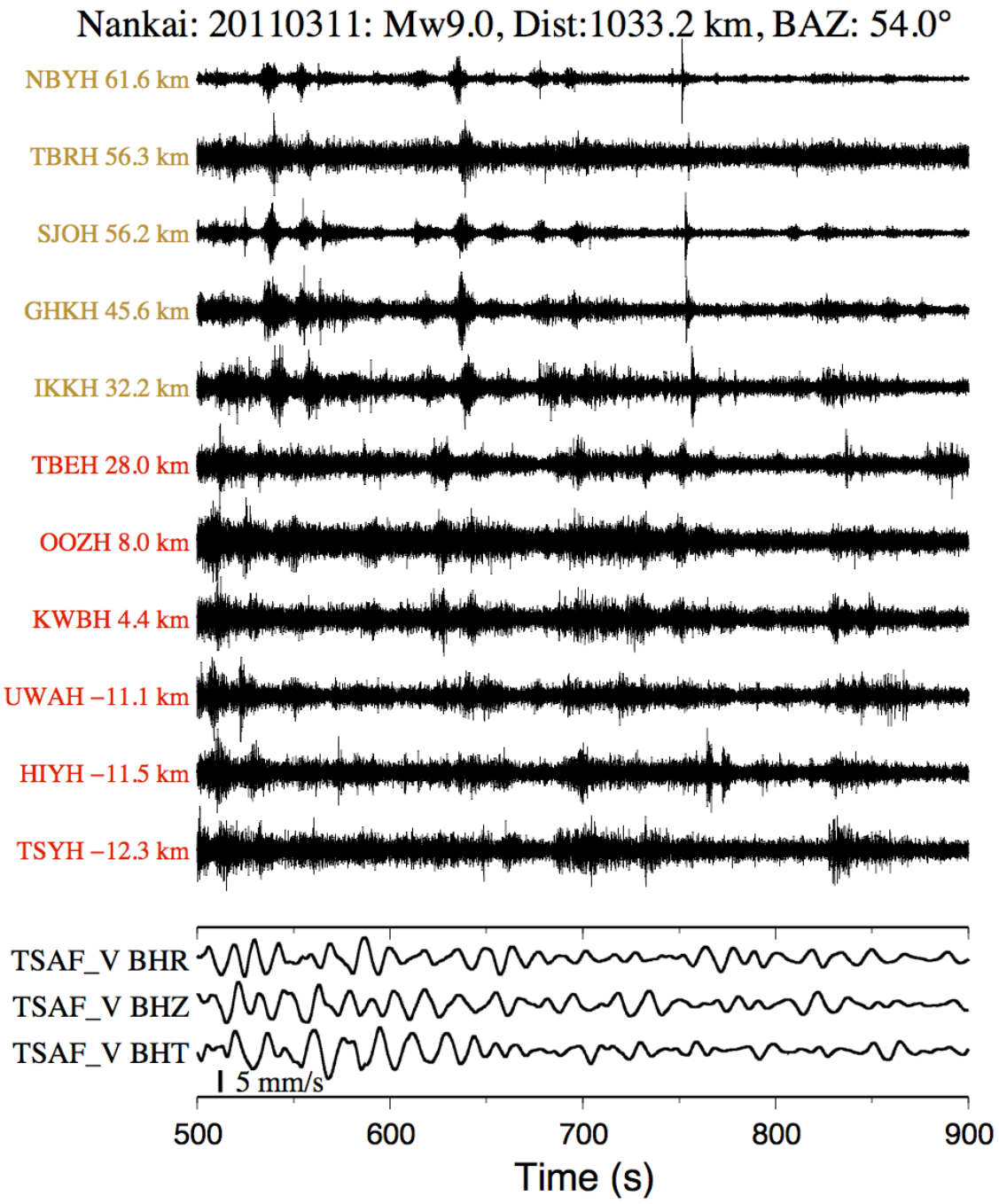

Figure S4.1 (a) Triggered tremor seismograms in Shikoku, Nankai around the 2011 Mw9.0 Tohoku-Oki mainshock. This figure is the same as Figure 4.3b but zoom in between 500 s and 900 s. The 5 Hz high-pass filtered seismograms in E-component showing the moveout of triggered tremor at multiple source regions in Shikoku. The along-strike distance to the tremor source in western Shikoku (Tables S4.1 and S4.2) and the station names are marked to the left of the seismograms. The tremor bursts used to

locate different tremor source are marked with vertical dotted lines and different colors. The bottom three traces show the instrument-corrected strong motion velocity (V) seismograms in radial (BLR), vertical (BLZ), and transverse (BLT) components at the F-net station TSAF. The study region, magnitude (M) of the 2011/03/11 Tohoku-Oki mainshock, and the epicenter distance (Dist) and back azimuth (BAZ) relative to the station TSAF are shown above the seismograms. The zero time corresponds to the origin time of the Tohoku-Oki mainshock. The arrow marks the predicted arrival of S-wave of the mainshock. The thick vertical bar marks the amplitude scale of surface waves.

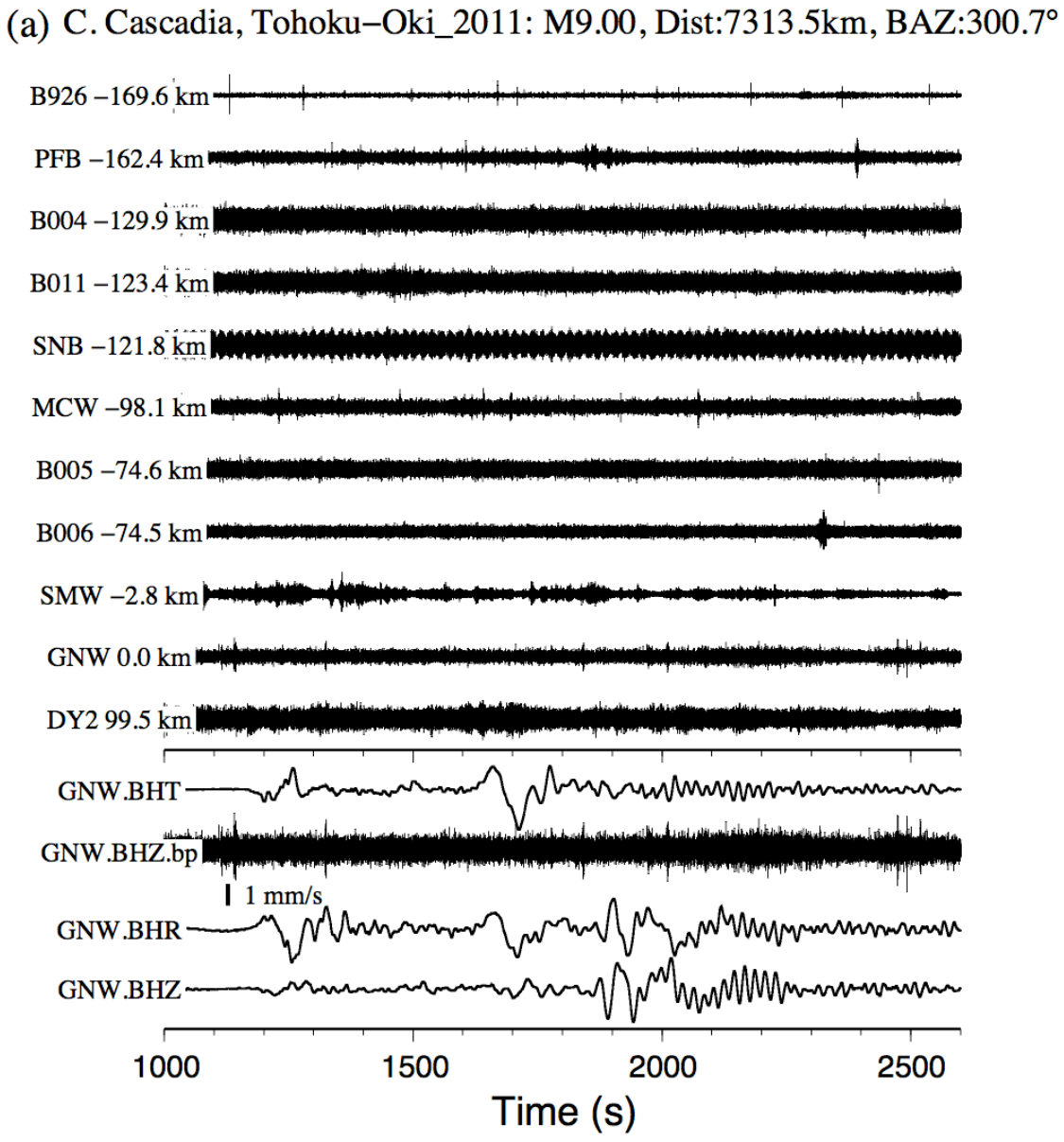

Figure S4.2 No tremor triggered by the Tohoku-Oki earthquake in central Cascadia with 5-Hz high-pass-filtered seismograms in Z-component. The seismograms are plotted along

the strike of the Cascadia sunduction zone. The bottom three traces show the instrument-corrected broadband velocity seismograms at station UW.GNW. Other notations are the same as in Figure S4.1.

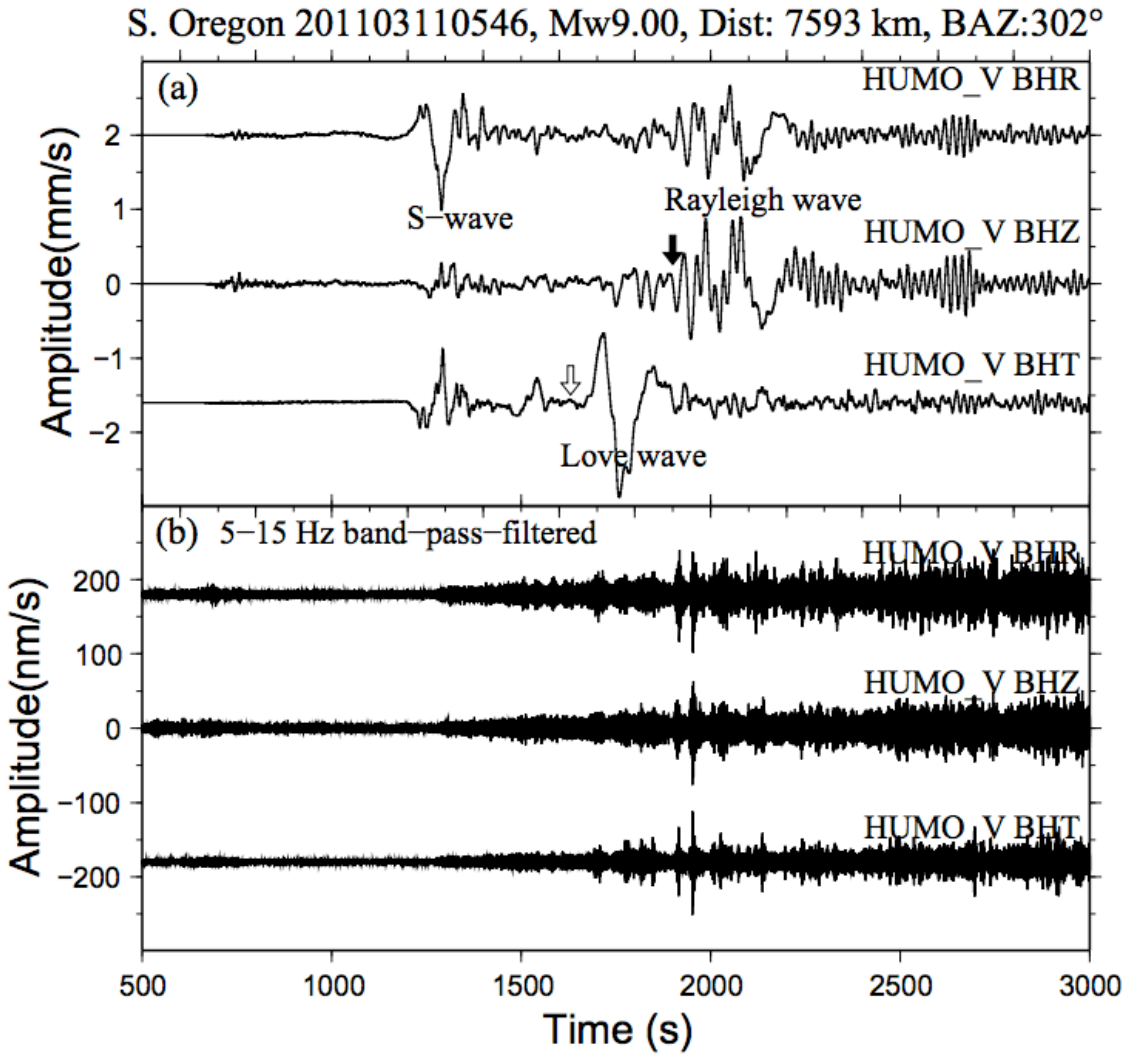

Figure S4.3 Clear triggered tremor example in south Oregon. A comparison of the (a) broadband station BK.HUMO and (b) 5– 15 Hz band-pass-filtered seismograms on radial (R), vertical (Z), and transverse (T) components at station HUMO. The open and solid arrows mark the approximate arrival times of the Love and Rayleigh waves, respectively.

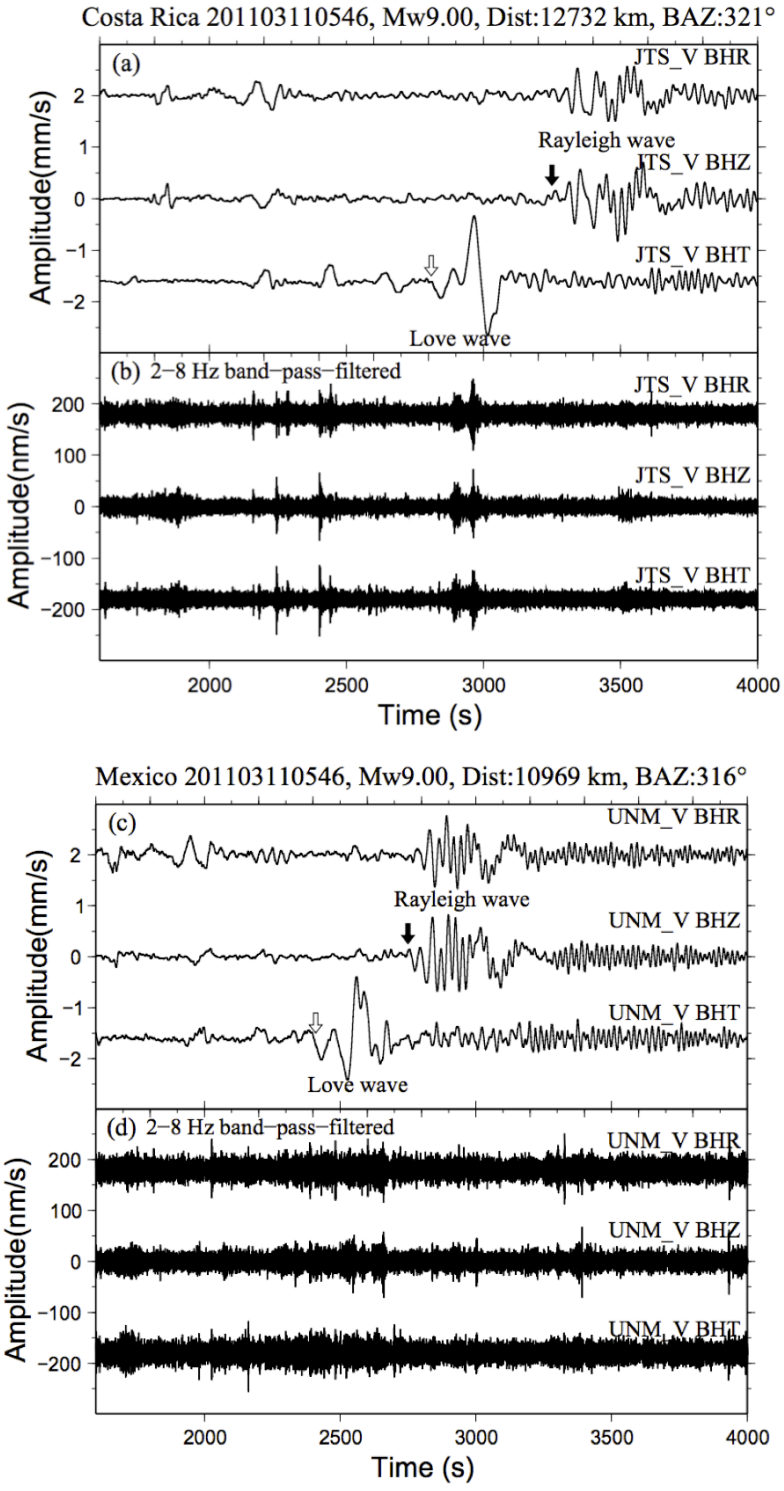

Figure S4.4 No clear triggered tremor examples in Costa Rica (a-b) and Mexico (c-d). A comparison of the (a) broadband station II.JTS and (b) 2–8 Hz band-pass-filtered

seismograms at JTS, and the (c) broadband station G.UNM and (d) 2–8 Hz band-pass-filtered seismograms at UNM. Other notations are the same as in Figure S4.3.

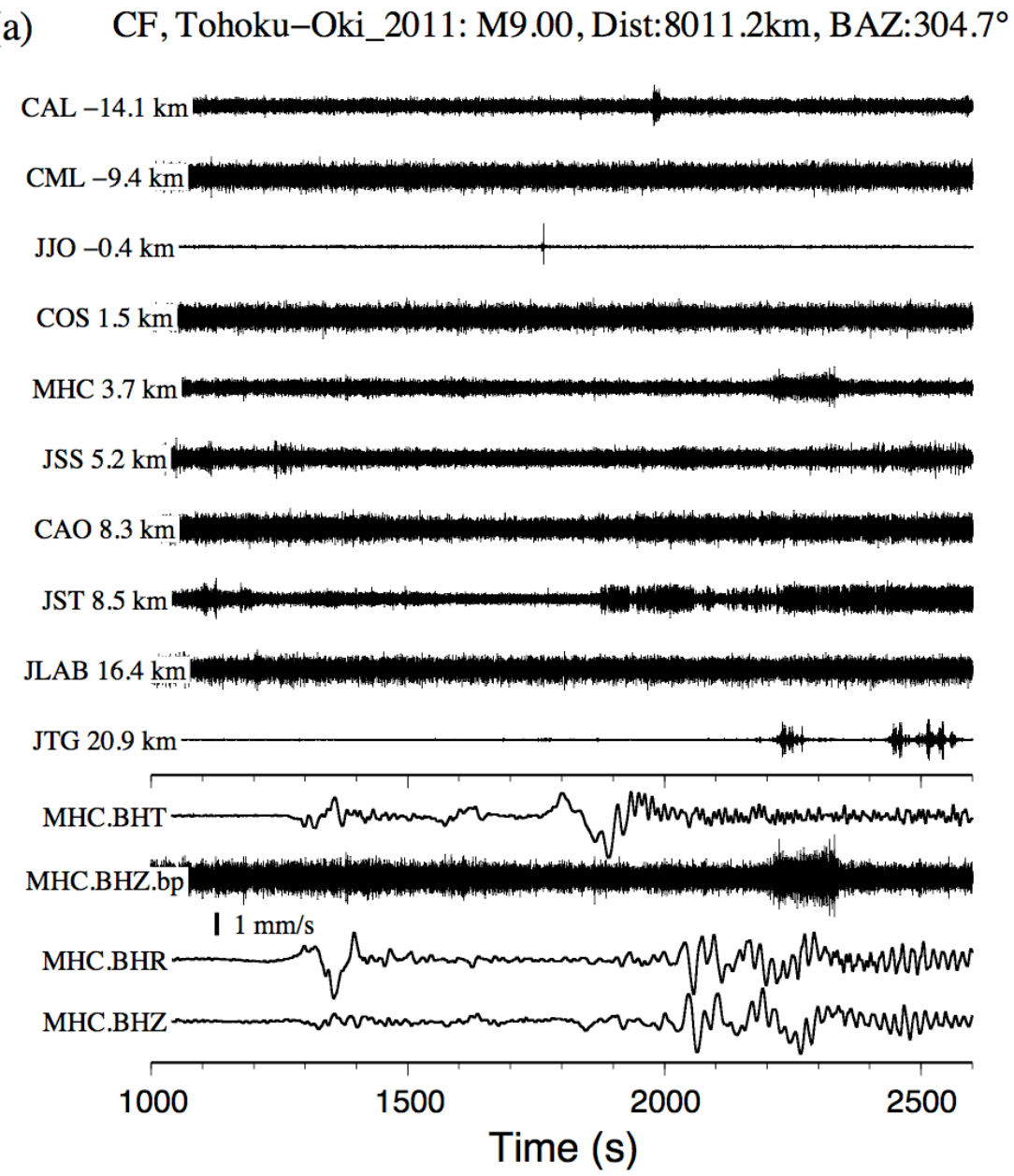

Figure S4.5 No tremor triggered by the Tohoku-Oki earthquake in Calaveras Fault with 2-8-Hz band-pass-filtered seismograms in Z-component. Other notations are the same as in Figure S4.1.

Table S4.1 Triggered tremor locations

Online version:
http://kevinchao.com/KChao/papers/Chao_etal_BSSA_2013_Table_S1.txt

```
# Table S1
# Triggered tremor locations in different regions
#(1)     (2)   (3)  (4)     (5)  (6)      (7)      (8)
#lon     lat   dep  RMS     stn stn_lon   stn_lat  region
-146.06  61.67 45.0 2.8415  KLU -145.923  61.4925  Alaska
-166.26  53.97 45.0 3.7762 AKRB -166.071  54.1292  Aleutian-C
-166.90  53.59 45.0 4.2311 OKFG -167.911  53.4107  Aleutian-W
-163.27  55.26 45.0 0.2418 SSLN -163.998  54.8109  Aleutian-E
   0      0     0   0       MHC -121.643  37.3416  CF
   0      0     0   0       JTS  132.748  33.5022  CostaRica
   0      0     0   0      GTBY -75.1108  19.9268  Cuba
 132.78  33.45 35.0 1.1406 KWBH  132.748  33.5022  Nankai-W
 133.24  33.83 35.0 2.0922 SJOH  133.184  33.8650  Nankai-C
 176.52 -39.15 45.0 0.4202  BKZ  176.492 -39.1674  NZ-SW
 176.76 -38.96 45.0 5.1761 NMHZ  176.806 -39.0988  NZ-NE
   0      0     0   0       HUMO  176.492 -39.1674  Oregon
-120.31  35.76 25.0 N/A     PKD -120.542  35.9452  Parkfield
-116.64  33.58 25.0 1.2204  RDM -116.848  33.6300  SJF
 120.88  23.05 25.0 2.1996 TPUB  120.630  23.3005  Taiwan-S
 121.43  24.27 25.0 1.8082 NACB  121.595  24.1738  Taiwan-1
 121.85  24.61 25.0 1.9611  TWC  121.859  24.6081  Taiwan-NZ
-127.39  50.31 35.0 4.6100  PHC -127.433  50.7067  Vancouver
   0      0     0   0       UNM -99.178   19.3290  Mexico
#
# (1) (2) (3): longitude(degree), latitude(degree), and depth(km) of triggered tremor sources
# (4): minumum root-mean-square(RMS) value, unit is in second
# (5) (6) (7): staion that is used to record triggered tremor for tremor amplitude corrections.
# (8): name of study region. CF: Calaveras Fault; NZ: New Zealand; SJF: San Jacinto Fault.
#
# In Parkfiled: LFE locations triggered by the 2011 Tohoku-Oki maikshock
# is calculated from David Shelly's LFEs Catalog
# Love window:     1750-2000s to MS or 22534-22784 s of 03/11
# Rayleigh window: 2000-2400s to MS or 22784-23184 s of 03/11
# LFE during Love:     -120.297 35.737 23.768
# LFE during Rayleigh: -120.321 35.779 25.300
# average location:    -120.31  35.76  25.0
```

Table S4.2 List of the information and measured parameters in all 17 regions used in this study. See the title within the file for the details of each field.

Online version:
http://kevinchao.com/KChao/papers/Chao_etal_BSSA_2013_Table_S2.txt

```
# Table S2
#(1) (2) (3)      (4)     (5)     (6)      (7)    (8) (9)  (10)     (11) (12)(13) (14)    (15)   (16)    (17)      (18)    (19) (20)
#S/N      S:nm     N:nm  tr_dist  S_cor    N_cor PGV_T     cm/s      KPa  PGV_Z    cm/s    KPa  stn_dist baz      region  num
 KLU BH  0.27180  0.03143 21.1   149.27    17.26  KLU BH  0.1270   9.30  KLU BH  0.1310  11.20  5415.1 276.1     Alaska  1   S_15.bp.disp
AKRB BH  3.79388  0.61607 21.6  2116.25   343.65 AKRB BH  0.4460  32.60 AKRB BH  0.4750  40.70  4237.1 267.0  Aleutian1  2   S_15.bp.disp
OKFG BH  0.88267  0.23510 70.1  4113.49  1095.63 OKFG BH  0.3850  28.20 OKFG BH  0.5020  43.00  4111.2 266.4  Aleutian2  3   S_15.bp.disp
 MHC BH  0.17219  0.17299  0.0     0.00     0.00  MHC BH  0.1110   8.10  MHC BH  0.0909   7.80  8016.9 304.7         CF  4   S_15.bp.disp
 JTS BH  0.11192  0.10776  0.0     0.00     0.00  JTS BH  0.1270   9.30  JTS BH  0.0826   7.10 12736.3 320.5  CostaRica  5   S_15.bp.disp
GTBY BH  0.21599  0.09536  0.0     0.00     0.00 GTBY BH  0.1290   9.40 GTBY BH  0.0750   6.40 12479.5 328.9       Cuba  6   S_15.bp.disp
KWBH BL  3.71684  0.08291  6.5   739.41    16.49 TSAF EH  2.8200 206.30 TSAF EH  1.7400 149.10  1033.2  54.0    Nankai1  7   S_15.bp.disp
SJOH BL  5.25960  0.09373  6.5  1045.83    18.64 OKWF EH  3.2300 236.30 OKWF EH  2.3800 204.00   942.5  55.7    Nankai2  8   S_15.bp.disp
 BKZ HH  0.21822  0.25856  3.1    87.08   103.18  BKZ HH  0.1150   8.40  BKZ HH  0.1670  14.30  9253.0 333.6        NZ1  9   S_15.bp.disp
NMHZ HH  0.87671  0.71166 15.9   420.34   341.21  BKZ EH  0.1150   8.40  BKZ EH  0.1670  14.30  9253.0 333.6        NZ2 10   S_15.bp.disp
HUMO BH  0.15924  0.02820  0.0     0.00     0.00 HUMO BH  0.1140   8.30 HUMO BH  0.0894   7.70  7599.8 302.5     Oregon 11   S_15.bp.disp
 PKD BH  0.28571  0.03746 29.4    71.01     9.31  PKD BH  0.0916   6.70  PKD BH  0.1180  10.10  8186.6 305.5   Parkfield 12   S_15.bp.disp
 RDM BH  0.16714  0.14809 20.1    25.25    22.37  RDM HH  0.1030   7.50  RDM HH  0.1340  11.50  8611.1 307.6        SJF 13   S_15.bp.disp
TPUB BH  2.36128  0.27814 37.7   952.30   112.17 TPUB HH  0.8520  62.30 TPUB HH  0.6350  54.40  2650.7  46.2     Taiwan1 14   S_15.bp.disp
NACB BH  0.95185  0.11615 19.8   142.14    17.34 NACB HH  0.9160  67.00 NACB HH  0.6640  56.90  2512.8  46.6     Taiwan2 15   S_15.bp.disp
 PHC BH  0.03340  0.02195 44.3    28.83    18.95  PHC BH  0.2300  16.80  PHC BH  0.1130   9.70  6856.6 296.6   Vancouver 16   S_15.bp.disp
 UNM BH  0.86969  1.45184  0.0     0.00     0.00  UNM BH  0.1210   8.90  UNM BH  0.0821   7.00 10972.6 315.6      Mexico 17    S_9.bp.disp
#
# (1): S/N: station name that used to measure tremor/nontremor amplitude
# (2): type of instrument, BH: Broadband High gain, HH: High broadband High gain, BL: Broadband Low gain (strong motion)
# (3): Singnal(S): median tremor/non-tremor amplitude measured from displacement seismogram, unit is in nm.
# (4): Noise(N): median noise amplitude measured from displacement seismogram 600-s before the occurrene of mainshock, unit is in nm.
# (5): tr_dist: epicentral distance between station and tremor sources (see Table S1)
# (6): S_corr: Singal (3) after correction
# (7): N_corr: Signal (4) after correction
# (8): PGV_T: station name that used to measure PGV(peak ground velocity) in tranverse (T) component
# (9): station type band of (8), see (2).
# (10): PGV, unit is in cm/s
# (11): corresponding dynamics stress, unit is in KPa
# (12): PGV_Z: station name that used to measure PGV(peak ground velocity) in vertical (Z) component
# (13): station type band of (12), see (2).
# (14): PGV, unit is in cm/s
# (15): corresponding dynamics stress, unit is in KPa
# (16): stn_dist: epicentral distance between station and the Tohoku-Oki mainshock epicenter
# (17): baz: back azimuth bewteen station and the Tohoku-Oki mainshock
# (18): study regions. CF: Calaveras Fault; NZ: New Zealand; SJF: San Jacinto Fault.
# (19): numbers that are marked on Figure 2 and 11.
# (20): band-pass filter used for (2) and (3)
```

Table S4.3 1-D velocity model used to locate triggered tremor in each region

Online version:
http://kevinchao.com/KChao/papers/Chao_etal_BSSA_2013_Table_S3.txt

```
# Table S3
# Velocity models used in this study
#   (1)      (2)
# Vs(km/s) depth(km)
# Vs: S-wave velocity
#
#Alaska
% from Eberhart-Phillips et al., JGR, 2006 (Table 1, P.7)
2.914  2.0
3.457  6.0
3.629 15.0
3.771 24.0
4.086 33.0
4.497 48.0
4.640 65.0
#
#Aleutian
% from Kennett et al., GJI, 1995 (p.122); other ref: Hauksson JGR 1985
3.46  0.0
3.85 20.0
4.48 35.0
4.49 77.5
#
#Cascadia
% from Aaron Wech. The PNSN's puget sound velocity model
3.11778 0.0
3.68360 4.0
3.80485 9.0
3.88568 16.0
3.96074 20.0
4.01270 25.0
4.50346 51.0
4.61894 81.0
#
#Nankai
% from Bogdan Enescu. NIED
2.844 0.0
3.012 1.0
3.157 2.0
3.278 3.0
3.375 4.0
3.431 5.0
3.451 6.0
3.471 7.0
3.491 8.0
3.511 9.0
3.531 10.0
3.552 11.0
3.572 12.0
3.593 13.0
3.614 14.0
3.634 15.0
3.657 16.0
3.680 17.0
3.704 18.0
3.729 19.0
3.754 20.0
3.782 21.0
3.803 22.0
3.831 23.0
3.858 24.0
```

3.885 25.0
3.915 26.0
3.944 27.0
3.974 28.0
4.003 29.0
4.032 30.0
4.059 31.0
4.086 32.0
4.113 33.0
4.140 34.0
4.161 35.0
4.186 36.0
4.210 37.0
4.232 38.0
4.254 39.0
4.274 40.0
4.294 41.0
4.311 42.0
4.329 43.0
4.344 44.0
4.356 45.0
4.367 46.0
4.375 47.0
4.382 48.0
4.388 49.0
4.393 50.0
4.396 51.0
4.399 52.0
4.404 53.0
4.406 54.0
4.409 55.0
4.410 56.0
4.411 57.0
4.413 58.0
4.414 59.0
4.415 60.0
#
#New Zealand
% Fry et al., GRL, 2010
3.30 0.0
3.70 12.0
4.60 33.0
4.90 45.0
#
#San Jacinto Fault
% Hutton et al., BSSA, 2010 (originla from Kanamori 1977)
3.20 0.0
3.60 5.5
3.90 16.0
4.50 32.0
#
#Taiwan-south
% Southern CR of Taiwan
% from Tang et al., GRL, 2010
2.20 0.0
2.93 2.0
3.24 4.0
3.31 6.0
3.31 9.0
3.42 13.0
3.46 17.0
3.50 21.0
3.65 25.0
3.78 30.0
4.02 35.0
4.60 50.0
4.82 70.0
#
#Taiwan-north
% Northern CR of Taiwan

% from Wu et al., GJI, 2009
2.15 0.0
2.65 2.0
2.93 4.0
3.07 6.0
3.32 9.0
3.48 13.0
3.60 17.0
3.75 21.0
3.88 25.0
4.05 30.0
4.25 35.0
4.56 50.0
4.67 70.0

Table S4.4 Fault orientations in different regions and inforamtion of the 2011 Tohoku-Oki earthquake

Online version:
http://kevinchao.com/KChao/papers/Chao_etal_BSSA_2013_Table_S4.txt

```
# Table S4
#(1)   (2)   (3)  (4)   (5)      (6)  (7)         (8)
#stn   baz    strike    in      type region      reference paper
 KLU  276.1  N55E 055  138.9    Subd Alaska      Peterson_Christensen_JGR_2009
AKRB  267.0  N64E 064  157.0     Subd Aleutian    Peterson_etal_BSSA_2011
 MHC  304.7  N35W 325   20.3    R-SS CF          Chao_etal_BSSA_2012
 JTS  320.5  N55W 305  -15.5    Subd CostaRica   Outerbridge_etal_JGR_2010
GTBY  328.9  N82E 082  113.1    L-SS Cuba        Gonzalez-Huizar_etal_GRL_2012
KWBH   54.0  N41E 041  -13.0     Subd Nankai      Hill_BSSA_2010
 BKZ  333.6  N34E 034   60.4    Subd NZ          Fry_etal_GRL_2011
HUMD  302.5  N10W 350   47.5    Subd Oregon      Wech_Creager_NGEO_2011
 PKD  305.5  N41W 319   13.5     R-SS Parkfield   Hill_BSSA_2010
 ROM  307.6  N49W 311    3.4    R-SS SJF         Chao_etal_BSSA_2012
TPUB   46.2  N16E 016  -30.2    Coll Taiwan      Chao_etal_GJI_2012
 PHC  296.6  N38W 322   25.4     Subd Cascadia   Hill_BSSA_2010
# R-SS: left-lateral strike-slip
# L-SS: right-lateral strike-slip
# Subd: subduction
# Coll: collision environment
#
# Information of the 2011 Tohoku-Oki, Japan earthquake
# event-ID     Year mon day hr min sec    lon.      lat.      depth  mag
# 201103110546 2011 03  11  05 46  24.12  142.3730  38.2970   29.00  9.00
```

APPENDIX A

METHOD FOR LOCATING TRIGGERED TREMOR

The tremor location is calculated by performing a grid search of the minimal root-mean-square (RMS) between the theoretical and observed travel time differences ($\Delta T_{i,j}$) for all station pairs ($pair^{i,j}$) (Chao *et al.*, 2012d; Peng and Chao, 2008; Peng *et al.*, 2009). We first compute the envelope function of seismograms that record clear tremor bursts in horizontal component because tremor is primarily generated by shear failure at depth. If there are n stations used to locate tremor, the total number of station pairs is $pair^{i,j} = n(n-1)/2$. The equation for computing the RMS for each grid point ([x, y, z] or [longitude, latitude, depth]) is

$$RMS_{(x,y,z)} = \sqrt{\sum_{i=1,j=2}^{n} (\Delta T_{i,j})^2 \Big/ n} = \sqrt{\left(\sum_{i=1,j=2}^{n} (\Delta t_{i,j}^{theo} - \Delta t_{i,j}^{obs})^2 \Big/ n \right)}$$

$$= \sqrt{\frac{(\Delta t_{1,2}^{theo} - \Delta t_{1,2}^{obs})^2 + (\Delta t_{1,3}^{theo} - \Delta t_{1,3}^{obs})^2 + ...+ (\Delta t_{2,3}^{theo} - \Delta t_{2,3}^{obs})^2 + ...+ (\Delta t_{i=n-1,j=n}^{theo} - \Delta t_{i=n-1,j=n}^{obs})^2}{n}}$$

(A1).

where *theo* and *obs* denote the theoretical and observed travel time difference ($\Delta T_{i,j}$) for all pairs ($\sum pair^{i,j}$). For each single $pair^{i,j}$, the theoretical travel time difference ($\Delta t_{i,j}^{theo}$) is computed from the difference of S-wave travel time from a common source (x,y,z) to

different stations *i* and *j* based on a 1D velocity model in each region (Table S4.3). The observed travel time difference ($\Delta t_{i.j}^{obs}$) is computed from cross-correlation of envelope functions for each tremor burst.

The best tremor location $(x,y,z)^{best}$ for each tremor burst corresponds to the minimum RMS among the entire grid search space. The final tremor location for each triggering event is calculated by averaging the locations from different tremor burst weighted by the RMS.

Because the tremor depth is generally not well constrained, in this study we fix the tremor depth to a certain value in each region (Table S4.1). Hence, the grid search is only performed in the longitude and latitude in a grid space of 0.01^{o}.

For regions with multiple tremor sources, we first separate the observed tremor signals into several groups based on their different waveform characteristics and moveout. Then we compute the RMS for each tremor source separately. Finally, we take the smallest RMS of all tremor sources at each grid point to obtain a composite RMS contour map in each region.

For more information of the tutorial on how to search for triggered tremor and locate tremor sources can be found on this webpage: http://kevinchao.com/login/login.php
(Email me for username and password: kevinchao@gmail.com)

REFERENCES

Aki, K. and P. G. Richards (2002). Quantitative Seismology, **2nd ed.,** 700 pp., Univ. Sci. Books, Sausalito, Calif.

Beroza, G. C. and S. Ide (2009). Deep tremors and slow quakes, *Science* **324,** 1025-1026.

Beroza, G. C. and S. Ide (2011). Slow Earthquakes and Nonvolcanic Tremor, *Annu. Rev. Earth Planet. Sci.* **39,** 271-296.

Boore, D. M. (2003). Simulation of ground motion using the stochastic method, *Pure and Applied Geophysics***,** 635-676.

Bouchon, M., H. Karabulut, M. Aktar, S. Özalaybey, J. Schmittbuhl, and M.-P. Bouin (2011). Extended Nucleation of the 1999 Mw 7.6 Izmit Earthquake, *Science* **331**.

Brodsky, E. E. and S. G. Prejean (2005). New constraints on mechanisms of remotely triggered seismicity at Long Valley Caldera, *J. Geophys. Res.* **110,** B04302.

Brown, J. R., G. C. Beroza, S. Ide, K. Ohta, D. R. Shelly, S. Y. Schwartz, W. Rabbel, M. Thorwart, and H. Kao (2009). Deep low-frequency earthquakes in tremor localize to the plate interface in multiple subduction zones, *Geophys. Res. Lett.* **36,** L19306.

Brown, J. R., S. G. Prejean, G. C. Beroza, J. S. Gomberg, and P. J. Haeussler (2012). Deep Low-Frequency Earthquakes in Tectonic Tremor Along the Alaska-Aleutian Subduction Zone in prep.

Chao, K., Z. Peng, C.-C. Tang, C.-H. Lin, and C. H. Chen (2010). Deep Tremor Activities beneath the Central Range in Taiwan and Their Relationship to Local, Regional, and Teleseismic Earthquakes, *Eos Trans. AGU* **91(50),** Fall Meet. Suppl., Abstract S23A-2106.

Chao, K., Z. Peng, D. Hill, D. Shelly, B. Enescu, B. Fry, and C. Aiken (2011). Triggered Non-volcanic Tremor following the 2011 Tohoku-Oki Earthquake, *SCEC Annual Meeting***,** Palm Springs, California, 11–15 September 2011.

Chao, K., Z. Peng, A. Fabian, and L. Ojha (2012a). Comparisons of Triggered Tremor in California, *Bull. Seismol. Soc. Am* **12,** 2.

Chao, K., Z. Peng, H. Gonzalez-Huizar, C. Aiken, B. Enescu, H. Kao, A. A. Velasco, K. Obara, and T. Matsuzawa (2012b). Global Search of Triggered Tremor Following the 2011 Mw9.0 Tohoku- Oki Earthquake, *Bull. Seismol. Soc. Am***,** submitted.

Chao, K., Z. Peng, A. Wech, C. Wu, C.-C. Tang, L. Y. Chuang, K. H. Chen, and C.-H. Lin (2012c). Deep Non-volcanic Tremor Activities in Taiwan before and after the Local Mw6.3 Jiasian Earthquake, *Geophys. Res. Lett***,** Submitted.

Chao, K., Z. Peng, C. Wu, C.-C. Tang, and C.-H. Lin (2012d). Remote triggering of non-volcanic tremor around Taiwan, *Geophys. J. Int.* **188,** 1, 301-324.

Delahaye, E., J. Townend, M. Reyners, and G. Rogers (2009). Microseismicity but no tremor accompanying slow slip in the Hikurangi subduction zone, New Zealand, *Earth and Planetary Science Letters* **277,** 1-2, 21-28.

Enescu, B., K. Chao, K. Obara, and Z. Peng (2012). Non-volcanic tremor triggered in south-west Japan by the 2011 M9.0 Tohoku earthquake and its aftershocks: a detailed investigation of the triggering process, *Bull. Seismol. Soc. Am***,** in prep.

Flinchum, B. A. and M. R. Brudzinski (2011). Non-volcanic Tremor Triggered by Teleseismic Surface Waves in South-Central Alaska, *Eos Trans. AGU***,** Fall Meet. Suppl., Abstract S23B-2254.

Fry, B., K. Chao, S. Bannister, and Z. Peng (2011). Deep tremor beneath the Hikurangi margin in New Zealand triggered by the 2010 Mw 8.8 Chile earthquake, *Geophys. Res. Lett* **38,** L15306.

Geller, R. J. (1976). Scaling relations for earthquake source parameters and magnitudes, *Bull. Seismol. Soc. Am* **66,** 5, 1501-1523.

Ghosh, A., J. E. Vidale, Z. Peng, K. C. Creager, and H. Houston (2009). Complex nonvolcanic tremor near Parkfield, California, triggered by the great 2004 Sumatra earthquake, *J. Geophys. Res.* **114,** B00A15.

Gomberg, J., J. L. Rubinstein, and Z. Peng (2008). Widespread triggering of nonvolcanic tremor in California, *Science* **319,** 173.

Gomberg, J. (2010). Lessons from (Triggered) Tremor, *J. Geophys. Res.* **115,** B10302.

Gomberg, J., t. C. 2007, and B. W. Group (2010). Slow-slip phenomena in Cascadia from 2007 and beyond: A review, *GSA Bulletin* **122,** 7/8, 963-978.

Gonzalez-Huizar, H. and A. A. Velasco (2011). Dynamic Triggering: Stress Modeling and a Case Study, *J. geophys. Res* **116,** B02304.

Gonzalez-Huizar, H., A. A. Velasco, Z. Peng, and R. Castro (2012). Remote Triggered Seismicity Caused by the 2011, M9.0 Tohoku, Japan Earthquake, *Geophys. Res. Lett***,** Submitted.

Guilhem, A., Z. Peng, and R. M. Nadeau (2010). High-frequency identification of non-volcanic tremor triggered by regional earthquakes, *Geophys. Res. Lett* **37,** L16309.

Hill, D. (2008). Dynamic stresses, Coulomb failure, and remote triggering, *Bull. Seismol. Soc. Am* **98,** 1, 66-92.

Hill, D. P. (2010). Surface-Wave Potential for Triggering Tectonic (Nonvolcanic) Tremor, *Bull. Seismol. Soc. Am* **100,** 5A, 1859-1878.

Hill, D. P., Z. Peng, D. R. Shelly, and C. Aiken (2012). Tectonic tremor beneath the Parkfield, CA, section of the San Andreas Fault triggered by S waves and surface waves from the Mw 9.0 Tohoku-Oki, Japan, Earthquake, *Bull. Seismol. Soc. Am***,** submitted.

Hillers, G. and J. P. Ampuero (2009). Systematic search for spontaneous non-volcanic tremor in Southern California, *Eos Trans. AGU* **90(54),** Fall Meet. Suppl., Abstract T13D-1918.

Ide, S., D. Shelly, and G. C. Beroza (2007). Mechanism of deep low frequency earthquakes: Further evidence that deep non-volcanic tremor is generated by shear slip on the plate interface, *Geophys. Res. Lett.* **34,** L03308.

Ide, S. (2010). Striations, duration, migration and tidal response in deep tremor, *Nature* **466,** 356-359.

Ide, S. (2012). Variety and spatial heterogeneity of tectonic tremor worldwide, *J. Geophys. Res.* **117,** B3.

Jaeger, J. C. and N. G. W. Cook (1979). *Fundamentals of Rock Mechanics***,** 3rd ed. Chapman and Hall, New York.

Jiang, T., Z. Peng, W. Wang, and Q.-F. Chen (2010). Remotely triggered seismicity in Continental China by the 2008 Mw7.9 Wenchuan earthquake, *Bull. Seismol. Soc. Am* **100,** 5B, 5274-5289.

Kao, H. and S.-J. Shan (2004). The Source-Scanning Algorithm: mapping the distribution of seismic sources in time and space, *Geophys. J. Int.* **157,** 2, 589-594.

Kao, H., S.-J. Shan, H. Dragert, and G. Rogers (2009). Northern Cascadia episodic tremor and slip: A decade of tremor observations from 1997 to 2007, *J. Geophys. Res.* **114,** B00A12.

Kao, H., K. Wang, H. Dragert, J. Y. Kao, and G. Rogers (2010). Estimating seismic moment magnitude (Mw) of tremor bursts in northern Cascadia: Implications for the "seismic efficiency" of episodic tremor and slip, *Geophysical Research Letters* **37,** 19.

Kato, A., K. Obara, T. Igarashi, H. Tsuruoka, S. Nakagawa, and N. Hirata (2012). Propagation of Slow Slip Leading Up to the 2011 Mw 9.0 Tohoku-Oki Earthquake, *Science* **335,** 6069, 705-708.

Kim, M. J., S. Y. Schwartz, and S. Bannister (2011). Non-volcanic tremor associated with the March 2010 Gisborne slow slip event at the Hikurangi subduction margin, New Zealand, *Geophysical Research Letters* **38,** 14.

La Rocca, M., D. Galluzzo, S. Malone, W. McCausland, and E. Del Pezzo (2010). Array analysis and precise source location of deep tremor in Cascadia, *J. Geophys. Res.* **115**.

Lay, T. and T. C. Wallace (1995). Modern Global Seismology, *Academic***,** San Diego, Calif.

Liu, C., A. T. Linde, and I. S. Sacks (2009). Slow earthquakes triggered by typhoons, *Nature* **459,** 833-836.

Mazzotti, S. and J. Adams (2004). Variability of near-term probability for the next great earthquake on the Cascadia subduction zone, *Bull. Seismol. Soc. Am* **94,** 5, 1954-1959.

McCaffrey, R., L. M. Wallace, and J. Beavan (2008). Slow slip and frictional transition at low temperature at the Hikurangi subduction zone, *Nature Geoscience* **1,** 5, 316-320.

Miller, M. M., T. Melbourne, D. J. Johnson, and W. Q. Sumner (2002). Periodic Slow Earthquakes from the Cascadia Subduction Zone, *Science* **295,** 2423.

Miyazawa, M. and J. Mori (2005). Detection of triggered deep low-frequency events from the 2003 Tokachi-oki earthquake, *Geophys. Res. Lett.* **32,** L10307.

Miyazawa, M. and J. Mori (2006). Evidence suggesting fluid flow beneath Japan due to periodic seismic triggering from the 2004 Sumatra-Andaman earthquake, *Geophys. Res. Lett.* **33,** L05303.

Miyazawa, M. and E. Brodsky (2008). Deep low-frequency tremor that correlates with passing surface waves, *J. Geophys. Res.* **113,** B01307.

Miyazawa, M., E. Brodsky, and J. Mori (2008). Learning from dynamic triggering of low-frequency tremor in subduction zones, *Earth Planets Space* **60,** e17-e20.

Miyazawa, M. (2011). Propagation of an earthquake triggering front from the 2011 Tohoku-Oki earthquake, *Geophysical Research Letters* **38,** 23.

Nadeau, R. M. and D. Dolenc (2005). Nonvolcanic tremors deep beneath the San Andreas fault, *Science* **307,** 389.

Nadeau, R. M. and A. Guilhem (2009). Nonvolcanic Tremor Evolution and the San Simeon and Parkfield, California, Earthquakes, *Science* **325,** 191-193.

Obara, K. (2002). Nonvolcanic Deep Tremor Associated with Subduction in Southwest Japan, *Science* **296,** 1679-1681.

Obara, K. and H. Hirose (2006). Non-volcanic deep low-frequency tremors accompanying slow slips in the southwest Japan subduction zone, *Tectonophysics* **417,** 33-51.

Obara, K., S. Tanaka, T. Maeda, and T. Matsuzawa (2010). Depth-dependent activity of non-volcanic tremor in southwest Japan, *Geophysical Research Letters* **37,** 13.

Obara, K. (2011). Characteristics and interactions between non-volcanic tremor and related slow earthquakes in the Nankai subduction zone, southwest Japan, *Journal of Geodynamics* **52,** 3-4, 229-248.

Outerbridge, K. C., T. H. Dixon, S. Y. Schwartz, J. I. Walter, M. Protti, V. Gonzalez, J. Biggs, M. M. Thorwart, and W. Rabbel (2010). A tremor and slip event on the Cocos−Caribbean subduction zone as measured by a global positioning system (GPS) and seismic network on the Nicoya Peninsula, Costa Rica, *J. Geophys. Res.* **115,** B10408.

Payero, J. S., V. Kostoglodov, N. Shapiro, T. Mikumo, A. Iglesias, X. Perez-Campos, and R. W. Clayton (2008). Nonvolcanic tremor observed in the Mexican subduction zone, *Geophys. Res. Lett.* **35,** L07305.

Peng, Z. and K. Chao (2008). Non-volcanic tremor beneath the Central Range in Taiwan triggered by the 2001 Mw7.8 Kunlun earthquake, *Geophys. J. Int.* **175,** 2, 825-829.

Peng, Z., J. E. Vidale, K. C. Creager, J. L. Rubinstein, J. Gomberg, and P. Bodin (2008). Strong tremor near Parkfield, CA, excited by the 2002 Denali Fault earthquake, *Geophys. Res. Lett.* **35,** L23305.

Peng, Z., J. E. Vidale, A. G. Wech, R. M. Nadeau, and K. C. Creager (2009). Remote triggering of tremor along the San Andreas Fault in central California, *J. Geophys. Res.* **114,** B00A06.

Peng, Z. and J. Gomberg (2010). An integrated perspective of the continuum between earthquakes and slow-slip phenomena, *Nature Geosci.* **3,** 599 - 607.

Peng, Z., D. P. Hill, D. R. Shelly, and C. Aiken (2010a). Remotely triggered microearthquakes and tremor in central California following the 2010 Mw8.8 Chile Earthquake, *Geophys. Res. Lett.* **37,** L24312.

Peng, Z., W. Wang, Q.-F. Chen, and T. Jiang (2010b). Remotely triggered seismicity in northeast China following the 2008 Mw7.9 Wenchuan earthquake, *Earth Planets Space* **62,** 893-898.

Peng, Z., L. T. Long, and P. Zhao (2011). The Relevance of High-frequency Analysis Artifacts to Remote Triggering, *Seismological Research Letters* **82,** 5, 654-660.

Peng, Z., K. Chao, C. Wu, B. Fry, B. Enescu, and C. Aiken (2012). Global Observations of Triggered Tectonic Tremor, *SSA Annual Meeting***,** San Diego, California, 17-19 April 2012.

Peterson, C. and D. Christensen (2009). Possible relationship between nonvolcanic tremor and the 1998–2001 slow slip event, south central Alaska, *J. Geophys. Res.* **114,** B06302.

Peterson, C., S. McNutt, and D. Christensen (2011). Nonvolcanic Tremor in the Aleutian Arc, *Bull. Seismol. Soc. Am* **101,** 6, 3081–3087.

Rogers, G. and H. Dragert (2003). Episodic Tremor and Slip on the Cascadia Subduction Zone: The Chatter of Silent Slip, *Science* **300,** 1942-1943.

Rubinstein, J. L., J. E. Vidale, J. Gomberg, P. Bodin, K. C. Creager, and S. D. Malone (2007). Non-volcanic tremor driven by large transient shear stresses, *Nature* **448,** 579-582.

Rubinstein, J. L., J. Gomberg, J. E. Vidale, A. G. Wech, H. Kao, K. C. Creager, and G. Rogers (2009). Seismic wave triggering of nonvolcanic tremor, episodic tremor and slip, and earthquakes on Vancouver Island, *J. Geophys. Res.* **114,** B00A01.

Rubinstein, J. L., D. R. Shelly, and W. L. Ellsworth (2010). Non-Volcanic Tremor: A Window into the Roots of Fault Zones, *New Frontiers in Integrated Solid Earth Sciences***,** International Year of Planet Earth, 287-314, ed. Cloetingh, S., Negendank, J., Springer, Berlin.

Rubinstein, J. L., G. C. Beroza, J. R. Brown, M. R. Brudzinski, K. Chao, J. Gomberg, S. D. Malone, D. Oppenheimer, Z. Peng, S. G. Prejean, H. Savage, D. Shelly, A. Wech, and M. West (2011). Widespread Triggering of Earthquakes and Tremor by the 2011 M9.0 off-Tohoku Earthquake, *Seismological Society of America annual meeting in Memphis, TN*.

Schwartz, S. Y. and J. M. Rokosky (2007). Slow slip events and seismic tremor at circum-Pacific subduction zones, *Rev. Geophys.* **45,** 3.

Shearer, P. M. (1999). Introduction to Seismology**,** Cambridge University Press, Cambridge.

Shelly, D. R., G. C. Beroza, S. Ide, and S. Nakamula (2006). Low-frequency earthquakes in Shikoku, Japan, and their relationship to episodic tremor and slip, *Nature* **442,** 7099, 188-191.

Shelly, D. R., G. C. Beroza, and S. Ide (2007). Non-volcanic tremor and low-frequency earthquake swarms, *Nature* **446,** 7133, 305-307.

Shelly, D. R. (2009). Possible deep fault slip preceding the 2004 Parkfield earthquake, inferred from detailed observations of tectonic tremor, *Geophys. Res. Lett.* **36,** L17318.

Shelly, D. R., W. L. Ellsworth, T. Ryberg, C. Haberland, G. S. Fuis, J. Murphy, R. M. Nadeau, and R. Bürgmann (2009). Precise location of San Andreas Fault tremors near Cholame, California using seismometer clusters: Slip on the deep extension of the fault?, *Geophys. Res. Lett.* **36,** L01303, doi:10.1029/2008GL036367.

Shelly, D. R. (2010). Migrating tremors illuminate complex deformation beneath the seismogenic San Andreas fault, *Nature* **463,** 648-652.

Shelly, D. R. and J. L. Hardebeck (2010). Precise tremor source locations and amplitude variations along the lower-crustal central San Andreas Fault, *Geophysical Research Letters* **37,** L14301.

Shelly, D. R., Z. Peng, D. P. Hill, and C. Aiken (2011). Triggered creep as a possible mechanism for delayed dynamic triggering of tremor and earthquakes, *Nature Geosci* **4,** 384-388.

Shin, T. and T.-L. Teng (2001). An overview of the 1999 Chi-Chi, Taiwan, earthquake, *Bull. Seismol. Soc. Am* **91,** 5, 895-913.

Smith, E. F. and J. Gomberg (2009). A search in strainmeter data for slow slip associated with triggered

and ambient tremor near Parkfield, California, *J. geophys. Res* **114,** B00A14.

Stein, S. and M. Wysession (2003). An Introduction to Seismology, Earthquakes and Earth Structure, *Blackwell Publishing*.

Suppe, J. (1981). Mechanics of mountain building and metamorphism in Taiwan, *Memoir of the Geological Society of China* **4,** 67-89.
Swiecki, Z. and S. Y. Schwartz (2010). Ambient Tremor, But No Triggered Tremor at the Northern Costa Rica Subduction Zone, *Eos Trans. AGU*.
Tang, C.-C., Z. Peng, K. Chao, C.-H. Chen, and C.-H. Lin (2010). Detecting low−frequency earthquakes within non−volcanic tremor in southern Taiwan triggered by the 2005 Mw8.6 Nias earthquake, *Geophys. Res. Lett.* **37,** L16307.
Tang, C.-C., L. Zhu, C.-H. Chen, and T.-L. Teng (2011). Significant crustal variation across the Chaochou fault, southern Taiwan: new tectonic implications for convergent plate boundary, *J. Asian Earth Sci.* **41,** 6, 564-570.
Thomas, A. M., R. M. Nadeau, and R. Bürgmann (2009). Tremor-tide correlations and near-lithostatic pore pressure on the deep San Andreas fault, *Nature* **462,** 7276, 1048-1051.
van der Elst, N. J. and E. E. Brodsky (2010). Connecting near-field and far-field earthquake triggering to dynamic strain, *J. Geophys. Res.* **115,** B7.
Velasco, A. A., H. Gonzalez-Huizar, and S. Hernandez (2009). Dynamic stress modeling for the triggering of non-volcanic tremors *Eos Trans. AGU* **90,** 52, Fall Meet. Suppl., Abstract T11C-1820.
Wallace, L. M., J. Beavan, R. McCaffrey, and D. Darby (2004). Subduction zone coupling and tectonic block rotations in the North Island, New Zealand, *J. Geophys. Res.* **109,** B12.
Wallace, L. M. and J. Beavan (2010). Diverse slow slip behavior at the Hikurangi subduction margin, New Zealand, *J. Geophys. Res.* **115,** B12.
Walter, J. I., S. Y. Schwartz, J. M. Protti, and V. Gonzalez (2011). Persistent tremor within the northern Costa Rica seismogenic zone, *Geophys. Res. Lett.* **38,** L01307, doi:01310.01029/02010GL045586.
Wang, T. and E. S. Cochran (2009). Study of triggered tremor characteristics and triggering threshold in Anza region, Southern California, *Eos Trans. AGU* **90(54),** Fall Meet. Suppl., Abstract T13D-1917.
Wang, W., X. Gong, Z. Peng, Q. Chen, and C. Wu (2011). Dynamic triggering around Fangshan Pluton near Beijing, China, *Eos Trans. AGU***,** Fall Meet. Suppl., Abstract S22B-06 presented at 2011 Fall Meeting, AGU, San Francisco, Calif., 2015-2019 Dec.
Wech, A. and K. Creager (2007). Cascadia tremor polarization evidence for plate interface slip, *Geophys. Res. Lett.* **34,** L22306.
Wech, A. G. and K. C. Creager (2011). A continuum of stress, strength and slip in the Cascadia subduction zone, *Nature Geoscience* **4,** 9, 624-628.
West, M., J. Sanchez, and S. McNutt (2005). Periodically triggered seismicity at Mount Wrangell, Alaska, after the Sumatra earthquake, *Science* **308,** 5725, 1144-1146.
Wu, C., Z. Peng, W. Wang, and Q.-F. Chen (2011). Dynamic triggering of shallow earthquakes near Beijing, China, *Geophys. J. Int.* **185,** 1321-1334.
Wu, Y.-M., C.-H. Chang, L. Zhao, J. B. H. Shyu, Y.-G. Chen, K. Sieh, and J.-P. Avouac (2007). Seismic tomography of Taiwan: Improved constraints from a dense network of strong motion stations, *J. Geophys. Res.* **112,** B08312.
Yeh, T.-C. (2011). Dynamic triggering of earthquakes and tremors in Taiwan, Master Thesis, National Taiwan University, Taipei.

Yu, S., H. Chen, and L. Kuo (1997). Velocity field of GPS stations in the Taiwan area, *Tectonophysics* **274,** 41-59.

Zechar, J. D. and R. M. Nadeau (2012). Predictability of repeating earthquakes near Parkfield, California**,** submitted.

Zigone, D., D. Rivet, M. Radiguet, M. Campillo, C. Voisin, N. Cotte, A. Walpersdorf, N. M. Shapiro, G. Cougoulat, P. Roux, V. Kostoglodov, A. Husker, and J. S. Payero (2012). Triggering of Tremors and Slow Slip event in Guerrero (Mexico) by the 2010 Mw 8.8 Maule, Chile, Earthquake, *J. geophys. Res***,** revised.